UNIVERSITÉ DE MONTRÉAL

SYNTHESIS, CHARACTERIZATION AND MODIFICATION OF $LiFePO_4$ BY DOPING WITH PLATINUM AND PALLADIUM FOR LITHIUM-ION BATTERIES

MAJID TALEBI-ESFANDARANI

DÉPARTEMENT DE GÉNIE CHIMIQUE

ÉCOLE POLYTECHNIQUE DE MONTRÉAL

THÈSE PRÉSENTÉE EN VUE DE L'OBTENTION

DU DIPLÔME DE PHILOSOPHIAE DOCTOR

(GÉNIE MÉTALLURGIQUE)

DÉCEMBRE 2013

© Majid Talebi-Esfandarani, 2013.

UNIVERSITÉ DE MONTRÉAL

ÉCOLE POLYTECHNIQUE DE MONTRÉAL

Cette thèse intitulée:

SYNTHESIS, CHARACTERIZATION AND MODIFICATION OF $LiFePO_4$ BY DOPING WITH PLATINUM AND PALLADIUM FOR LITHIUM-ION BATTERIES

présentée par: TALEBI-ESFANDARANI Majid

en vue de l'obtention du diplôme de : Philosophiae Doctor

a été dûment acceptée par le jury d'examen constitué de :

M. AJERSCH Frank, Ph.D., président

M. SAVADOGO Oumarou, D. d'état, membre et directeur de recherche

M. PATIENCE Gregory, Ph.D., membre

M. MOHAMEDI Mohamed, Ph.D., membre

DEDICATION

To my beloved mother

For always believing in me and supporting me

ACKNOWLEDGEMENT

I owe my sincere gratitude to those who helped me in the completion of this dissertation. The first and most important person I would like to thank is my advisor Professor Oumarou Savadogo. He provided me with the opportunity to carry out this research and has taught me how to conduct research independently and patiently.

I extend my gratitude to all my committee members, Professor Frank Ajersch, Professor Gregory Patience and Professor Mohamed Mohamedi, for their precious time to read this thesis and give me helpful comments on this work.

I am so thankful to Dr. Fredrick Omenya at university of Binghamton for his warm compassions and helpful discussions regarding the synthesis of materials. I would like to extend my thanks to my colleagues and friends in Ecole Polytechnique for sharing their friendship and knowledge with me, particularly Mr. Ali Seifitokaldani and Mr. Mohsen Keshavarz. Many thanks to all the secretaries and technical staff of the Chemical engineering department, particularly Mrs. Carole Massicotte and Mr. Robert Delisle. I would like to deeply thank Mrs. Hanen Touihri for her warm and quick response to my request for translating parts of this thesis to French.

I would like to extend my gratitude to all my friends in Montreal for their unforgettable favors and for all the memorable moments I had with them; Very special thanks to Mr. Khalil Shahverdi, Mr. Jaber Shabanian, Mrs. Laleh Dashtban and Mr. Hesamoddin Tabatabaei who were always there, ready to hear me and support me in any conditions.

My special thanks also goes to Mrs. Roksana Bavand Savadkouhi for helping me to analyze the XPS results. I wish to deeply thank Mr. Sobhan Hassanshahi not only for revising my thesis, but

also for his generous nature and warm supporting. I would also like to thank Mr. Milad Aghabararnejad for helping me to take the BET measurements.

I could not have done this without my family. I am thankful to my sister and brothers for their supports and encouragements. Finally, from the very depth of my heart, I would like to express my undying gratitude to my beloved mother for confidence, sacrifices and endless support in my whole life. There will never be a right word to express my feeling of appreciation for her unconditional love.

RÉSUMÉ

Le phosphate de fer lithié ($LiFePO_4$), caractérisé par son excellente stabilité chimique et structurale, sa non-toxicité, son faible coût, et son abondance dans la nature, est l'un des matériaux de cathode le plus prometteur pour être utilisé dans les batteries aux ions lithium. Cependant, il souffre d'une faible conductivité électrique et d'une diffusion ionique très limitée, Ce matériau fonctionne uniquement à des taux faibles de charge/décharge de courants. Dans cette thèse, une double approche du dopage métallique et le revêtement de carbone a été utilisée pour résoudre le problème mentionné précédemment. Ce travail porte pour la première fois sur l'étude, de l'effet du dopage de $LiFePO_4$ avec le platine ou le palladium sur ses propriétés physico-chimiques. L'effet de dopage de ce matériau avec Pt ou Pd sur ses performances comme cathode pour les la battéries au Li-ion sera déterminé. La méthode de préparation sol-gel et hydrothermique ont été utilisées pour la synthèse des matériaux à base de cathode de $LiFePO_4$ dopés et non dopés. Les matériaux préparés ont été caractérisés par différentes méthodes telles que la diffraction des rayons X (XRD), la spectroscopie des photoelectrons (XPS), la microscopie électronique à balayage (MEB) et la mesure de surface active par BET (Brunauer Emmett Teller). Les techniques de caractérisation électrochimiques comme le test de charge/décharge, la voltammétrie cyclique (CV), l'impédance électrochimique (EIS) et le cyclage ont également été utilisés. Les effets du dopage des métaux sur les propriétés physico-chimiques, les tailles des particules, la morphologie, la structure et la pureté des électrodes ont été étudiés et leur corrélation avec les propriétés électrochimiques des matériaux a été étudiés.

Dans la première section, nous avons déterminé à l'aide du MEB la quantité optimale de support de carbone et la morphologie des particules de $LiFePO_4$ qui sont revêtues par le support. Ceci a permis d'identifier la composition optimum de la cathode de $LiFePO_4$/C qui permet d'obtenir

d’excellentes performances électrochimiques dans une pile au Li-ion. On a constaté que lorsque la quantité de carbone utilisé dépasse la valeur optimisée, la capacité de décharge du matériau $LiFePO_4$/C diminue. Ceci pourrait indiquer une faible diffusion des ions Li^+ à travers les couches de carbone au cours du processus de charge/décharge. Pour une quantité de carbone inférieure à la quantité optimum, la cathode de $LiFePO_4$/C présente une capacité de charge/décharge très inférieure à celle obtenue avec le carbone optimisé. Ceci est attribué à la faible valeur de sa conductivité électrique due à la faible quantité de carbone. Par conséquent, la qualité et la quantité de revêtement de carbone à la surface des particules de $LiFePO_4$ sont importantes et seulement la teneur optimisée en carbone peut conduire à une répartition plus uniforme de carbone. La surface et la conductivité optimisées, qui donnent une haute performance électrochimique, ne peuvent être atteintes que si la teneur en carbone appropriée et la bonne méthode de préparation de l'électrode ont été identifiées.

Dans la deuxième partie, nous avons étudié l'effet de doper $LiFePO_4$/C avec Pt et Pd sur sa structure, sa composition chimique et ses propriétés électrochimiques. Les électrodes ont été préparées en utilisant le procédé sol-gel. L'analyse de la composition chimique par XPS des électrodes dopées au Pd a dé montré que le Pd est présent dans les nano matériaux composites de $LiFePO_4$/C. Pour l’électrode de $LiFePO_4$/C dopé au Pt, le Pt a été détecté dans des matériaux composites à base de nanoparticules de ce matériau. Les résultats sur la structure et la morphologie des électrodes non dopées et dopées ont montré que le dopage au palladium a facilité la formation de l’impureté Li_3PO_4 dans les électrodes $LiFe_{0.98}Pd_{0.02}PO_4$/C et $LiFe_{0.96}Pd_{0.04}PO_4$/C. Par conséquent, la présence du Pd dans l'échantillon dopé réduit les paramètres de maille, augmente la taille des particules et provoque leur agglomération. Les performances électrochimiques des électrodes ont montré que la capacité spécifique diminue

quand la teneur en palladium augmente. Ensuite, les électrodes dopées au Pd et fabriquées en utilisant la méthode sol-gel ont une capacité de décharge plus faible que celle des électrodes de $LiFePO_4$/C non dopées. La diminution de la performance est attribuée à plusieurs facteurs comme la diminution des paramètres du réseau cristallin, les formations l'impureté Li_3PO_4 et l'augmentation de la taille des particules suite au dopage de $LiFePO_4$. En revanche, pour $LiFePO_4$/C dopé au Pt en utilisant la méthode sol-gel, il a été constaté que la cristallinité et les paramètres de maille du matériau nano-composite $LiFe_{0.96}Pt_{0.04}PO_4$/C ont augmenté en comparaison avec l'électrode $LiFePO_4$/C seul. Aucune impureté n'a été formée dans l'électrode Pt-dopé. En outre, les échantillons dopés au Pt montraient des particules de tailles plus petites (100-200 nm) que l'électrode non dopée (200-500 nm). Des particules plus homogènes et uniformes ont également été obtenues avec $LiFe_{0.96}Pt_{0.04}PO_4$/C comparativement à celles obtenues avec $LiFePO_4$/C. Par conséquent, le dopage au platine pourrait fournir plus d'espace pour la diffusion des ions Li^+; ce qui facilite le déplacement des ions Li^+ dans la structure de $LiFe_{0.96}Pt_{0.04}PO_4$/C pendant les réactions d'oxydoréductions à la cathode de la batterie, améliorant ainsi les capacités de décharge.

Dans la troisième partie de cette étude, $LiFe_{1-x}Pd_xPO_4$/C (x = 0,00, 0,02, 0,04) et nano matériaux de cathode composite $LiFe_{0.96}Pt_{0.04}PO_4$/C ont été synthétisés par voie hydrothermique et les effets de Pd et Pt ont été examinés. Les résultats indiquent que la quantité optimale de teneur en palladium (0,02%) dans l'électrode ($LiFe_{0.98}Pd_{0.02}PO_4$/C) réduit la taille des particules composites. Cela pourrait faciliter la diffusion des ions Li^+ et par conséquent améliorer la réversibilité et diminuer la résistance de transfert de charge. La teneur optimisée en Pd dans l'électrode pourrait agir comme un pilier pour éviter le rétrécissement et l'effondrement de la structure initiale de la maille de $LiFePO_4$. Cela pourrait aider à la stabilisation de la structure

cristalline au cours du processus d'intercalation/dé-intercalation des ions Li^+. Cependant, en augmentant la teneur en palladium à 4%, les capacités spécifiques ont diminué en raison de la formation d'impuretés Li_3PO_4 et de l'augmentation de la taille des particules. La présence de ces impuretés peut produire une petite aire de surface pour la réaction redox, et provoque des difficultés pour la diffusion d'ions Li^+ pendant le processus d'oxydo-réduction électrochimique. En conséquence, le dopage au palladium à une teneur optimisée est utile pour améliorer les performances électrochimiques du matériau $LiFePO_4$/C. La cathode à base de $LiFe_{0.96}Pt_{0.04}PO_4$/C nano matériau qui a été préparée par la méthode hydrothermique a présenté une meilleure performance en comparaison avec l'échantillon de $LiFePO_4$/C. L'amélioration de la performance électrochimique peut être attribuée à la combinaison des aspects suivants liés à la présence de Pt dans l'électrode. L'élément platine pourrait agir comme un pilier pour stabiliser la structure cristalline pendant le processus de charge/ décharge. Il pourrait aussi contribur à l'amélioration de la vitesse de la réaction d'oxydo-réduction avec l'augmentation de la surface spécifique de l'électrode composite. L'électrode de $LiFe_{0.96}Pt_{0.04}PO_4$/C présente aussi des petites particules homogènes qui pourraient faciliter le taux de diffusion des ions Li^+.

Les résultats montrent que les propriétés structurales et chimiques et les performances électrochimiques des électrodes à base de $LiFePO_4$/C dopées de Pd et Pt pour donner $LiFe_{1-x}Pd_xPO_4$/C et $LiFe_{1-x}Pt_xPO_4$/C comme cathodes de la pile au lithium-ion sont très affectées par la méthode de préparation des matériaux et de l'élément dopant.

ABSTRACT

Lithium iron phosphate ($LiFePO_4$) with features of excellent thermal stability, non-toxicity, low cost and abundance in nature is one of the most promising cathode materials to be used in lithium ion batteries. However, as it suffers from the low electrical conductivity and poor ionic diffusion, it operates only at low charge/discharge current rates. In this thesis, a dual approach of metal doping and carbon coating was employed to solve the aforementioned problem. This work is mainly on the study, for the first time, of the effect of platinum and palladium doping of $LiFePO_4$ on its physical-chemical properties. The effect of Pt and Pd doping on the $LiFePO_4$ performance as Li-ion cathode will be also shown. Sol-gel and hydrothermal methods were used to synthesize the $LiFePO_4$ and doped-$LiFePO_4$ cathode materials. The prepared materials were characterized using different methods such as XRD (X-ray Diffraction), XPS (X-ray Photoelectron Spectroscopy), SEM (Scanning Electron Microscopy) and BET (Brunauer Emmett Teller). The electrochemical characterization techniques including charge/discharge test, CV (Cyclic Voltammetry), EIS (Electrochemical Impedance Spectroscopy) and cycling were also used. The effects of metals doping on chemical-physical properties, particles sizes, morphology, structure and purity of the electrodes were investigated and their correlation to the electrochemical properties of materials were studied.

In the first section, we determine the optimized amount of carbon support and morphology of the particles using SEM which help to obtain $LiFePO_4$/C cathode material with an excellent electrochemical performance. It was found that when the amount of coated carbon exceeds the optimized value, the discharge capacity of the $LiFePO_4$/C material decreased. This might indicate a low diffusion of the Li^+ ions through the carbon layers during the charge/discharge process. On the other hand, for $LiFePO_4$ coated with carbon quantity lower than the optimum value,

$LiFePO_4$/C cathode exhibited poor capacity performance due to its low electrical conductivity. Therefore, both the quality and quantity of carbon coating on the surface of $LiFePO_4$ particles are important and only optimized carbon content can lead to a more uniform carbon distribution. Optimized surface area and conductivity, which give high electrochemical performance, can be only achieved if the appropriate carbon content and method of electrode preparation are obtained.

In the second part, the effect of doping the $LiFePO_4$/C electrodes with Pt and Pd on the structure, their chemical compositions and electrochemical properties were investigated. The electrodes were prepared using sol-gel method. The chemical composition analysis by XPS of the Pd doped electrodes showed that Pd was detected in the Pd-doped nano composite materials. Also, for Pt doped electrode, Pt was detected in Pt-doped based nano composite materials. Based on the structure and morphology of the non doped and doped electrodes, the results showed that palladium doping facilitated formation of Li_3PO_4 impurity in the $LiFe_{0.98}Pd_{0.02}PO_4$/C and $LiFe_{0.96}Pd_{0.04}PO_4$/C electrodes. Consequently the presence of the Pd in the doped sample reduced the lattice parameters, increased the size of particles and caused their agglomeration. The electrochemical performances of the electrodes showed that their specific capacity decreased when the palladium content increases. Then, the Pd-doped electrodes fabricated using sol-gel method exhibit less discharge capacity than samples of the non-doped $LiFePO_4$/C electrode. The reduction in the level of performance is attributed to several reasons such as the shrinking of the lattice parameters, the formation of Li_3PO_4 impurity phase, and large particles size.

In contrast, for $LiFePO_4$/C doped with Pt using sol-gel method, it was found that the crystallinity and the lattice parameters of $LiFe_{0.96}Pt_{0.04}PO_4$/C nanocomposite material increased when compared with $LiFePO_4$/C electrode. No impurity was formed in the Pt-doped electrode. In addition, the Pt doped samples exhibited smaller particle sizes (100-200 nm) than the non doped

electrode (200-500 nm). More homogeneous and uniform particles were also obtained with $LiFe_{0.96}Pt_{0.04}PO_4/C$ than $LiFePO_4/C$ samples. Therefore, platinum doping might provide more space for the diffusion of Li^+ ions which facilitates the movement of Li^+ ions through the structure of $LiFePO_4/C$ material during the redox reactions in the battery, enhancing the discharge capacities.

In the third part of this study, $LiFe_{1-x}Pd_xPO_4/C$ (x = 0.00, 0.02, 0.04) and $LiFe_{0.96}Pt_{0.04}PO_4/C$ nano composite cathode materials were synthesized by a hydrothermal method and the effects of Pd and Pt were examined. The results indicated that the optimized amount of palladium content (0.02%) in the electrode ($LiFe_{0.98}Pd_{0.02}PO_4/C$) reduced the nano composite particle sizes. This facilitates the Li^+ ion diffusion and consequently enhances the reversibility and decreases the charge transfer resistance. The optimized Pd content in the electrode might act as a pillar to prevent the shrinking and collapse of the initial lattice structure. This might support the stabilization of the crystal structure during the intercalation/de-intercalation process of Li^+ ions. However, by increasing the palladium content to 4%, the specific capacities decreased due to the Li_3PO_4 impurity formation. The presence of such impurity may produce a small surface area for the redox reaction, and causes difficulty of Li^+ ion diffusion during the redox electrochemical process. As a result, the optimized palladium doping is helpful in improving the electrochemical performance of $LiFePO_4/C$ material. A $LiFe_{0.96}Pt_{0.04}PO_4/C$ based cathode nano material prepared by a hydrothermal method exhibited better performance when compared to the non-doped $LiFePO_4/C$ sample. The improvement in the electrochemical performances can be attributed to the combination of the following aspects related to the presence of Pt in the electrode. The platinum element can act as a stabilizing point of the crystal structure during the charge/discharge process. It contributes to the improvement of the redox reaction rate with the increase of the

specific surface area of the composite electrode. $LiFe_{0.96}Pt_{0.04}PO_4/C$ electrode exhibited homogeneous small particles which might facilitate the Li^+ ions diffusion rate.

The results show that the chemical and structural properties and electrochemical performances of Pd and Pt doped $LiFePO_4/C$ based electrodes to obtain $LiFe_{1-x}Pd_xPO_4/C$ and $LiFe_{1-x}Pt_xPO_4/C$ as Li-ion cathodes are significantly informed by the method of preparation of the materials and the doping element.

TABLE OF CONTENTS

LIST OF TABLES

LIST OF FIGURES

SYMBOLS AND ABBREVIATIONS

ν	Scan rate
σ_w	Warburg impedance coefficient
ω	Frequency
Ω	Ohm
°C	Degrees Celsius
Å	Angstrom
A	Ampere, area
AC	Alternating current
C	Current, Carbon, Concentration of Li^+ ions
cm	Centimeter
D	Diffusion coefficient of Li-ions
E_{ox}	Anodic peak potential
E_{red}	Cathodic peak potential
e^-	Electron
eV	Electron volt
F	Faraday constant
g	Gram
K	Kelvin
kg	kilogram
h	Hour
L	Liter
Li	Lithium

Li^+	Lithium ions
m	Meter
µm	Micronmeter
nm	Nanometer
mAh	MiliAmpere.hour
mg	Milli gram
mL	Milli liter
n	Number of electron
R	Resistance, Gas constant,
R_{ct}	Charge transfer resistance
R_e	Electrolyte resistance
R_s	Solution resistance
S	Siemens
s	Second
t	Time
T	Temperature
V	Volt
v	Volume
W	Watt
Wh	Watt.hour
wt%	Weight percent
Z', Z_{re}	Real axis
Z", Z_{im}	Imaginary axis
BET	Brunauer Emmett Teller

CPE	Constant phase element
CV	Cyclic voltammetry
CNT	Carbon nano tube
DEG	Diethylene glycol
DMC	Dimethyl carbonate
EC	Ethylene carbonate
EG	Ethylene glycol
EV	Electric vehicle
EIS	Electrochemical impedance spectroscopy
HEV	Hybrid electric vehicle
LFP	Lithium iron phosphate
LIB	Lithium ion battery
NMP	N-methyl pyrrolidone
PVDF	Poly vinylidene fluoride
OCV	Open circuit voltage
SEI	Solid electrolyte interphase
SEM	Scanning electron microscopy
TEG	Triethylene glycol
TTEG	Tetraethylene glycol
XRD	X-ray diffraction
XPS	X-ray photoelectron spectroscopy

CHAPTER 1 INTRODUCTION

Due to the increasing price of fossil fuel, global warming and pollution challenges, attention has increasingly turned to reducing or replacing fossil fuel by developing new energy sources in recent years. Electricity from battery sources is a clean and appropriate method to produce energy for a long term consideration in reducing the use of fossil fuel and, consequently, decreasing the amount of greenhouse gas generation and atmospheric pollution. The development of batteries, a technology dating back more than a century, plays critical roles in portable devices and mobile technologies used today. However, battery technologies have been incapable in providing the necessary performance for large devices at a competitive cost because batteries require features of high energy density, small size, low cost, fast charging rate which can store more charge and operate at higher current rates. Nevertheless, the application of batteries in large devices continues to grow.

A battery is a power device, which converts chemical energy to electrical energy. Batteries are mainly categorized into two groups: Primary and Secondary batteries. Primary batteries are generally disposable and non-rechargeable. Therefore, once discharged, they are discarded because the materials used in the primary batteries may not return to their original form as the chemical reaction is not easily reversed. Secondary batteries are known as rechargeable batteries i.e. they can be recharged many times after each discharge by applying an electric current to reverse the chemical reaction which occurs during discharging, making the battery reusable. Among different rechargeable batteries fabricated so far, the lithium ion battery (LIB) which is considered in this study shows the best volumetric and gravimetric energy density, compared to the other various types of rechargeable batteries, shown in Figure 1-1[1]. The most important

electrochemical performance parameters of LIB compared with other kinds of rechargeable batteries are summarized in Table 1-1. It shows that the energy density and cell voltage of LIBs are at least twice those of other types of rechargeable batteries. LIBs also feature low self-discharge, large operating temperature in range of -20 to +60 °C, a long life cycle, and stability, but significantly higher costs. In addition, there is almost no memory-effect for the LIBs and, hence, they can be recharged at any time. Considering these features, LIB devices can provide a reliable rechargeable system to meet the demand for clean and high-efficiency transportation. Since its first commercial production by SONY Company in 1991, LIBs became the most popular rechargeable battery as a power source for low energy, portable electric devices, such as cell phones, cameras, and laptop computers. However, the application of LIBs for high power tools and devices, such as electric bikes and cars, is still limited because of its low charge/discharge rate.

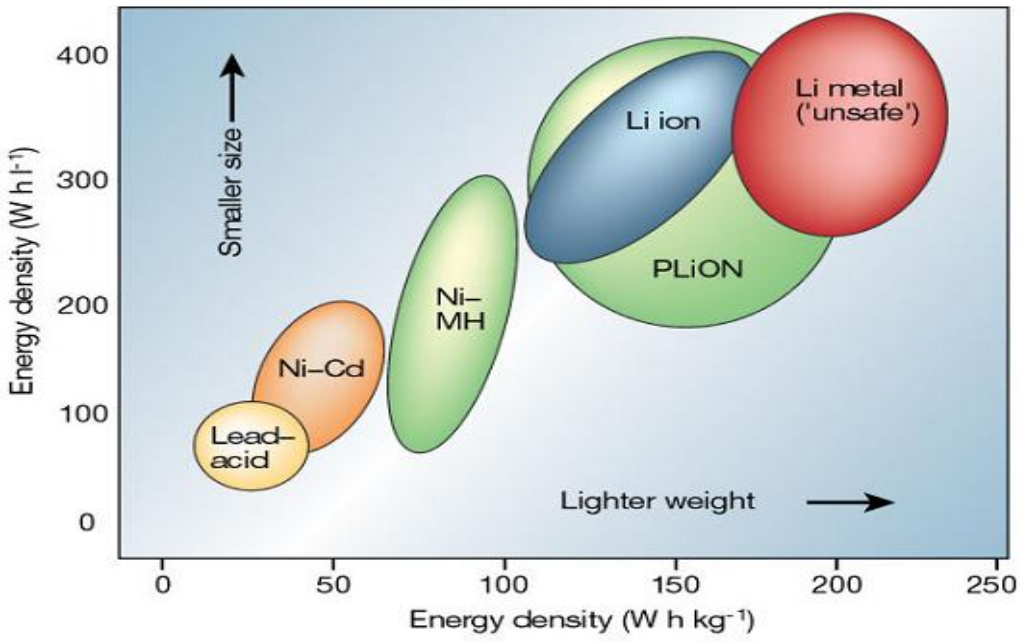

Figure 1-1: A comparison of different rechargeable battery technologies in terms of volumetric and gravimetric energy densities [1]

Therefore, it is difficult for a LIB to satisfy the requirements of powering a next generation of large devices such as electric vehicles (EV) or hybrid electric vehicles (HEV). As such, to accomplish high performance battery especially in the aspects of energy/power density, life cycle and safety issues, more investigation is required to enhance the performance of commonly used LIB.

There are many factors that can affect the performance of LIB, such as anode, cathode, and electrolyte components. However, these days, the main determining factor for energy density in LIBs is the cathode material because it has lower specific capacity compared with the graphite anode material [1]. In addition, Li transport/diffusion on the cathode is the main rate limiting step in a LIB system [2]. The common cathode material in LIB application is $LiCoO_2$. However, it is expensive and is not environmentally friendly due to the Co [3]. $LiFePO_4$ is one of the best alternatives that can be used as the cathode material because of its excellent thermal stability, low cost, non-toxicity and abundance in nature [4]. However, it has some drawbacks, such as poor ionic diffusion and low electrical conductivity, limiting its application in large devices and working only at low charge/discharge current densities [4]. These are the main challenges on the subject.

Table 1-1: The performance parameters of various rechargeable batteries

Types of battery	Energy density (Wh/kg)	Cycle durability	Self-discharge (Per month)	Cell voltage (V)	Charge time (h)
NiMH	30-80	500-1000	25%-30%	1.2	2-4
NiCD	40-60	1500	10%-20%	1.25	1
Lead-acid	30-40	600-800	5%-20%	2.1	8-16
Li-ion	100-170	1200	5%-12%	3.5	1-3

Many efforts have focused on solving these problems by decreasing the particles sizes, coating particles with a high conducting material, such as carbon, and doping with transition metal ions [5-7]. Consequently, improved performance at higher current rates is expected for those materials by optimizing the morphology, particle size, carbon coating and transition metal doping. Many researchers have examined the particle size reduction and carbon coating strategies to improve the electrochemical performance of $LiFePO_4$ material. However, the mechanism of doping strategy has not been completely understood due to its complexity. Therefore more investigation is needed in this strategy. Moreover, even with the exhaust of research on the improvement of $LiFePO_4$ material, the capacity is still below the requirements for the next generation of batteries, suggesting that $LiFePO_4$ based material with high energy density and good electrochemical property still needs more investigation.

The variations in the crystallinity, purity, particle size, morphology, and electrochemical performance of the $LiFePO_4$ material depend on the preparation methods and conditions [8-10]. Certainly, a successful method of synthesis and optimized preparation are needed to obtain high performance materials. Since the introduction of $LiFePO_4$ by Padhi et al. in 1997 [4], various methods for preparing the $LiFePO_4$ material have been proposed, including solid state, hydrothermal, sol-gel, co-precipitation, microwave processes, polyol process, etc [9-11]. The solid state synthesis method is the most conventional method because of its simple procedure and the ease in scaling-up. High energy consumption and high temperature calcinations for long periods are, however, disadvantages of the solid state method. In addition, this method suffers from agglomeration and uncontrollable particle growth.

Hydrothermal synthesis has advantages of low energy utilization, low cost, rapid and an easily scalable method to prepare $LiFePO_4$ material with well controlled morphology and fine crystal

particles [12-14]. Hydrothermal synthesis is also suitable for the preparation of metal-doped $LiFePO_4$ materials [15]. Sol-gel, as another significant method, ensures higher purity, homogeneity and small particle size due to better mixing of the precursors [16-18]. In addition, it is a simple and non-expensive method to prepare $LiFePO_4$ material. Therefore, hydrothermal and sol-gel methods are regarded as the best techniques to synthesize high quality $LiFePO_4$ materials which will be used in this research because the resulting products in these methods have higher uniformity, purity, controllable shapes and are suitable for the synthesis of metal-doped material.

Up to now, no noble metals with high stability and activity such as palladium and platinum have been doped on the $LiFePO_4$ material. Therefore, this research work is focused on studying the performance of doped-$LiFePO_4$ cathode materials, including the preparation with hydrothermal and sol-gel methods, characterization and electrochemical tests of doped-$LiFePO_4$ cathode materials, in order to investigate the effect of platinum and palladium doping on the crystal structure, particle size and the electrochemical properties of the prepared materials.

The objective of this study consists of conducting comprehensive and fundamental research work to provide more valuable information on how the size of the particle and the structure can change the performance of the cathode material in the LIB, with special attention to variations of doping with Pd and Pt. It is anticipated that more fundamental understanding of the effect of doping will be understood with Pt and Pd doping because they are expected to be more stable than the other doping elements used until now.

CHAPTER 2 BACKGROUND AND LITERATURE REVIEW

2.1 Lithium ion battery

The lithium ion battery (LIB) was first proposed by Whittingham in 1970, [19] and then commercialized in 1991 by Sony. An LIB is an energy conversion device that converts the chemical energy stored in its active materials into electric energy through electron and Li^+ ion movement caused by an oxidation-reduction reaction at the electrodes [2]. It contains one or more electrochemical cells that are connected in series or in parallel to provide the required voltage and capacity, respectively. In our work, LIB refers to a single electrochemical cell. Each cell contains two electrodes, the anode and cathode, non-aqueous electrolyte and separator.

The anode (negative electrode) is oxidized during the discharge and releases electrons. Normally, materials with low (negative) standard reduction potential are used as anodes. The cathode (positive electrode) accepts electrons and is reduced during the discharge. High (positive) standard reduction potential materials are chosen as cathodes. The electrolyte is a material that provides good ionic conductivity to transfer the Li^+ ion during charge/discharge processes, but no electrical conductivity, in order to prevent short circuiting. The separator is a porous polymer which is an electrically insulating material placed between the electrodes, preventing the direct contact of cathode and anode, while allowing ionic conduction. Typically, the main material used for the cathode is $LiCoO_2$, for the anode, graphite is used. The electrolyte is a lithium salt ($LiPF_6$, $LiBF_4$ or $LiClO_4$) in a mixture of organic solvent (ethylene carbonate, diethyl carbonate, or dimethyl carbonate) with some volumetric ratio [1, 2, 20]. The non-aqueous electrolyte is used because Li reacts strongly with water and also, water is not stable during oxidation at the high potentials, inherent to LIBs.

Discharging and charging of the LIB is attributed to the intercalation and de-intercalation of Li^+ ions into a host structure as illustrated in Figure 2-1. During discharge process, Li^+ ions flow internally from the anode to the cathode through the electrolyte and are transported to the cathode, while electrons transfer externally from the anode to the cathode across the connection outside the circuit, creating a current and providing electrical energy. However, the insertion of Li^+ ions on to the cathode would come to an end when the electrical potential of the cathode reaches the same value as that of the anode material. At this time, the chemical energy is totally converted to electrical energy. The reverse process, known as the de-intercalation of Li^+ ions from the host material, occurs during the charging of the battery by applying a current in opposite direction. During the charging process, Li^+ ions flow internally from the cathode to the anode, while electrons transfer externally from the cathode to the anode side to maintain charge.

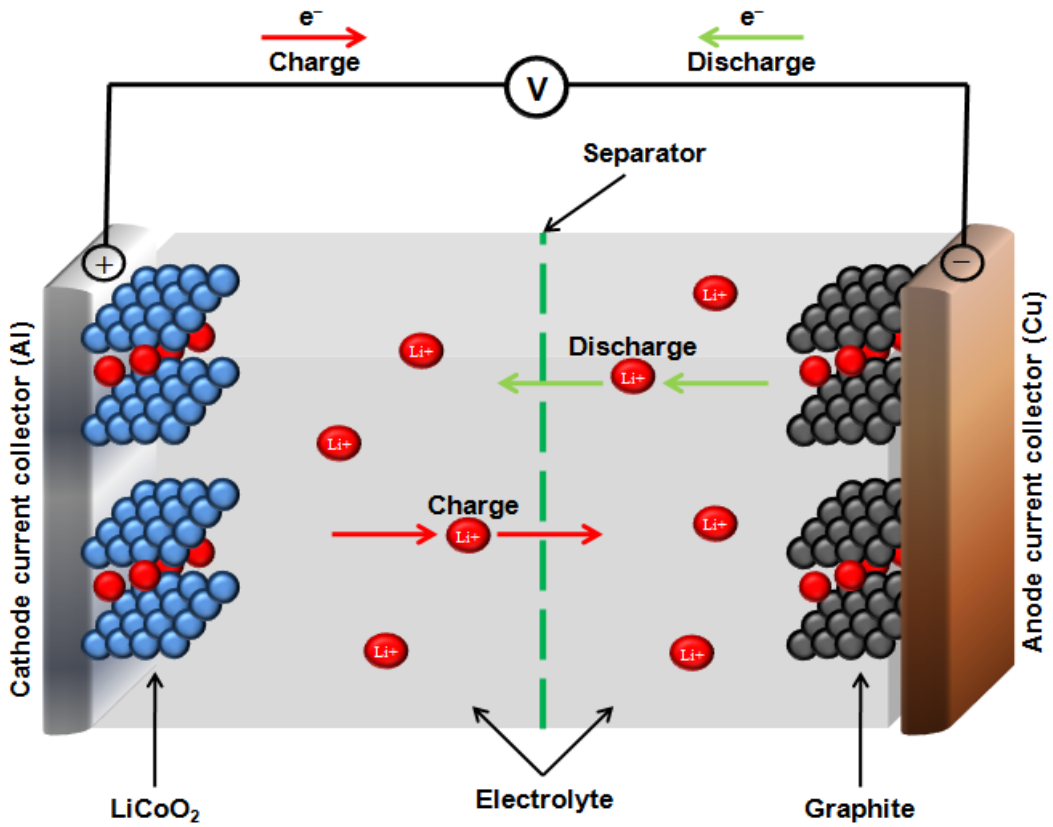

Figure 2-1: Charging and discharging processes in a rechargeable lithium ion battery

In addition, LIB is called a "rocking-chair cell" because the Li^+ ions are shuttled or rocked between the anode and cathode upon charging and discharging. The major factors that identify the electrochemical performances of a LIB are cell potential (V), energy density, cycling ability and rate capability. Cell potential depends on the intrinsic chemistry of materials. Energy density referring to the amount of energy stored per volume or mass, ascribes the ability of hosting lithium ions, in units of Wh/L or Wh/kg. The energy density is a function of the cell potential and material's reversible capacity. For high energy density, a material with high potential and large specific capacity is needed. Specific capacity is related to the maximum current in the active materials flowing for a given time in units of mAh/g. The cycling ability refers to the stability of performance of the cell after many charging/discharging cycles. A material with long storage time and minimal degradation of performance (capacity loss) is preferred. The rate capability in terms of electron and Li^+ insertion/ extraction through the material, is determined by the both the electric conductivity within the electrode and the ionic conductivity within the electrodes, the electrolyte, and across the electrolyte electrode interface.

To compare the performance of the different active materials, a C-rate (mA or A) is used to describe the amount of the current a battery is generating or accepting in either discharge or charge modes. It is represented as the ratio of the battery discharging or charging. Different C-rates such as 1C, 5C, 10C or 0.1C are often used to examine the capacities of the active materials. For example, 1C is defined as the amount of current necessary to use all of the specific capacity in one hour. If an operating current is xC, then the theoretical specific capacity is obtained in 1/x hour. In general, a material has a good performance, when the experimental capacity is close to the theoretical one, regardless of what C-rate is applied.

2.2 Materials for the Lithium ion battery

The performance of a LIB depends mainly on the anode, the cathode and the electrolyte components [1, 20]. Therefore, extensive studies have been carried out to improve or develop new materials for components of LIBs, especially on active materials for the anodes and the cathodes. Excellent active materials have the following key features:

- Large amount of Li^+ ions for intercalation/de-intercalation to maximize capacity;
- Efficient and rapid intercalation/de-intercalation of Li^+ ions and electrons;
- Good reversibility with small or no change in the host structure during Li^+ ions intercalation/de-intercalation process;
- Chemically stable when contacted by an electrolyte without reacting with the electrolyte;
- Good electrical conductor to minimize polarization and heat generation;
- Inexpensive, environmentally friendly, lightweight and easy to synthesize.

Since two decades ago when the LIB was introduced, studies have focused on positive electrode materials to improve the performance of LIBs because the cathode material suffers a much lower intercalation capacity, at least in long term cycles compared with the anode material [2]. Moreover, the positive cathode material additionally involves other characteristics such as safety issues, material costs, environmental toxicity and recyclability. Therefore, research on the lithium ion battery electrode is more concentrated on the cathode material. In addition to looking for new cathode materials, researchers have been trying to propose various methods to improve the intercalation capacity of already established cathode materials. Here is a brief review on the anode materials and a more extensive literature review on the cathode materials.

2.2.1 Anode materials

In the earliest LIB, lithium metal was used as the anode because it is lightest metal with high specific capacity (3826 mAh/g) as well as the lowest potential (-3.045 V), which can release the electron easily. However, the safety problem of using lithium metal as an anode became a serious drawback due to short circuits caused by the formation of lithium dendrites on the surface of the lithium metal anode during cycling, making it unsafe in the lithium battery [21]. Moreover, lithium metal is extremely reactive with oxygen and moisture. Therefore, glove boxes or dry-rooms are necessary for assembling the LIB. However, Li-Al alloys have improved the safety issue, but still could not avoid the fast capacity degradation [22].

After several investigations, graphite with specific capacity of 380 mAh/g was introduced as anode material which can host Li^+ ions during reaction with stochiometry of LiC_6 [23]. Graphite was commercialized as an anode in LIBs in 1991 by Sony [24]. Replacing the lithium metal with graphite not only solves the safety issue but also reduces the cost. In the meantime, other anode candidates such as metals, alloys, and oxides were investigated [25-27].

Recently, to improve the performance of anode materials, graphene was designed with its features of higher surface area, better electronic mobility and mechanical properties [28, 29]. In addition, SnO_2 is proposed as another alternative because of its high theoretical capacity [30, 31]. However, due to the large volume expansion of SnO_2 during battery operation, it is important to use nanocrystal-sized and carbon-coated SnO_2 [32]. Zhang et al. reported that graphene-SnO_2-CNT mixture delivers the specific capacity of 635 mAh/g at 0.25 A/g [33]. Also, SnO_2 nanowires, SnO_2 on carbon nanosheets, and TiO_2 on graphene substrate have shown good performance as anode materials for LIB, probably due to the short diffusion paths for the Li^+ insertion into the structure [31-35]. Currently, the study of anode materials is very popular,

because the new anode materials have a much higher specific capacity than the common graphite.

2.2.2 Cathode materials

Since the first introduction of LIBs, different types of cathode materials have been introduced. An excellent material should have the following features to be used as cathode in the LIB applications: [1, 2]

1) High redox potential;
2) High reactivity with lithium reversibility;
3) High lithium ions hosting to deliver sufficient capacity;
4) High surface area to increase reduction/oxidation reaction rates;
5) High electronic conductivity to transfer electron rapidly and minimize heat generation;
6) High ionic conductivity to ensure small polarization and high capability;
7) Low volume structure changing during Li^+ insertion/extraction to ensure cycling stability;
8) Less expensive, environmentally benign and easy prepare processing.

The intercalation cathode materials of LIBs are mainly classified into three types of layered, spinel, and olivine by their crystal lattice types as shown in Figure 2-2, which will be explained below [36].

2.2.2.1 Layered

These types of materials usually have a stable 2-dimensional structure consisting of metal-oxygen octahedral, with Li taking the interstitial sites as illustrated in Figure 2-3. During the charge and discharge process, Li can be extracted from the structure (charge) and inserted back to the structure (discharge) without significantly changing the structure. Li ion can diffuse

through the octahedral sites in the lithium layer. Goodenough first proposed the use of layered $LiCoO_2$ as a cathode material in 1980 [37]. Ever since its first use in commercial LIBs by SONY Company in 1991, $LiCoO_2$ has been the most common cathode material for portable electronics.

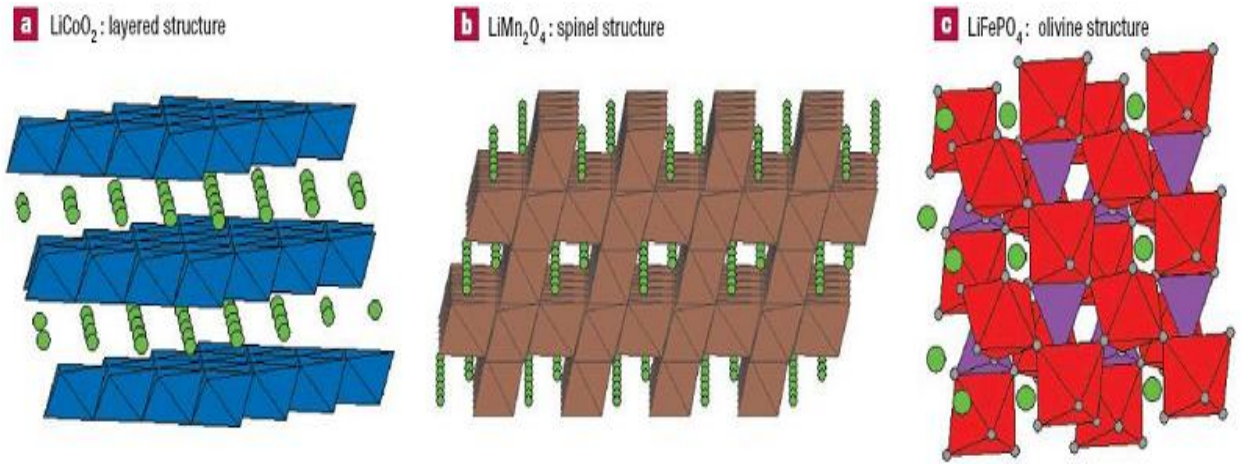

Figure 2-2: The crystal structure of (a) a layered type of $LiCoO_2$, (b) a spinel type of $LiMn_2O_4$, and (c) an olivine type of $LiFePO_4$. Li: green, Co: blue, Mn: brown, Fe: red, and P: purple [36]

Despite a high theoretical capacity of 274 mAh/g, the practical capacity of $LiCoO_2$ is about 130-150 mAh/g, with a working voltage of 3.5-4.2 V [38, 39]. Because in practice, only about 50% of the total Li can be reversibly intercalated and de-intercalated, extracting is limited to only 0.5 mol/mol of $LiCoO_2$. A change in the crystal structure occurs when more than half of the Li is removed, leading to irreversible capacity loss [38, 39]. Since cobalt is toxic and expensive, however, researchers are looking for other transition metals, which can replace Co. To solve these problems, many methods such as coating with metal oxide and, reducing the amount of Co have been investigated [3, 40]. $LiNiO_2$ has a layered structure and exhibits a higher practical capacity than $LiCoO_2$. In addition, nickel has lower toxicity and is less expensive than cobalt. However, $LiNiO_2$ has the drawbacks of fast capacity fading, synthesis difficulty, thermal instability, and poor safety [41, 42]. When Ga, In and Ti in $LiNi_{1-x}M_xO_2$ (M = Ga, In, Tl, and x =

0.010, 0.025 and 0.050) replace Ni, they all performed well. Among them, $LiNi_{1-x}Ga_xO_2$ with x =0.025 exhibits the best capacity (172.2 mAh/g) and relatively good cycling performance [43]. The $LiNi_{0.5}Mn_{0.5}O_2$ binary mix material and $LiCo_{1/3}Ni_{1/3}Mn_{1/3}O_2$ ternary mix material show good stability with reversible capacities of 200 mAh/g in the potential range of 2.5 to 4.5 V [44, 45]. However, less capacity fading was observed in mix materials compared with the single materials [46]. Layered $LiMnO_2$ appears to be a promising candidate because it is more environmentally benign and less costly than $LiCoO_2$ [47]. However, it suffers from structural change during charging/discharging process which results in capacity fading [48]. Also, it has poor performance in high temperature conditions. Coating with Al_2O_3, CoO or combinations of both in different proportions seems to improve the electrochemical performance of $LiMnO_2$, but it still has a low specific capacity and the problem of capacity diminishing [49].

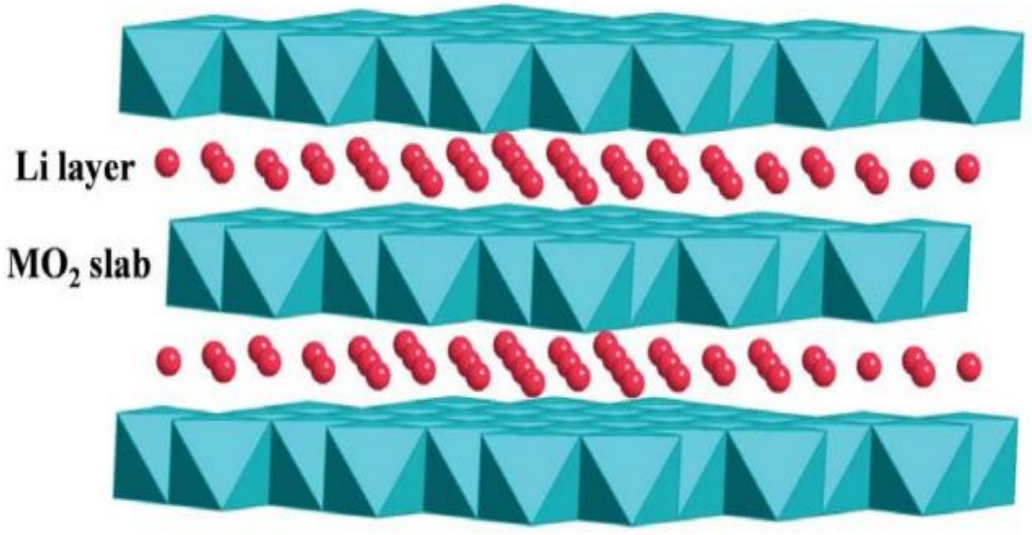

Figure 2-3: Crystal structure of layered $LiMO_2$ (Blue: transition metal ions such as Co, Ni, and Mn; Red: Li ions)

2.2.2.2 Spinel

These types of cathode materials usually have a 3-dimensional framework by edge sharing metal-oxygen octahedral, with Li taking the tetrahedral interstitial sites. This 3-dimensional style diffusion is expected to be more capable of high rate cycling than the 2-dimensional type as shown in Figure 2-4. Spinel $LiMn_2O_4$ material was originally introduced as cathode material with the theoretical capacity of 148 mAh/g [50]. The Mn ion with a potential of 4.1V provide high power capability and stability. In addition, it becomes attractive due to the low cost of Mn and being environmentally friendly compared to Co and Ni [51, 52]. However, $LiMn_2O_4$ material has problems with cycling and capacity fading, especially at elevated temperatures (55 ^oC) because of Mn dissolution in the $LiPF_6$ electrolyte that causes electrolyte decomposition and forms a non-active solid layer at the interface (SEI) between the electrolyte and the $LiMn_2O_4$ particles, resulting in degradation of charge capacity [53, 54]. However, some electrolyte modification and oxide coating significantly reduce the Mn dissolution [55].

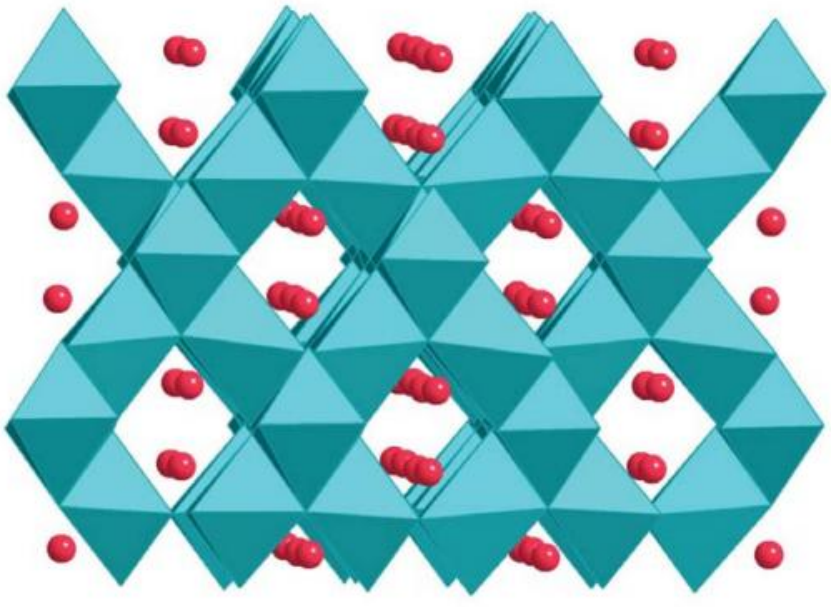

Figure 2-4: Crystal structure of spinel LiM_2O_4 (Blue: transition metal ions; Red: Li ions)

It has been reported that $LiNi_{0.5}Mn_{1.5}O_4$ can be an attractive cathode material because of its good cyclability and high potential of 4.7 V [56]. However, the synthesis of pure $LiNi_{0.5}Mn_{1.5}O_4$ material is difficult and also high working potential may cause the decomposition of electrolytes [56]. The coating with ZnO and $LiAl_xMn_{1-x}O_4$ was found also to improve electrochemical performance significantly [47]. Although $LiMn_2O_4$ is a promising cathode material with excellent electrochemical properties which can be improved, its discharge capacity is low due to its inherent structure. The partial replacement of metal cations to form the $LiMn_{2-x}M_xO_4$ solid solutions (M =Fe, Cu, Co^{3+}, Cr^{3+}, Zn^{2+}, Ni^{2+} and Mg^{2+}) enhance the structural stability with the capacities in the range of 100-110 mAh/g within the useful voltage below 4.4 V [57].

2.2.2.3 Olivine

Since Padhi et al. [4] introduced olivine-type $LiMPO_4$ (M= Fe, Co, Mn, or Ni) as cathode materials in LIBs, these kinds of compounds have been attracting much research and development interest. In phospho-olivines, which have an orthorhombic unit cell as shown in Figure 2-5 for the $LiFePO_4$, all of the oxygen ions form strong covalent bonds with P^{5+} to form PO_4^{3-} tetrahedral polyanion and stabilize the whole three dimensional framework [1]. Because of that, oxygen cannot be easily released, almost eliminating any threat of combustion or decomposing at high temperatures. Therefore, it guarantees superior thermal and chemical stability compared with other types of materials, encouraging the researcher to work on the olivine type cathode [58].

Among these olivine structures, $LiFePO_4$, with high theoretical capacity of around 170 mAh/g and operation potential of 3.45 V vs Li^+/Li, has been established as an attractive candidate for the next generation of cathode materials in LIBs [4, 59, 60]. $LiFePO_4$ has some advantages, such as excellent thermal stability, low cost, non-toxicity, abundance in nature, low capacity fading and

high cyclability [61]. In addition, the lower charging voltage (<4V) of the $LiFePO_4$ battery makes the material less reactive with electrolyte. The intercalation/de-intercalation of Li into the $LiFePO_4$ structure is almost 100% reversible.

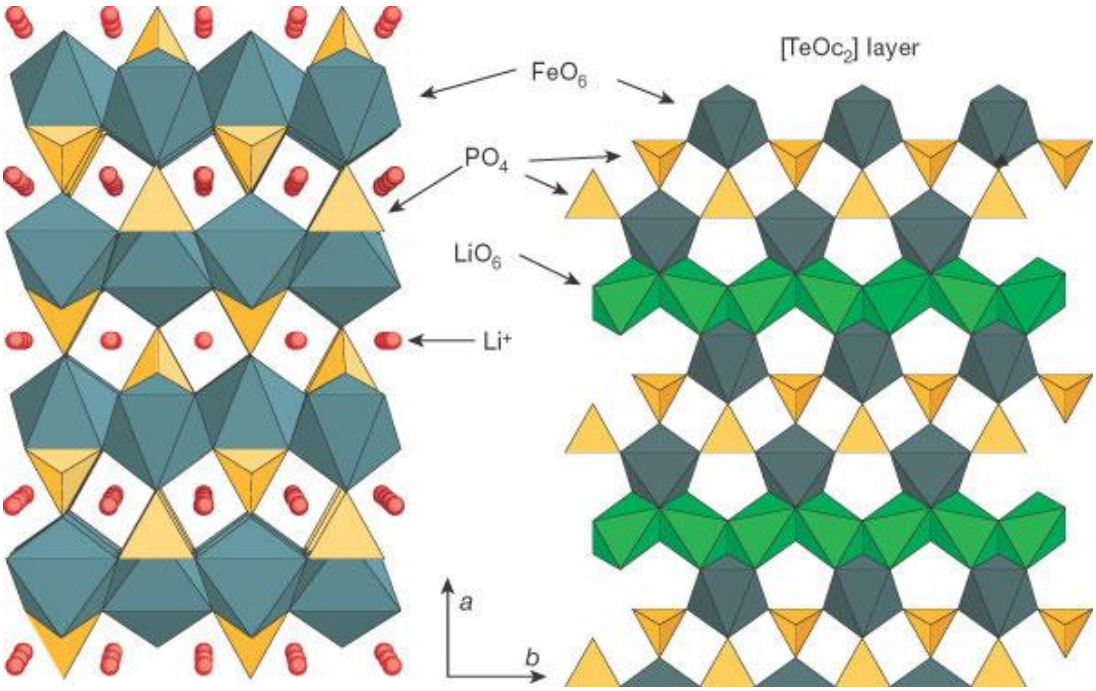

Figure 2-5: The crystal structure of olivine $LiFePO_4$ [1]

Other stable olivine phases with different transition metals are prepared such as $LiMnPO_4$, $LiNiPO_4$ and $LiCoPO_4$ [62-65]. $LiMnPO_4$ material with high operation potential of 4.1 V can be a remarkable choice due to the wide availability of Mn and its being inexpensive. However, after several investigations, the high performance was not observed. The conductivity of $LiMnPO_4$ material is lower than $LiFePO_4$, resulting in poor rate capability. Additionally, due to the low thermal stability and dissolution of Mn in the electrolyte, the capacity fading was observed for the $LiMnPO_4$ material [66]. $LiNiPO_4$ and $LiCoPO_4$ materials with olivine structure have the operation potential of 5.1 V and 4.8 V vs. Li/Li^+, respectively [63-65]. However, well-developed

electrolytes needed to be stable at these high potentials. Furthermore, the environmental concerns and increased cost the associated with Co and Ni have made their commercial application regrettable. However, mixed-metal phosphates have shown better performance than pure $LiMnPO_4$ or $LiCoPO_4$ [67].

Among all the cathode materials, $LiFePO_4$ obtains many superior features and has been considered as one of most promising substitution candidates of $LiCoO_2$. Therefore, in this work, $LiFePO_4$ will be considered as the main material. For comparison, some electrochemical parameters of the main cathode materials are listed in Table 2-1.

Table 2-1: Comparison of the main cathode materials (voltage and capacities)

Cathode	**Voltage (V)**	**Theoretical capacity (mAh/g)**	**Practical capacity (mAh/g)**
$LiCoO_2$	3.5-4.5	274	130-150
$LiMnO_2$	3	285	170-220
$LiNiO_2$	2.5-4.1	276	220
$LiMn_2O_4$	4	148	110-120
$LiFePO_4$	3.4-3.5	170	160

$LiFePO_4$ structure consists of PO_4 tetrahedra, distorted FeO_6 octahedra and LiO_6 octahedra as shown in Figure 2-5[1]. The Li ions, P atoms and Fe atoms occupy octahedral sites, tetrahedral sites and octahedral sites, respectively [68]. In $LiFePO_4$ structure, PO_4 tetrahedra share all their corners with the LiO_6 octahedra and FeO_6 octahedra share all their corners with the PO_4 tetrahedra. $LiFePO_4$ has an orthorhombic unit cell with space group Pmnb, accommodating four units of $LiFePO_4$. The oxygen ions form a hexagonal close-packed arrangement. The Li^+ ions

obtain one-dimensional channel in the structure for the diffusion of Li^+ that runs parallel to the planes of corner-sharing FeO_6 octahedra, along the [010] direction [69, 70]. Therefore, the Li^+ ions cannot jump from a channel to another channel, suggesting that any blockage in the channel will prevent the Li^+ ion movement [1].

The charge/discharge process of $LiFePO_4$ is based on the extraction/insertion reaction between the two phases of $LiFePO_4$ and the heterosite $FePO_4$ [4]. During the charge process, Li^+ is extracted from the olivine structure $LiFePO_4$ and converted to the heterosite structure $FePO_4$. During the discharge process, Li^+ inserts into the heterosite structure of $FePO_4$ and converts to the olivine structure $LiFePO_4$, as shown in Figure 2-6. These processes can be written as follows:

$$Li_xFePO_4 \rightarrow FePO_4 + xLi^+ + xe^- \qquad (\textbf{Charge Process})$$

$$FePO_4 + xLi^+ + xe^- \rightarrow Li_xFePO_4 \qquad (\textbf{Discharge Process})$$

However, pristine $LiFePO_4$ has the disadvantage of poor rate performances due to its weakness of diffusion limitation ($10^{-14}cm^2s^{-1}$) and low electrical conductivity (10^{-9} Scm^{-1}), limiting the powering performance of the batteries in the large devices. Basically, its poor electrical conductivity is the main problem preventing its use in commercial production. To overcome these barriers, various research groups have used different strategies, including particle size reduction, carbon coating and doping with elements [6, 17, 60, 71, 72].

A decrease in the grain size can obtain faster reactions because of easier diffusion of intercalation ions by decreasing the diffusion path, resulting in higher ion diffusion. However, using a smaller particle size needs to be considered carefully, since it has some disadvantages, such as poor thermal stability, a higher reactivity with electrolytes and increased solubility [17,

73]. The poor electrical conductivity of $LiFePO_4$ is overcome by coating the surface of the particles with conductive films of carbon or by grinding with carbon powder [7, 17, 18, 71]. In addition carbon coating could protect electrode materials from dissolution into the electrolyte, especially in case of nanostructure materials because of the large solid/liquid interface, indicating good cyclic stability [74]. However, large amount of coating reduces the capacity and volumetric energy. The volumetric capacity of the cell is difficult to increase because the addition of carbon decreases the particle density of the cathode material [75]. So the carbon coating must be optimized.

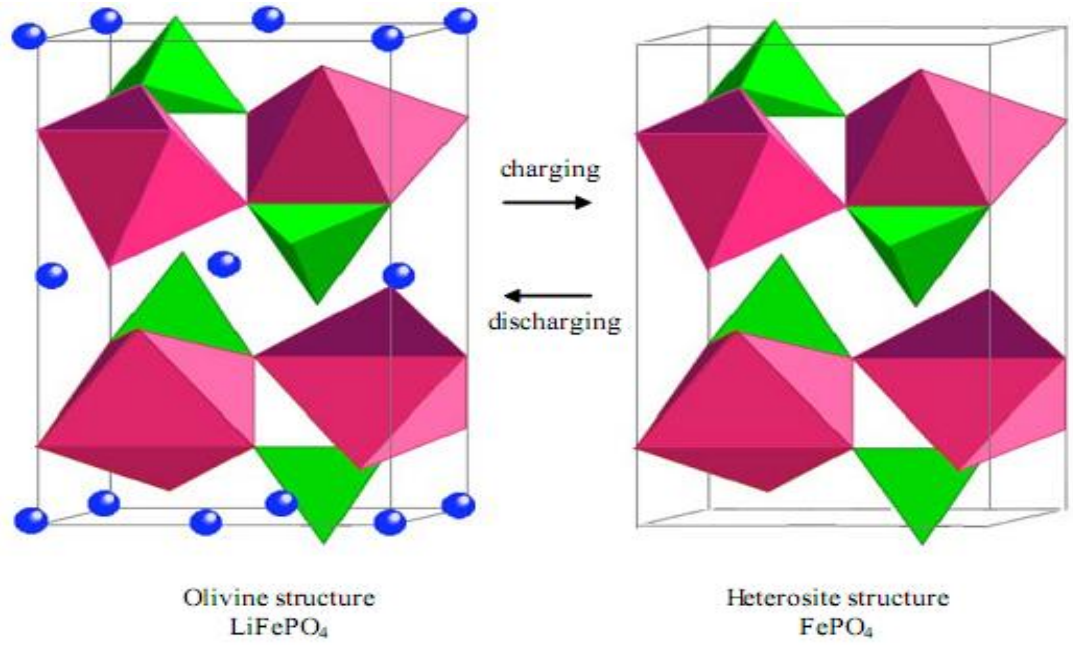

Figure 2-6: Crystal structures of $LiFePO_4$ (left) and $FePO_4$ (right) during the charge/discharge process

Both carbon content and particle size minimization must be optimized together. Because small particles have large surface area, they need a large amount of carbon to coat the particles. A large amount of carbon, however, decreases the energy density of the material [75]. Therefore, the amount of carbon and the size of the material must be carefully optimized. However, the low

diffusion and poor electrical conductivity of surface of $LiFePO_4$ can be solved by minimizing the particle size and adding conductive additives.

For nano structures, doping causes local disorder, which can be considered as defects of the structure. However, these defects may be able to facilitate the Li^+ ions intercalation capability of the compound due to the modified physical, chemical, and mechanical properties. In addition, doping agent can improve the electrical conductivity of bulk of $LiFePO_4$ material, as well as improving the ion diffusion. Doping in the host materials without a conductive coating, however, is not enough to improve the rate capacity and the charge/discharge performance. Thus, researchers usually have combined the elements of doping with carbon coating to increase the electrochemical performance of $LiFePO_4$.

There are mainly two different doping modes, at the M_1 (Lithium site) and M_2 (Iron site) sites. Doping at the M_1 site could cause the taking of the lithium vacancy to improve the electrochemical performance. However, in some cases, the presence of an unmoving dopant at the Li channel may probably block the diffusion of Li^+ ions [12]. Therefore, the doping at M_2 site could be an ideal and promising way to improve the electrochemical performance of $LiFePO_4$. In our research, metal doping will be carried out on the M_2 site.

Besides, in the earlier studies, synthetic $LiFePO_4$ was mainly produced using solid state methods [75-78]. The solid state synthesis method is currently the most effective method to expand to large scale industrialization. High temperature calcinations for long periods and high costs are, however, drawbacks of this method. There are several methods for preparing $LiFePO_4$ cathode materials to increase their ionic/electrical conductivity by the optimization and minimization of particles with suitable preparation procedures such as hydrothermal synthesis [12-14, 79-83], sol-gel [16-18, 84-91],co-precipitation [92, 93], microwave processes [94, 95], polyol process

[96, 97], molten salt synthesis [98], vapor deposition procedure [99], etc for particle morphological controls and to achieve fine particle size.

Large variations in the powder quality, the crystallinity, the morphology, the particle size, and the electrochemical performance of the material depend on the preparation methods and conditions [10]. The optimization conditions mainly focus on the development of homogeneous nanoparticles with controllability on particle size and high quality (thin and uniform) carbon coating [86].The sensitivity of Fe^{2+} ions in the $LiFePO_4$ preparation environment is very important [100, 101]. Improper preparation may lead to oxidation of Fe^{2+} to Fe^{3+}, leading to formation of impurity phases which reduces the electrochemical performance of battery. Although the attendance of sufficient amount of carbon is able to prevent the oxidation, the excessive carbon must be also avoided. Controlling the particle size can be done by cutting the synthesis time and temperature [77, 102].

Some researchers reported using surfactants such as the block co-polymer, sodium dodecyl sulphonate and poly methyl methacrylate to suppress particle growth during the synthesis procedure [8, 12, 103, 104]. However, the synthesis methods faced many obstacles from a laboratory process to large scale manufacture because of the complicated synthesis techniques, difficult-to-control synthesis situation and relatively high cost. Some methods were not useful for the large scale manufacture of $LiFePO_4$ cathode material such as microwave processes.

Among the methods of preparation, hydrothermal and sol-gel are simple, quick, easy, and cheaper methods to prepare $LiFePO_4$ materials. In addition, the products with these methods have higher uniformity, purity, a controllable shape and are suitable for the synthesis of multi-component material. Thus, these two methods are regarded as the best techniques to synthesize high quality $LiFePO_4$ materials which will be used in our work [15, 105, 106].

2.2.2.4 Literature review of $LiFePO_4$ doping

This work is mainly demonstrated with the cathode material, especially doped $LiFePO_4$ cathode material. Therefore, a supportive literature review related to doping of $LiFePO_4$ materials is presented as follows.

Jian et al. and others [107-110] studied the structure and electrochemical behavior of $LiFePO_4$ modified with vanadium. Vanadium can be embedded into the olivine structure on the phosphorus site, not on the iron site, with the unit cell decreasing in size when the presence of vanadium increases. They mentioned that the 5% vanadium doping has the highest electrical and ionic conductivities in comparison to others. Their results showed that the electrochemical reaction of $LiFePO_4$ became more reversible and easier to occur because vanadium doping increases the stable cycle life at a higher current rate.

Yen et al. [109] synthesized $Li_{1-x}Na_xFePO_4/C$ (x = 0, 0.01, 0.03, 0.05) by the carbonthermal reduction method and investigated the effect of doping. They indicated that doping Na does not destroy the lattice structure of $LiFePO_4$ when making the lattice volume bigger. Electrochemical test results showed that the $Li_{0.97}Na_{0.03}FePO_4/C$ sample exhibits the best electrochemical performance with an initial special discharge capacity of 158, 151, 142, 134, and 105 mAh/g when discharged at the rate of 0.1 C, 0.5 C, 1 C, 2 C, and 3 C, respectively. It may be attributed to its larger lattice parameters in *a* and *c* than those of other samples prepared in their study.

Jiao et al. [111] prepared a series of Mo-doped $LiFe_{1-3x}Mo_xPO_4/C$ (x = 0.000, 0.025, 0.050, 0.100, 0.150) cathode materials by sol-gel method. They indicate that the a and b unit cell parameters and cell volumes of crystal decrease slightly with increasing the amount of Mo. This may be due to the ionic radius of Mo^{6+} which is a little smaller than that of Fe^{2+}. In addition, with the increase in Mo doping, the P–O bonds become stronger enhancing the stability of PO_4 and

with the lengthening of Li–O bond, the Li^+ ions diffusion rate during the charge/discharge process is facilitated. Among the samples, $LiFe_{0.925}Mo_{0.02}5PO_4/C$ sample has shown the best electrochemical performance, with the discharge capacity of 162.3 mAh/g at 0.1 C rate. However, by increasing the amount of Mo, high polarization and large particles sizes reduce the Li^+ ion diffusion coefficient and poor electrochemical results are obtained. It is observed that proper Mo doping remarkably enhances the Li^+ ion diffusion coefficient by four orders of magnitudes in the doped materials compared with the undoped one which means excellent electrochemical performance.

Zhang et al. [112] synthesized $Li_{0.99}Mo_{0.01}FePO_4/C$ cathode material by an easy solution method followed by heat treatment at various temperatures. Their results showed that the mix doping method does not affect the olivine structure of cathode but largely improves its capacity and cycle performance. They indicated initial specific discharge capacities of 161 and 124 mAh/g with rates of 0.2 C and 2 C, respectively, which attribute the enhancement of the electrical conductivity to ion doping and carbon coating. The lower electrochemical polarization of the doped sample suggests that the increasing conductivity is induced by the doping method.

Hu et al. [113] synthesized a single phase of $Li_{l-4x}Ti_xFePO_4/C$ (x=0, 0.005, 0.010, 0.015) cathode materials using the solid state method. Their XRD results showed that doping at a low concentration Ti^{4+} does not affect the structure of the samples, but the electrochemical performance of the doped samples is better than the un-doped ones when the concentration of doping is less than 1.5%. A greater amount of Ti^{4+} doping on Li^+ sites may block the diffusion of lithium ion, because the diffusion coefficient of lithium is fast only in the tunnel c-axis [114].

Wang and co-workers [115] prepared Ti-incorporated $LiFe_{1-x}Ti_xPO_4$ (x= 0, 0.01, 0.03, 0.05, 0.07, 0.1, 0.15, 0.2) cathode materials via a two step solid-state reaction method. Their results

confirm that materials with doping amount of $x \leq 0.05$ obtain a single phase while those with higher amount of doping contain impurity phases such as $LiTi_2(PO_4)_3$ and TiP_2O_7. The initial discharge capacities of the $LiFe_{1-x}Ti_xPO_4$ (x= 0, 0.01, 0.03, 0.05, 0.07, 0.1, 0.15, 0.2) samples at 0.1 C are 134, 140, 144, 152, 147, 149, 142 and 143 mAh/g, respectively. Among the samples, $LiFe_{0.95}Ti_{0.05}PO_4/C$ shows the highest discharge capacity. The Ti incorporation causes lengthening of the Li–O bond and facilitates the insertion/de-insertion of the Li^+ ions. Appropriate amount of titanium doping is favorable for the enhancement in electrochemical performance of $LiFePO_4$ material.

Huang et al. [116] synthesized carbon coated $Li_{1+x}FePO_4$ (x = 0, 0.01, 0.02, 0.03, 0.04) and doped compositions of $Li_{1.03}Fe_{0.99}Ti_{0.01}PO_4$ by the thermal reduction method. Although the thermal reduction method could be used to synthesize $LiFePO_4$ cathode materials, the main disadvantage of this method is that the particle size is larger and its electrochemical properties are not as good. In addition, this method requires a high temperature (about 70°C), which can increase the possibility of grain growth that can decrease the electrochemical properties of the $LiFePO_4$ cathode material. Their results indicated that increasing the content in $Li_{1+x}FePO_4$ gives better electrochemical properties and cyclic performances until x=0.03, where $Li_{1.03}Fe_{0.9}Ti_{0.01}PO_4$ performs better in comparison to other samples under the 1 C rate. This sample showed a trend of increased capacity and reached the highest discharging rate capacity of 156 mAh/g at 60 cycles when the $Li_{1.03}Fe_{0.9}Ti_{0.01}PO_4/C$ sample cycled before 60 times. The initial charge/discharge capacity of the $Li_{1+x}FePO_4/C$ (x = 0, 0.1, 0.2, 0.3, 0.4) samples at room temperature, respectively, are 112, 119, 128, 129 and 109 mAh/g, which has a similar change law with the particle size of samples. Their results suggested that particle size has a strong dependence on the electrochemical properties of positive active material. Li_3PO_4 and $Li_4P_2O_7$ are

types of conductive impurity. It can exist on the particle surface or interior and form a conductive layer improving the electronic and Li ion conductivity of samples. The impurity Li_3PO_4, however, can prevent the growth of the $LiFePO_4$ particle during the sintered process. Also, the layer of Li_3PO_4 can reduce the direct contact of active material with the electrolyte and avoid corrosion from the electrolyte that results in enhancing the cyclic performances of positive active material. The $LiFePO_4$ sample has a better rate capability and cycling life attributed to the small particle distribution, as well as improved electronic conductivity.

The reason for increasing the electrochemical performance of $LiFePO_4$ is that Ti doping with a small degradation of overall capacity can turn a relatively small amount of Li^+ into vacancies at the Li site. Secondly, the synergetic effect of the super valency of the doped sample will make a longer Li–O bond of the olivine structure. The longer Li–O bond is the smaller binding energy as a result of the easy migration of Li^+ due to the reduction of the energy barrier [117]. These vacancies change the structure of the ion transport route and reduce the energy barrier that can lead to an increase in the Li^+ mobility in the olivine structure so as to enhance the ionic conductivity.

Wu et al. [118] synthesized $LiFePO_4$ and Ti^{4+} doped $LiFe_{1-x}Ti_xPO_4$ ($0.01 \leq x \leq 0.09$) powder material by a solution method followed by heat treatment at 700 °C for 8 h under N_2 flowing atmosphere. Among the prepared powders, $LiFe_{0.97}Ti_{0.03}PO_4$ showed the most promising cycling performance with a specific discharge capacity of 135, 127, 116, 107, and 81 mAh/g at the rate of 0.1C, 0.2C, 0.5C, 1C, and 3C, respectively. From their results for prepared samples, the doped Ti^{4+} ions did not occupy the Fe^{2+} sites. However, the occupancy of the doped Ti^{4+} ions was still not clear, and theoretical calculations are needed for more understanding. The $LiFe_{0.97}Ti_{0.03}PO_4$ sample heat treated at 700 °C for 8 hours showed the highest discharge capacity

of 135 mAh/g among the prepared $LiFe_{1-x}Ti_xPO_4$ ($0 \leq x \leq 0.09$) samples at the 0.1C rate. Doping Ti^{4+} maybe cause to occupy Li^+ sites because the cation radiometry of lithium (Li^+=68 pm) is close to that of titanium (Ti^{4+}=64 pm). The discharge capacities of $LiFePO_4$/C, $Li_{0.98}Ti_{0.005}FePO_4$/C, $Li_{0.96}Ti_{0.01}FePO_4$/C and $Li_{0.94}Ti_{0.015}FePO_4$/C cathode obtained the initial discharge capacity of 128.4, 139.5, 146.7 and 99.5 mAh/g, respectively. They noted that the charge transfer resistance of the samples could be decreased greatly by doping an appropriate amount of Ti^{4+} which indicates by electrochemical impedance the spectroscopy result. Yaoqin et al. [85] synthesized $LiFePO_4$, $Li_{0.98}Mg_{0.01}FePO_4$ and $Li_{0.96}Ti_{0.01}FePO_4$ by the sol-gel method and using a variety of processing conditions. For comparison, $LiFePO_4$was also synthesized from iron acetate by a solid state method. They suggested that the inherent electrical conductivity of these materials is not significantly better than un-doped $LiFePO_4$.

Arumugam et al. [119] synthesized nano crystalline of $LiFePO_4$ and $LiMg_{0.05}Fe_{0.95}PO_4$ cathode materials using the sol-gel method in an argon atmosphere by using succinic acid as a chelating agent. $LiMg_{0.05}Fe_{0.95}PO_4$ exhibits the initial charge and discharge capacities of 159 and 141 mAh/g at the 0.2 C rate, respectively, as compared to 121 and 107 mAh/g for bare $LiFePO_4$. Furthermore, $LiMg_{0.05}Fe_{0.95}PO_4$ retained more than 89% of the capacity even after 60 cycles. Hence, $LiMg_{0.05}Fe_{0.95}PO_4$ is a promising cathode material for rechargeable lithium ion batteries.

Liu and coworkers [120] prepared the spherical $LiFePO_4$/C and $LiFe_{0.9}Mg_{0.1}PO_4$/C powders from spherical $FePO_4$ by a simple uniform phase precipitation method at normal pressure, using $FeCl_3$ and H_3PO_4 as the reactants. The excellent specific capacities of 148 and 157 mAh/g with a rate of 0.1 C achieved for the $LiFePO_4$/C and $LiFe_{0.9}Mg_{0.1}PO_4$/C, respectively.$LiFe_{0.9}Mg_{0.1}PO_4$/C exhibits a better high rate and cycle performances than the undoped $LiFePO_4$/C. The tap density of $LiFePO_4$ powder is usually 1.0-1.3 g/cm, which is much lower than the tap density of

commercially used $LiCoO_2$ (2.3-2.5 g/cm). The low tap density of $LiFePO_4$ limits the energy density of lithium ion batteries. The powders composed of spherical particles have a higher density than the powders composed of irregular particles. Therefore, to obtain a high tap density of $LiFePO_4$ powder, preparing spherical powders is expected as an effective way. The tap density of the spherical $LiFePO_4$/C and $LiFe_{0.9}Mg_{0.1}PO_4$/C powders are 1.75 and 1.77 g/cm, respectively, which are remarkably higher than the non-spherical $LiFePO_4$ powders (the tap-density is 1.0-1.3 g/cm). The $LiFePO_4$/C and $LiFe_{0.9}Mg_{0.1}PO_4$/C demonstrated discharge capacities of 110 and 120 mAh/g at the 1C rate, respectively.

$Li_{1-x}Mg_xFePO_4$ (x= 0.00, 0.02) synthesized from LiOH, H_3PO_4, $FeSO_4$ and $MgSO_4$ by the hydrothermal method at 180 °C for 6 h and heat treatment at 750 °C for 6 h. The carbon coated composites of both the doped and undoped sample show discharge capacities of 146 mAh/g and 144 mAh/g at the 0.2 C rate, 140 mAh/g and 138 mAh/g at the 1 C rate, 124 mAh/g and 123 mAh/g at the 5 C rate, respectively [15].

Wang and co-workers [121] prepared samples of $LiFe_{0.9}M_{0.1}PO_4$ (M=Ni, Co, Mg) by solid state reactions. $LiFePO_4$ doped materials showed improvement in performance and cyclic stability. The capacities of $LiFe_{0.9}M_{0.1}PO_4$ (M=Ni, Co, Mg) reached 81.7, 90.4 and 88.7 mAh/g at the 10 C rate, respectively, in comparison with 53.7 mAh/g for undoped $LiFePO_4$ and 54.8 mAh/g for carbon-coated $LiFePO_4$ ($LiFePO_4$/C). The capacity retention is 95% after 100 cycles for doped samples and this value is only 70% for $LiFePO_4$ and $LiFePO_4$/C. It illustrated that the capacities for $LiFe_{0.9}M_{0.1}PO_4$ (M=Ni, Co, Mg) are around 140 mAh/g under 0.2 C and 82, 90 or 89 mAh/g under 10 C, respectively.

Chen et al. [122] synthesized a series of olivine $LiFe_{1-x}Co_xPO_4$ (X=0, 0.25, 0.5, 1) composites by a hydrothermal method under reductive atmosphere. The XRD result shows that the lattice

parameters and unit cell volume of samples reduce a little with increasing the amount of Co doping. This result can be related to the small ionic radius of Co^{2+} (0.75Å) in comparison with the Fe^{2+} (0.78Å). $LiFePO_4$ exhibits a discharge capacity around 150 mAh/g in 0.1C rate with voltage plateau around 3.4V, whereas $LiCoPO_4$/C only delivers a discharge capacity of 93 mAh/g with a small voltage plateau around 4.5V. Among the doped samples, the $LiFe_{3/4}Co_{1/4}PO_4$/C sample shows high discharge capacity around 170 mAh/g at 0.1C rate, which is close to the theoretical capacity of $LiFePO_4$. In addition, $LiFe_{3/4}Co_{1/4}PO_4$/C sample obtains a higher discharge voltage plateau around 3.5V which is higher than the voltage plateau of pure $LiFePO_4$ sample. However, other investigation reported that low amount of Co doping did not increase the redox potential [123]. Therefore, high amount of cobalt doping is essential to enhancing the voltage plateau of $LiFePO_4$.

Hsu and co-workers [124] synthesized $Li_{0.99}Al_{0.01}FePO_4$/C composite particles by the sol-gel process. They found that the electrochemical properties of the synthesized $Li_{0.99}Al_{0.01}FePO_4$/C composite improved because of its small grain size and good electronic conductivity. They concluded that increasing the sintering time leads to a decrease in the conductivity of the $Li_{0.99}Al_{0.01}FePO_4$/C composite powders because the carbon content is too low to form a conductive network when the sintering time is higher than 3 h. The electrical conductivity of the $Li_{0.99}Al_{0.01}FePO_4$/C composites is greatly improved, reaching a value of 8×10^{-2} S/cm at room temperature.

Liu [125] prepared 1.5%, 2.5%, and 5% ZnO-doped $LiFePO_4$ to improve the electrochemical performance of cathode material. Their results showed that 2.5% ZnO-doped $LiFePO_4$ has higher electrochemical reactivity for lithium insertion and extraction than the rest of the samples. The results indicated that the zinc atoms prevent the collapse of the $LiFePO_4$ lattice structure. Also,

during the lithium ion intercalation and de-intercalation processes, the doped zinc atoms protect the $LiFePO_4$ crystal from shrinking and it can provide more space for the movement of lithium ions. Consequently, it causes increasing in the conductivity and the lithium ion diffusion coefficient after doping. The initial specific discharge capacity for the 2.5% ZnO-doped $LiFePO_4$ sample is about 167 mAh/g after 150 cycles.

Liu et al. [126] reported Zn-doped $LiFePO_4$ material forming homogeneous $LiZn_{0.01}Fe_{0.99}PO_4$ for the first time. The Zn doping does not destroy the lattice structure of $LiFePO_4$ because of the low doping concentration. On the other hand, the distortion of the lattice is negligible because of the almost similar ion radius of Zn^{2+} (radius=0.083 nm) and Fe^{2+}. They showed that after doping the charge capacity increases from 100 to 163 mAh/g, and the discharge capacity from 88 to 133 mAh/g. The Zn doping contributes the formation of a crystal structure, expands the lattice volume and provides more space for lithium ion intercalation/de-intercalation. In addition, the doping improves the reversibility of lithium intercalation and de-intercalation, decreases the charge transfer resistance and increases the diffusion of lithium ions due to the effect of the doped Zn atoms. As a result, zinc doping is very promising for the improvement of the electrochemical performance of $LiFePO_4$. Both discharge capacity and rate capability are greatly improved. In the same way, another report shows the improvement of electrochemical properties of ZnO-doped $LiFePO_4$ materials prepared with hydrothermal method. Because ZnO doping reduces the size of particles, Li^+ migration path becomes shorter, and the crystal lattice is expanded which facilitate Li^+ ion intercalate/de-intercalate during process [127].

Zhao et al. [128] synthesized $LiFe_{1-x}Nd_xPO_4/C$ (x = 0, 0.01, 0.02, 0.04, 0.06, 0.08) cathode materials by solid-state reaction method and they optimized the synthesis condition by thermal analysis and magnetic properties to obtain the pure phase of $LiFePO_4$ material. They indicate that

the sample calcined at 700 ^{o}C contains less impurity phase than the sample calcined at 750 ^{o}C. The result shows that the small amount of Nd^{3+} ion doped does not affect the structure of $LiFePO_4$ material, but the size of particles reduce from 400 nm to 150 nm after doping. Among the doped samples, $LiFe_{0.4}Nd_{0.6}PO_4/C$ sample exhibits the best discharge capacity of 165 mAh/g at 0.2C rate because it exhibits smaller particle sizes and it allows higher lithium ion diffusion. However, the discharge capacity decreases when the amount of doping is increased up to 8%. Therefore, the optimized amount of Neodymium doping could improve the electrochemical performance of $LiFePO_4$ materials.

Croce and co-workers [84] suggested improving the electrochemical kinetics of the $LiFePO_4$ electrode by the sol-gel synthesis method based on a critical step involving the dispersion of metal (copper or silver) at a very low concentration (1wt%). This metal addition does not affect the structure of cathode, but it seems to prefer the growth of small size particles and decrease the inter-particle resistance. So, it can improve the capacity and life cycle. They showed that increasing the capacity from the standard to the modified electrode is clearly a change from 120 to 145 mAh/g. Their results indicated that the electrode response of the $LiFePO_4$ electrode may be enhanced by the addition of dispersed metal powders during the synthesis procedure.

Yang and co-workers [129] synthesized Cu doped $LiFePO_4$ material by the co-precipitation method, followed by sintering at high temperature for crystallization. They indicated that the unit cell parameter and unit cell volume of $LiFePO_4$ doped by 1% Cu^{2+} has changed clearly where the length of a-axis, b-axis, c-axis, and unit cell volume are all decreased. They showed that, compared with the pure $LiFePO_4$, the unit cell parameter and unit cell volumes of $Li_{0.98}Cu_{0.01}FePO_4$ have both shrunk. The reason is that the ion radius of Cu^{2+} is 0.073 nm and smaller than 0.076 nm, that of Li^{+}, and it caused a decrease in the length of the c-axis. Another

reason is that the binding force between Cu^{2+} and O^{2-} is larger than that between Li^{+} and O^{2-} and the unit cell volume of $Li_{0.98}Cu_{0.01}FePO_4$ shrank. The Cu-doped $LiFePO_4$ demonstrated a better electrochemical property in terms of delivery capacity, cycle performance, and electrochemical properties, which is related to the enhancement of the electrical conductivity by ion dopant, compared with undoped $LiFePO_4$. The small size of $Li_{0.98}Cu_{0.01}FePO_4$ material may allow the intercalation and de-intercalation of Li^{+} ions to occur easily during the charge/discharge processes and exhibit high discharge capacity and good reversibility.

Heo and co-workers [130] synthesized carbon $LiFePO_4$, $Li_{1.05}FePO_4$, $LiFe_{0.997}Cu_{0.003}PO_4$, and $Li_{1.05}Fe_{0.997}Cu_{0.003}PO_4$ materials at 660 °C in Ar atmosphere using a solid state method. They indicated that the replacement of Li and Cu metal ions in the $LiFePO_4$ structure resulted in a small change in the powder morphology, which improved the electric conductivity and battery performance of the $LiFePO_4$ electrode. Among the samples, the $Li_{1.05}Fe_{0.997}Cu_{0.003}PO_4$ showed the highest discharge capacity of 145 mAh/g and an excellent cycle retention rate over 90% after 30 cycles. They suggested that this material can be prepared easily without any additional treatment for improving cycle performance, such as carbon coating and ball milling.

Chang et al. [131] prepared $LiFe_{1-x}Cu_xPO_4/C$ (x = 0, 0.01, 0.015, 0.02, 0.025) cathode materials with a high tap density using a solid state method at high temperature reaction in an inert atmosphere by using $Cu(Ac)_2$ as a dopant and $FePO_4$ as a precursor. They showed that the cathode material has excellent charge/discharge capacities, about 150 mAh/g and 297 mAh/cm at a rate of 0.1C and more than 127 mAh/g and 252 mAh/cm at a rate of 2C. They indicated from the SEM results that Cu-doped $LiFePO_4$ plays an important role in the particle growth of $LiFePO_4$ particles during the synthesis process. Also, they mentioned that the smaller size of the

particle can expand contact between the electrolyte solution and sample surface, decreasing the transmission way in the solid phase, improving the insertion and extraction of Li ions.

Shin and co-workers [132] prepared the carbon coat of $LiFePO_4$ and doped particles with Cr using a mechanochemical process. They suggested that improving performance can be done by chromium doping, which facilitates the phase transformation between triphylite and heterosite during cycling, and increases conductivity by carbon coating. From their results, the $LiFe_{0.97}Cr_{0.03}PO_4/C$ showed excellent rate performance and obtained the discharge capacity of 120 mAh/g at the 10 C rate. The capacity delivered in the first discharge at 0.1 C is 127 mAh/g and it decreased to 118 mAh/g in the subsequent four cycles when using bare $LiFePO_4$.

Kang et al. [133] synthesized $LiFePO_4$ and $LiFe_{0.97}Sn_{0.03}PO_4$ cathode materials by a simplified sol-gel method for the first time. Their results show that the Sn doping reduces the size of particles with uniform distribution and increases the electrical conductivity of material. The smaller particles with uniformly distribution could offset the barrier to the sluggish charge transport of phosphate [5]. In addition, Sn doping expands Li–O bond length with lower energy barrier and facilitates the Li^+ intercalation/de-intercalation, resulting in the improvement of the electrochemical properties of $LiFePO_4$, especially the high-rate charge/discharge performance. $LiFe_{0.97}Sn_{0.03}PO_4$ sample delivers specific capacity of 158, 154, 146 and 128 mAh/g at 0.5C, 1C, 5C and 10C, respectively, in comparison with 147, 134, 119 and 107 mAh/g for $LiFePO_4$. Moreover, the doping of Sn does not influence the cycle capability, even at 10 C [133].

Liu and co-workers [134] synthesized a series of cation doped $Li_{1-x}M_{0.01}Fe_{0.99}PO_4/C$ composites (M=Ti, Zr, V, Nb, and W) by the solid state reaction method. After doping, the lattice structure of $LiFePO_4$ is not destroyed and the reversibility of lithium ion intercalation and de-intercalation is improved. They mentioned that the diffusion coefficient of lithium ions depends on the radius

of the heteroatoms. As the radius of the heteroatom is larger, the diffusion coefficient increases. However, only when the radius of the doped heteroatom is bigger than or equal to Fe^{3+}, the diffusion behavior can be improved. The heteroatom doping enlarges the volume of the crystal lattice, making the redox reversibility easier for the de-intercalation and intercalation of lithium ions. It may, however, block the ion diffusion channel.

Wang and co-workers [135] prepared Ru-doped $LiFePO_4$/C cathode materials by a simple rheological phase reaction method. Their results indicated that the Ru-doped $LiFePO_4$/C materials exhibit a discharge capacity of 101 mAh/g at 5C for a current and stable cycle life. Their results can be explained by the small shrinkage of the lattice of $LiFePO_4$ after Ru doping, because the diameter of Ru^{3+} is smaller than Fe^{2+}. In the undoped $LiFePO_4$/C, the cell volume decreases as Fe^{2+} is oxidized to Fe^{3+} during de-intercalation of Li^+ because the diameter of Fe^{3+} is smaller than Fe^{2+}. It found that when the doping amount of Ru is too high, the lattice structure of $LiFePO_4$ changed too much and the electrochemical performance was very poor. They showed that the Ru-doped $LiFePO_4$/C materials have a more stable lattice structure, increase the conductivity and diffusion coefficient of Li^+ where Ru^{3+} acts as a pillar in the lattice structure to prevent the collapse of crystal during cycling.

Luo et al. [136] synthesized a series of samples of lanthanum doped $Li_{1-x}La_xFePO_4$ (x=0.0025, 0.005, 0.0075, 0.01) using the solid state method. The effect of La showed that doping reduced crystal size to nano materials, increased conductivity and enhanced the diffusion rate of lithium ion. The lattice volume of La doped $Li_{1-x}La_xFePO_4$ are larger than the pure $LiFePO_4$. The lattice volume values increase with the increasing La doping amount, which makes it easier for Li^+ to insert and de-insert into doped materials. The optimum material with $Li_{0.99}La_{0.01}FePO_4$ cathode showed a relatively high capacity of 123 mAh/g or close to 73% of the theoretical capacity for

the 0.5C discharge rate, which indicated a superior cycle capacity value and long term stability characteristics compared to other cells at ambient temperature. The roles of doping include decreasing the particle size, increasing electrical conductivity and affecting charge and mass transfer resistances of cells.

Li and co-workers [7] prepared carbon-coated $Li_{1-x}La_xFePO_4$(x=0.005, 0.01, 0.015, 0.02, 0.025) by a microwave assisted, room temperature, solid state method. The lanthanum doping does not collapse the lattice structure of $LiFePO_4$ due to the low doping content of lanthanum. Their results for electrochemical measurements indicated that the carbon coating and lanthanum doping with small and uniform particles (25-50 nm) provided an initial discharge capacity of 145 mAh/g with an excellent rate capacity and long cycling stability when the amount of lanthanum is x=0.02. The sample achieves the best cycling performance, which make it attractive for large scale applications.

Choet al. [137] synthesized $LiFePO_4$ cathode materials with carbon coating and La doping by a high temperature solid state method. The mixtures were milled in an inert atmosphere to avoid the oxidation of Fe^{2+} to Fe^{3+} in a planet mixer for 3 h. Their results indicated that the La-ion dopants do not affect the structure of the material, but they improve its rate capacity performance and cyclic stability. Among the materials, the $LiFe_{0.99}La_{0.01}PO_4$/C composite presents the best electrochemical behavior, having a discharge capacity of 156 mAh/g between 2.8 and 4.0 V at 0.2 C compared to 104 mAh/g for undoped $LiFePO_4$. They mention the exceptional thermal stability, which is attributed to good anion bonding and the stability of phosphate materials with its shorter P–O bond and more strongly bound oxygen. The excellent safety performance of the olivine structure could allow LIBs to move the traditional low rate markets more to high rate strong systems.

Using a solution method, Rong and coworkers [117] synthesized $LiFe_{0.95}M_{0.05}PO_4$ by doping with ($M=Mg^{2+}$,Ni^{2+},Al^{3+} and V^{3+}) ion, which has an atomic radius similar or smaller than the Fe^{2+} ion. They showed that the effect of the cation and larger atomic size of the doping element causes the lattice expansion and Li–O bond lengthening of the olivine structure. The lengthening and weakening of the Li–O bond will be useful to the electrochemical performance of cathode materials especially under the high C rate. Hence, the $LiFe_{0.95}V_{0.05}PO_4$ powder with the largest volume of unit cells (longest Li–O bond length) recorded the highest discharging capacity of 152 and 136 mAh/g at 0.1C and 1C rates, respectively. They concluded that the samples with a doping element of higher valency demonstrated a higher specific discharge capacity, especially when a high C rate charge/discharge is carried out.

Up to now, most of interests have examined the cation doping. However, anion doping has recently become important for the $LiFePO_4$ material. Zhou and co-workers [138] synthesized F-doped $LiFePO_4$/C nanoparticles via a low-temperature hydrothermal method followed by heat treatment. The F-doped $LiFePO_4$/C sample shows a high discharge capacity of 165.6 mAh/g, in contrast, $LiFePO_4$/C sample delivers a discharge capacity of 153.4 mAh/g. Their result indicate that the F doping increases the conductivity of $LiFePO_4$/C and facilitates the Li^+ ion diffusion. Introduction of F into the structure has caused the weakness of Li–O bonds to improve Li^+ ion diffusion and also reduction in the length of P–O bonds, implying higher stability for the $LiFePO_4$ structure [138].

Liao et al. [139] synthesized a series of F-substituted $LiFe(PO_4)_{1-x}F_{3x}$/C (x = 0.025, 0.05, 0.1) cathode materials by adding LiF and studied the effects of fluorine substitution on the electrochemical properties of $LiFePO_4$/C. The results of electrochemical measurement showed that F-substitution can improve the rate capability of these cathode materials. The

$LiFe(PO_4)_{0.9}F_{0.3}$/C sample showed the best performance, with a discharge capacity of 110 mAh/g at 10C rate and a discharge voltage of 3.0-3.3V. The $LiFe(PO_4)_{0.9}F_{0.3}$/C sample also indicated a better cycling life at high temperature than the other samples. The $LiFe(PO_4)_{0.9}F_{0.3}$/C sample delivered a lower discharge capacity of 151.6 mAh/g compared to 159.4, 163.88 and 157.9 mAh/g for $LiFe(PO_4)_{1-x}F_{3x}$/C (x = 0.025, 0.05, 0), respectively. Another group synthesized anion Cl-doped $LiFePO_4$/C cathode materials via a carbothermal reduction route [140]. Cl-doping also improves the electrical conductivity and Li^+ ions diffusion in the bulk of $LiFePO_4$ in the same way as F-doping. The pristine $LiFePO_4$/C delivers a discharge capacity of 132.1 mAh/g; in contrast, Cl-doped $LiFePO_4$/C presents a discharge capacity of 162 mAh/g.

In addition, it is worth noting that the coating of conductive carbon on the surface of $LiFePO_4$ crystals can reduce the contact resistance between particles and markedly increase the apparent diffusion coefficient of Li^+ by at least one order of magnitude in comparison with that of $LiFePO_4$ without carbon coating and, thus, also enhance significantly the electrical conductivity of the composites [141, 142]. Recent reviews [9-11, 143-149] summarized the material processing techniques, material doping and coating, particle size optimizing and other parameters, which applied to the fabrication of LIBs and their components.

Most of the cathode materials are transition metal oxides, which have poor electrical conductivity. This may in some systems limit the current density on the cathode. Therefore, improving the electrical conducting of the cathode is very important for improving the cycling rate of LIBs. The Li diffusion on the cathode side is believed to be the rate limit step in most cases. Improving both the ionic and electrical conduction of the cathode is the key to developing high rate LIBs.

In conclusion, despite the quantity of doping elements used to improve the performances of the $LiFePO_4$/C cathode materials, there is no commercial Li-ion battery based on metal doped $LiFePO_4$/C cathode materials. The fundamental reasons of the effect of the metal doping on the performance of the $LiFePO_4$/C cathodes are not elucidated. Furthermore, how the method of preparation may impact the effect of the doping element on the cathode performance is not well understood.

2.3 Objectives

The main objective of this work is to determine and optimize experimental conditions to prepare high performance $LiFePO_4$ doped with noble metals as cathode material for LIBs applications. This has never been done before.

To support the main objective, the following specific objectives must be accomplished:

(1) Synthesis of $LiFePO_4$ cathode materials via sol-gel and hydrothermal methods.

(2) Carbon coating optimization of $LiFePO_4$ material to obtain high performance $LiFePO_4$/C material.

(3) Synthesis of palladium doped $LiFePO_4$/C materials by hydrothermal and sol-gel methods.

(4) Synthesis of platinum doped $LiFePO_4$/C materials by hydrothermal and sol-gel methods.

(5) Charactering the prepared materials by XRD, SEM, XPS and BET to determine the effect of the doping on the physical-chemical parameters of $LiFePO_4$/C materials.

(6) Determining the electrochemical performance of the Li-ion battery based on these cathode materials, such as charge-discharge test, CV, EIS and cycling.

(7) Investigating the effect of metal doping and preparation methods on the physical-chemical properties and electrochemical performance of $LiFePO_4$/C materials.

CHAPTER 3 ORGANIZATION OF ARTICLES AND THESIS STRUCTURE

In chapter 4, optimized amount of carbon for coating of $LiFePO_4$ particles were investigated. Therefore, uniform and optimized carbon coating is determined to achieve high performance $LiFePO_4$/C material for all the experiments. The results are presented in an article with the title of "*Improvement of the electrochemical and electrical properties of $LiFePO_4$ coated with citric acid*".

In Chapter 5, the influence of palladium & platinum doping on the physical-chemical properties and electrochemical performance of $LiFePO_4$/C material prepared via sol-gel method was investigated using XRD, XPS, SEM, BET techniques and electrochemical test measurements. The results of this chapter are presented in two articles titled "*Effects of palladium doping on the structure and electrochemical properties of $LiFePO_4$/C prepared using the sol-gel method*" and "*Synthesis and characterization of Pt-doped $LiFePO_4$/C composites using sol-gel method as the cathode material in lithium-ion batteries*".

Chapter 6 discusses in detail the effects of palladium & platinum doping on the structure, purity, morphology and electrochemical properties of $LiFePO_4$/C material synthesized using a hydrothermal method. The results of this chapter are presented in two articles by titles of "*Synthesis and characterization of palladium doped $LiFePO_4$/C nano composites using hydrothermal method for Li-ion batteries application*" and "*Enhancement of electrochemical properties of Platinum doped $LiFePO_4$/C cathode material synthesized using hydrothermal method*".

Chapter 7 is a general discussion and summary of results obtained in this study. Moreover, the most important factors affecting the performance of doped-$LiFePO_4$/C material are presented. Chapter 8 concludes the main achievements of this thesis and offers recommendations for future work.

CHAPTER 4 ARTICLE 1: IMPROVEMENT OF THE ELECTROCHEMICAL AND ELECTRICAL PROPERTIES OF $LIFEPO_4$ COATED WITH CITRIC ACID

M. Talebi-Esfandarani and O. Savadogo*

Laboratory of New Materials for Electrochemistry and Energy
École Polytechnque de Montréal
C.P. 6079, Succ. Centre Ville, Montréal, QC, Canada H3C 3A7
*Corresponding author: osavadogo@polymtl.ca, Phone: +1 514 3404725

Submitted to Journal of Material Sciences, November 21, 2013

Abstract

$LiFePO_4$ was synthesized using the hydrothermal method and coated with different amounts of citric acid as the carbon source. The samples were characterized by X-ray powder diffraction (XRD), scanning electron microscopy (SEM), surface area measurement (BET), discharge capability, cyclic voltammetry (CV), and electrochemical impedance spectroscopy (EIS). The results show that the quality and thickness of the carbon coating on the surface of the $LiFePO_4$ particles are very important, and that only a specific content (about 30%) can lead to a more uniform carbon distribution. Electrochemical results show that the samples containing 20%, 30%, 40%, and 50% carbon deliver a discharge capacity of 105, 167, 151, and 112 mAh g^{-1} respectively at the rate of 0.1C. An increase in carbon leads to a decrease in the discharge capacity of the $LiFePO_4$/C, owing to fact that the excess carbon delays the diffusion of the Li^+ ions through the carbon layers during the charge/discharge procedure, and $LiFePO_4$/C with a

low carbon content exhibits poor electrochemical performance because of its low electrical conductivity. Therefore, the amount of carbon must be optimized in order to achieve excellent electrochemical performance of $LiFePO_4$/C for application in a lithium-ion battery.

Keywords: $LiFePO_4$, Lithium ion batteries, Carbon coating

4.1 Introduction

Lithium iron phosphate ($LiFePO_4$) is well known to be a promising candidate to replace lithium cobalt oxide as the cathode in a lithium ion battery application, owing to its low cost, excellent thermal stability, lack of toxicity, abundance in nature, and high cyclability [1-3]. There are several methods for preparing $LiFePO_4$ cathode materials, such as the sol-gel method [4], the hydrothermal method [5, 6], co-precipitation [7], microwave processes [8], the solid-state method [9], etc. The disadvantage of pristine $LiFePO_4$ is its low electrical conductivity (10^{-9} Scm^{-1}) and its poor ability to diffuse ions ($10^{-14}cm^2s^{-1}$), which limit its practical use in large applications [10]. To solve these problems, various strategies, including particle size reduction, carbon coating, and metal doping, have been proposed [11-14]. However, experimental results show that carbon coating has a more significant effect on performance than doping and particle size reduction, and so most researchers in this field are of the opinion that carbon coating is worth further study [15, 16].

Low electrical conductivity can be overcome by coating the surface of particles with porous films of carbon which are conductive [17]. Also, carbon coating will protect the active material from dissolution in the electrolyte and prevent percolation of the electrolyte, as it will solve the problem of direct contact between the electrode and the electrolyte [18]. In addition, a carbon coating will prevent undesirable particle growth during the preparation of $LiFePO_4$, and it will act as a reducing agent, stopping the oxidation of Fe^{2+} to Fe^{3+} [19, 20]. Many sources of carbon,

such as ascorbic acid [19], lactose [20], sucrose [21], glucose [22], carbon nanotube [23], graphene [24], etc., have been recognized as suitable for this purpose. However, the carbon source must be inexpensive, the amount used must be optimized, and the carbon coating must be uniform, in order to guarantee an excellent conducting network on the $LiFePO_4$ particles [25, 26]. It is not necessary to use large amount of carbon to ensure a better coating. In fact, too much carbon would have significant side-effects, such as the reduction of $LiFePO_4$ to Fe_2P, a decrease in energy density, and a decrease in porosity [27, 28]. It seems that achieving a uniform, homogeneous carbon coating on the surface of $LiFePO_4$ particles is a major challenge [29]. Based on the results in the literature, no carbon coating has yet been found that meets the criteria for lithium-ion batteries. An optimal relation between the amount of carbon used for the coating, the uniformity of the coating, and its physicochemical properties, and the performance of the cell based on these electrodes need to be established. The objective, then, is to optimize the amount of carbon to obtain a uniform coating without sacrificing its energy density. In this work, $LiFePO_4$, with different amounts of citric acid as the carbon source, is synthesized to investigate the effect of carbon on the structure, morphology, performance, and electrochemical properties of $LiFePO_4$.

4.2 Experimental

4.2.1 Synthesis of $LiFePO_4$

$LiFePO_4$ was prepared using the hydrothermal method from precursors of $FeSO_4 \cdot 7H_2O$, H_3PO_4, and $LiOH \cdot H_2O$ in a molar ratio of 1:1:3. $FeSO_4 \cdot 7H_2O$ and H_3PO_4 were dissolved in deionized water under magnetic stirring to obtain a solution. Then, a $LiOH \cdot H_2O$ solution was added dropwise to the first solution while stirring. A small amount of hydrazine and some ethylene glycol (EG) were then added to the solution. The whole procedure was carried out in a nitrogen

atmosphere. The mixture was quickly sealed in a Teflon-lined autoclave purged with nitrogen and heated at 190°C for 6 h. Once the hydrothermal reaction was completed, the autoclave was cooled down to room temperature. The precipitate was filtered out of the cooled liquid and washed several times with deionized water and acetone. After drying at 120°C overnight in a vacuum oven, presynthesized $LiFePO_4$ was mixed with different amounts of citric acid in deionized water as the carbon source. The dried sample was annealed at 500°C for 5 h under a nitrogen atmosphere. The samples are hereafter reported as LF for $LiFePO_4$ and LF/20C, LF/30C, LF/40C, and LF/50C for 20%, 30%, 40%, and 50% citric acid, by weight of $LiFePO_4$, respectively.

4.2.2 Sample characterization

The structure and crystallinity of the samples were analyzed by X-ray diffractometry (Philips X'pert) with CuKα radiation (λ=1.54056 A°). The diffraction patterns were recorded between scattering angles of 10° and 80° in steps of 0.03°. The morphology of the prepared powders was observed using scanning electron microscopy (JSM-7600TFE). The specific surface area of the samples was then measured (Autosorb-1, Quantachrome instruments). The carbon content of the samples was determined using carbon-detector (LECO Co., CS 400).

4.2.3 Cell fabrication and electrochemical tests

The composite electrode was prepared by mixing the active material, with carbon black (Super C65- Timcal) as a conductive additive, and polyvinylidene fluoride (PVDF) in a weight ratio of 80:10:10 in N-methyl-2-pyrrolidone. The resulting slurry was spread onto aluminum foil and dried in a vacuum oven at 70°C overnight. The loading of the composite cathode was 7-10 mg/cm^2. The cells (2032) were assembled in an argon-filled glove box with the lithium metal as

the anode, $LiFePO_4$/C as the cathode, with a Celgard 2400 as the separator, and 1 mol/L $LiPF_6$ in ethylene carbonate-dimethyl carbonate (1:1 in W/W) as the electrolyte. The charge/discharge tests were performed at between 2.5 and 4.2V (vs. Li/Li^+) with a Solartron battery test analyzer. cyclic voltammetry was carried out using a potentiostat, PAR 273A, in the potential range of 2.5-4.2V (vs. Li/Li^+) at room temperature with scan rates of 0.1 mVs^{-1}. The EIS measurements were performed on a Solartron 1260 over a frequency range of 0.01 Hz-1 mHz by applying an AC signal of 10 mV.

4.3 Results and discussion

The XRD patterns of the samples are shown in Figure 4-1. The peaks for all the samples can be indexed as a well-crystallized $LiFePO_4$ phase with an orthorhombic structure, the P_{nmb} space group, based on patent no. JCPDS 40-1499. No evidence of diffraction peaks for citric acid appears in the diffraction pattern of the samples, even when the amount of carbon is increased to

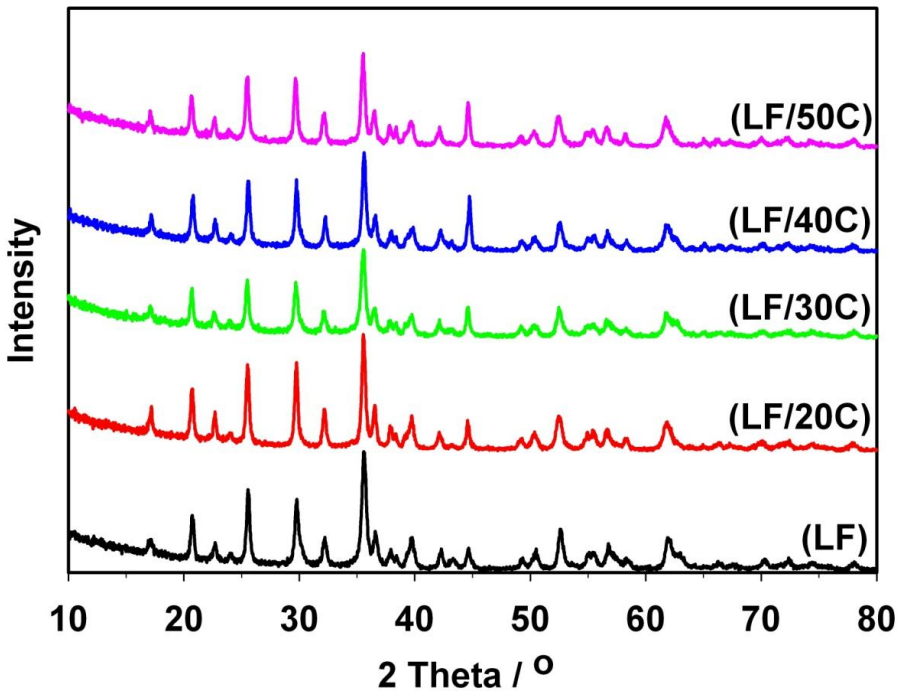

Figure 4-1: XRD patterns for synthesized $LiFePO_4$/C with the different amount of carbon

50%, since carbon has an amorphous structure. Also, the carbon has not changed the structure of $LiFePO_4$, since the carbon coating was added after the $LiFePO_4$ had been synthesized. All the samples have narrow diffraction peaks, indicating a high degree of crystallinity, due to the annealing of the samples. Note that no impurities were detected by X-ray diffraction analysis. This is because hydrazine was added during the synthesis process to prevent their formation [19].

Figure 4-2 shows the SEM images of $LiFePO_4$ coated with different amounts of carbon. The LF particles are fine-grained, because EG was added during synthesis to reduce the solubility of the metal ions. This means that crystal growth is inhibited by EG, and so smaller particles are produced [16, 30]. The LF sample shows a particle size of about 0.5-1μm. We know that the LF/20C sample contains insufficient carbon, because the $LiFePO_4$ particles could not be coated completely. In contrast, we see that the carbon is uniformly dispersed on the LF/30C sample, and is therefore optimized. The addition of more carbon causes cracks and holes to appear, as we can see in the LF/40C sample. The carbon contents are 1.8 wt%, 4.1 wt%, 6.3 wt% and 6.9 wt% for the LF/20C, LF/30C, LF/40C and LF/50C samples, respectively. The BET measurements in Table 4-1 show clearly that the specific surface area of the electrode increases with the carbon content as a result of mixing LF powder with citric acid in the liquid phase and the evaporation of the solution. In Figure 4-2, we see the pores that have increased the surface area of the electrode, and can conclude from this that the high discharge capacity on some electrodes is due to their large surface area.

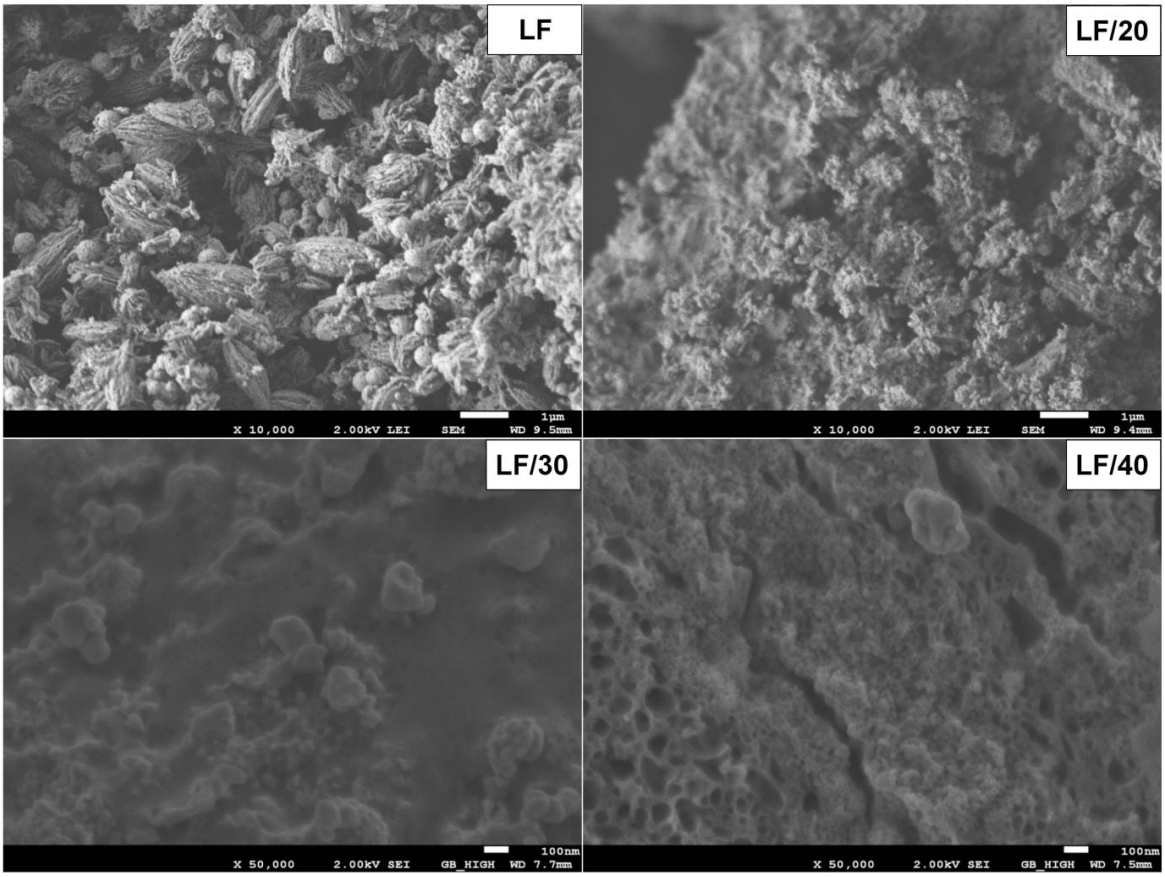

Figure 4-2: SEM images of $LiFePO_4$/C with the different amount of carbon

Table 4-1: The BET results of samples

Sample	**BET(m^2 g^{-1})**
LF	17
LF/20	25
LF/30	34
LF/40	45
LF/50	48

The discharge curves of samples prepared with various amounts of carbon are shown in Figure 4-3. The low specific capacity of the pristine LF samples can be attributed to low electrical

conductivity, and this can be confirmed by measuring resistivity. We see an initial specific discharge capacity of 105, 167, 151, and 112 mAh g^{-1} for the LF/20C, LF/30C, LF/40C and LF/50C samples respectively. The performance of the $LiFePO_4$ particles surface-coated with carbon has improved greatly, in terms of specific capacity, due to an increase in electrical conductivity and an enlargement of the specific surface area, both of which improve the reaction, as indicated by the BET results. But the amount of carbon must be optimized, to ensure that the carbon content is not too high, as this would result in too much carbon on the surface of the particles. A thick layer of carbon would prevent the surface electrons from interacting and make it difficult for the ions to diffuse through the powder structure, as revealed with the LF/50C samples.

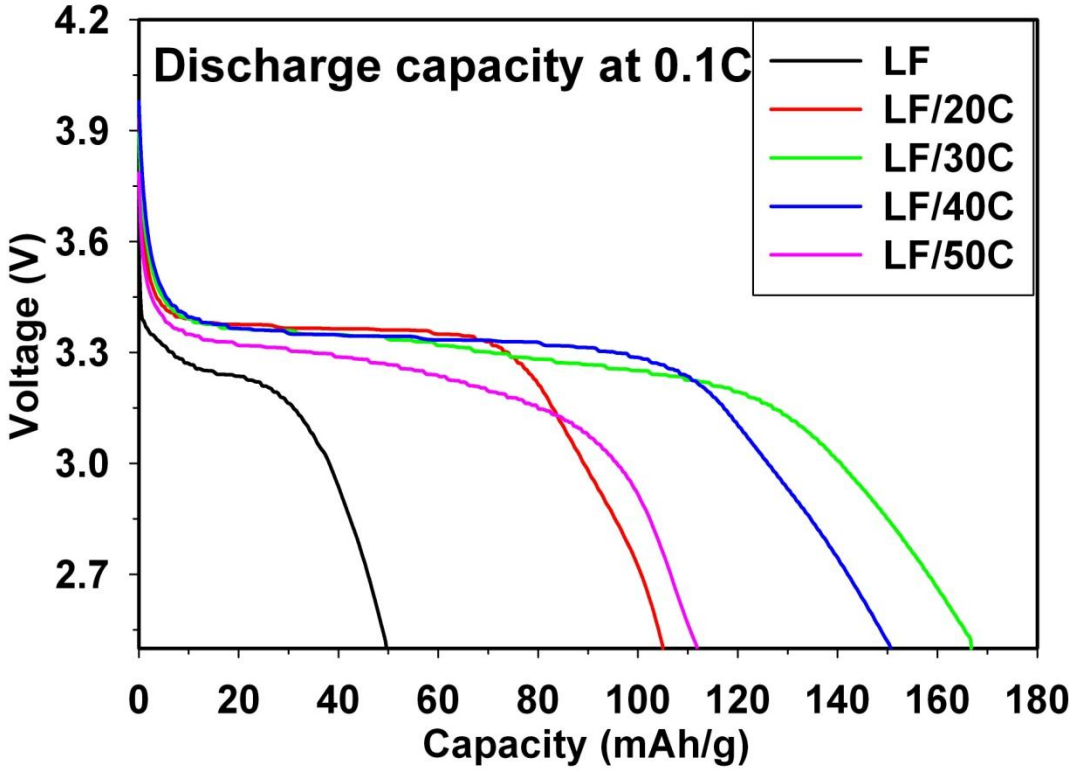

Figure 4-3: Discharge curves of LF, LF/20C, LF/30C, LF/40C and LF/50C samples at 0.1C rate

As we can see in Figure 4-3, if the particles have a uniform carbon coating of the appropriate thickness (LF/30C), they could have a discharge capacity of 167 mAh g^{-1}, which is close to the theoretical capacity for $LiFePO_4$, which is 170 mAh g^{-1}.

The CV curves of the LF, LF/20C, LF/30C, LF/40C, and LF/50C samples are presented in Figure 4-4. For all the samples, there are oxidation and reduction peaks. These are attributed to the two-phase reaction between lithiated phase, $LiFePO_4$, and the delithiated phase, $FePO_4$. However, for the optimized LF/30C sample, the potential separation between the cathodic (3.57V) and anodic (3.30V) peaks is shorter (around 0.27V) than those of non optimized samples. This shorter distance between the cathodic and anodic peaks (0.27V) indicates a low polarization potential during the redox process. In addition, the oxidation/reduction peaks for the LF/30C sample are sharper and more symmetrical, which indicates better reversibility and

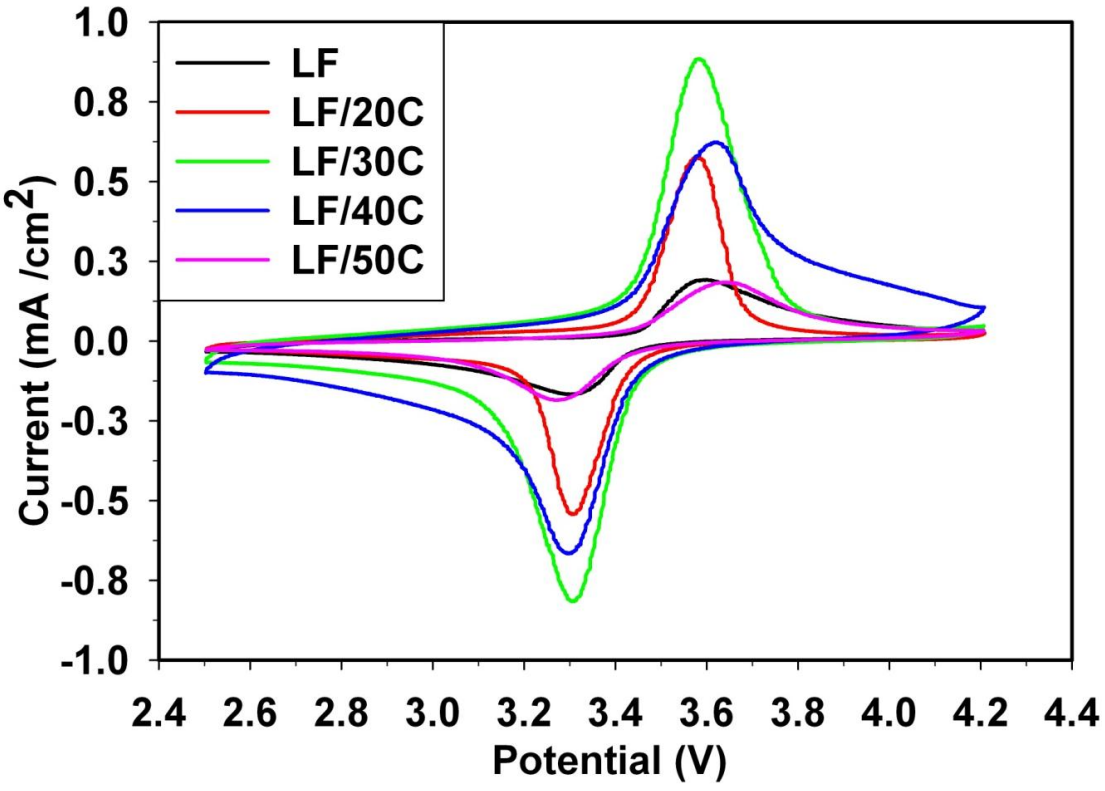

Figure 4-4: CV curves of LF, LF/20C, LF/30C, LF/40C and LF/50C samples

electrochemical activity during the lithium intercalation and de-intercalation processes [31].Electrochemical impedance spectroscopy (EIS) was performed to investigate the lithium ion diffusion through the $LiFePO_4$ structure. The EIS curves of all the samples are shown in Figure 4-5. The intercept impedance on the real axis corresponds to the resistance, Re, of the electrolyte. The depressed semicircle in the high frequency region is related to the charge transfer resistance (Rct), and the diameter of the semicircle on the Z' axis is approximately equal to Rct. The sloping line at the lower frequency is attributed to the Li^+ diffusion resistance in the bulk of the material, which is called the Warburg diffusion [32]. The impedance data can be fitted to the equivalent circuit, as shown in the inset in Figure 4-5. The parameters of the equivalent circuit are presented in Table 4-2.

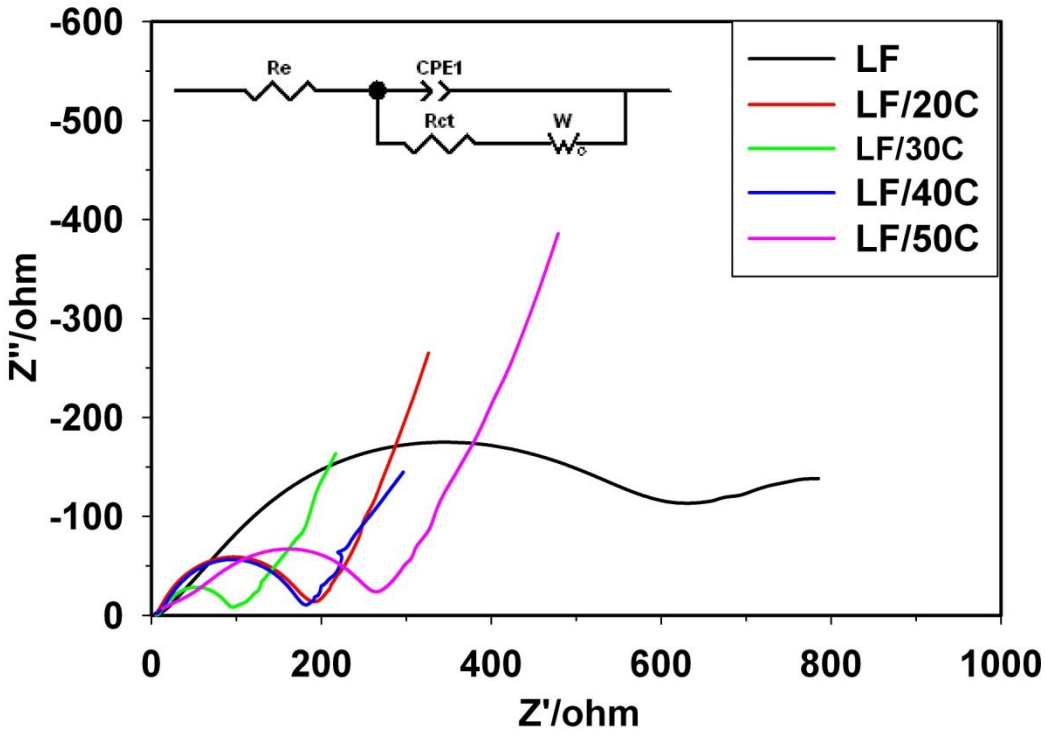

Figure 4-5: The EIS plots of LF, LF/20C, LF/30C, LF/40C and LF/50C samples. The inset shows an equivalent circuit

Table 4-2: The impedance parameters of the different samples

Sample	Re(Ω)	R_{ct}(Ω)	σ_w($\Omega cm^2 s^{-0.5}$)	D($cm^2 s^{-1}$)
LF	11.5	498.5	91.03	2.83×10^{-15}
LF/20	6.3	182.7	15.31	1.00×10^{-13}
LF/30	5.1	78.9	12.02	1.62×10^{-13}
LF/40	5.2	168.8	14.51	1.11×10^{-13}
LF/50	9.52	260.5	51.37	8.89×10^{-15}

The relation of Z_{re} vs. the reciprocal root square of the frequency ($\omega^{-0.5}$) in the low frequency region is shown in Figure 4-6. Using Eq. (1), the Warburg impedance coefficient, σ_w, of the samples can be obtained, and are listed in Table 4-2. Consequently, the Li^+ diffusion coefficients, D, of the samples were calculated using Eq. (2):

$$Z_{re} = R_e + R_{ct} + \sigma_w \omega^{-0.5} \qquad (1)$$

$$D = R^2T^2 / 2A^2F^4n^4C^2\sigma_w^2 \qquad (2)$$

Where R is a gas constant (8.314 J mol^{-1} K^{-1}), T is the temperature (298 K), A is the electrode surface area (cm^2), F is the Faraday constant (96486 C mol^{-1}), n is the number of electrons involved in the reaction, and C is the concentration of Li^+ ions.

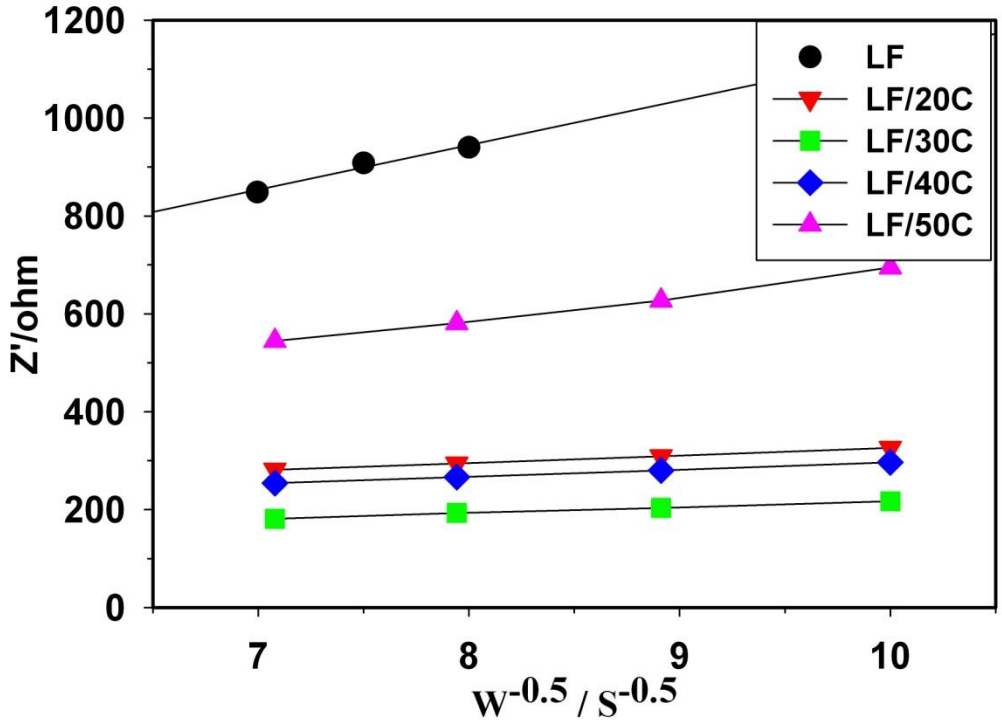

Figure 4-6: The relationship between Z_{re} and $\omega^{-0.5}$ at low frequency

The LF/30C sample shows a lower value for R_{ct}, due to the high electrical conductivity, and this indicates that the impedance of the electrochemical reaction is reduced by the optimization of the amount of carbon. The result is consistent with the difference between the peak potentials in the cyclic voltammograms, as shown in Figure 4-4. Also, the lithium ion diffusion for the LF/30C sample is high (1.62×10^{-13} cm^2s^{-1}), in comparison with that of the other samples presented in Table 4-2. Consequently, the enhancement of the electrochemical properties of the LF30/C sample can be attributed to its high electrical conductivity, large surface area, and short lithium ion diffusion path through the structure of the material, which facilitates fast kinetics and the achievement of a high rate capacity [33]. This result shows that the lithium ion diffusion initially increases with an increasing amount of carbon and then decreases with the addition of more carbon. We can conclude that carbon coating can enhance the electrical conductivity of $LiFePO_4$;

however, a too thick coating could make difficult the Li^+ ion diffusion through the $LiFePO_4$ structure, which is compatible with Jiang's result [34]. Also, annealing the samples completes carbonization of the citric acid, as well as increasing the crystallinity of $LiFePO_4$ powders for better ion diffusion [14]. It has been pointed out that an excellent electrochemical performance can be achieved by optimizing other factors during synthesis, including particle size, morphology, homogeneity, crystallinity, and purity of the material.

4.4 Conclusion

In this work, $LiFePO_4$ material was synthesized using a hydrothermal method and by carbon coating the material with different amounts of carbon. The results indicate that carbon coating does not change the structure of the $LiFePO_4$, but it can significantly improve the electrochemical properties of the material by enhancing its electrical conductivity and specific surface area. Electrochemical results show that the LF, LF/20C, LF/30C, LF/40C and LF/50C samples deliver a discharge capacity of 50, 105, 167, 151, and 112 mAh g^{-1}, respectively at the rate of 0.1C. $LiFePO_4$ coated with a small amount of carbon results in poor electrochemical performance, and too much carbon can prevent Li^+ diffusion through the structure of the material and decrease its specific capacity. The thickness of the carbon coating was found to be optimized at around 5-10 nm.

References

[1] AK Padhi, KS Nanjundaswamy, JB Goodenough (1997) Journal of The Electrochemical Society 144: 1188. Doi:10.1149/1.1837571

[2] J Liu, J Wang, X Yan, et al. (2009) Electrochimica Acta 54: 5656. Doi:10.1016/j.electacta.2009.05.003

[3] A Yamada, SC Chung, K Hinokuma (2001) Journal of The Electrochemical Society 148: A224. Doi:10.1149/1.1348257

[4] J-K Kim, J-W Choi, GS Chauhan, et al. (2008) Electrochimica Acta 53: 8258. Doi:10.1016/j.electacta.2008.06.049

[5] Q Song, X Ou, L Wang, G Liang, Z Wang (2011) Materials Research Bulletin 46: 1398. Doi:10.1016/j.materresbull.2011.05.015

[6] S Yang, PY Zavalij, M Stanley Whittingham (2001) Electrochemistry Communications 3: 505. Doi:10.1016/s1388-2481(01)00200-4

[7] Y Ding, Y Jiang, F Xu, et al. (2010) Electrochemistry Communications 12: 10. Doi:10.1016/j.elecom.2009.10.023

[8] XZ F. Deng, J. Zou, J. Huang, X. Xiong, X. Li, H. Sheng (2011) Journal of New Materials for Electrochemical Systems 14: 27.

[9] WB W. Xiaoyue, Y. Kai, Y. Xuankun, W. Chuan, W. Feng, W. Feng, C. Shi, L. Gewei (2009) Journal of New Materials for Electrochemical Systems 12: 213.

[10] FLC S. Franger, C. Bourbon, H. Rouault (2002) Electrochemical and Solid-State Letters 5: A231.

[11] J.-T. Son (2010) Journal of New Materials for Electrochemical Systems 13: 301.

[12] A Kuwahara, S Suzuki, M Miyayama (2010) Journal of Electroceramics 24: 69. Doi:10.1007/s10832-008-9442-1

[13] D Arumugam, G Paruthimal Kalaignan, P Manisankar (2009) Journal of Solid State Electrochemistry 13: 301. Doi:10.1007/s10008-008-0533-3

[14] XQ Ou, GC Liang, JS Liang, SZ Xu, X Zhao (2008) Chinese Chemical Letters 19: 345. Doi:http://dx.doi.org/10.1016/j.cclet.2007.10.052

[15] W-J Zhang (2010) Journal of The Electrochemical Society 157: A1040. Doi:10.1149/1.3460840

[16] MK Devaraju, I Honma (2012) Advanced Energy Materials 2: 284. Doi:10.1002/aenm.201100642

[17] G Wang, H Liu, J Liu, et al. (2010) Advanced Materials 22: 4944. Doi:10.1002/adma.201002045

[18] NA Chernova, M Roppolo, AC Dillon, MS Whittingham (2009) Journal of Materials Chemistry 19: 2526.

[19] J Chen, MJ Vacchio, S Wang, N Chernova, PY Zavalij, MS Whittingham (2008) Solid State Ionics 178: 1676. Doi:http://dx.doi.org/10.1016/j.ssi.2007.10.015

[20] K Zaghib, A Mauger, F Gendron, CM Julien (2007) Chemistry of Materials 20: 462. Doi:10.1021/cm7027993

[21] J Yang, Y Bai, C Qing, W Zhang (2011) Journal of Alloys and Compounds 509: 9010. Doi:10.1016/j.jallcom.2011.07.021

[22] G Liang, L Wang, X Ou, X Zhao, S Xu (2008) Journal of Power Sources 184: 538. Doi:10.1016/j.jpowsour.2008.02.056

[23] G Wang, X Shen, J Yao (2009) Journal of Power Sources 189: 543. Doi:10.1016/j.jpowsour.2008.10.044

[24] X Zhou, F Wang, Y Zhu, Z Liu (2011) Journal of Materials Chemistry 21: 3353.

[25] K Saravanan, P Balaya, MV Reddy, BVR Chowdari, JJ Vittal (2010) Energy & Environmental Science 3: 457.

[26] F-Y Su, C You, Y-B He, et al. (2010) Journal of Materials Chemistry 20: 9644.

[27] BE P.S. Herle, N. Coombs, L.F. Nazar (2004) Nat Mater 3: 147.

[28] M Doeff, J Wilcox, R Yu, A Aumentado, M Marcinek, R Kostecki (2008) Journal of Solid State Electrochemistry 12: 995. Doi:10.1007/s10008-007-0419-9

[29] R Dominko, M Bele, M Gaberscek, et al. (2005) Journal of The Electrochemical Society 152: A607. Doi:10.1149/1.1860492

[30] W Kang, C Zhao, R Liu, F Xu, Q Shen (2012) CrystEngComm 14: 2245.

[31] L Wang, H Wang, Z Liu, et al. (2010) Solid State Ionics 181: 1685. Doi:http://dx.doi.org/10.1016/j.ssi.2010.09.056

[32] MD Levi, G Salitra, B Markovsky, et al. (1999) Journal of The Electrochemical Society 146: 1279. Doi:10.1149/1.1391759

[33] J Ni, M Morishita, Y Kawabe, M Watada, N Takeichi, T Sakai (2010) Journal of Power Sources 195: 2877. Doi:http://dx.doi.org/10.1016/j.jpowsour.2009.11.017

[34] Z Jiang, Z-j Jiang (2012) Journal of Alloys and Compounds 537: 308. Doi:http://dx.doi.org/10.1016/j.jallcom.2012.05.066

CHAPTER 5 ARTICLES 2 AND 3: SUMMARY OF DOPING WITH SOL-GEL METHOD

This chapter consists of the following two publications;

1. Effects of palladium doping on the structure and electrochemical properties of $LiFePO_4$/C prepared using the sol-gel method

2. Synthesis and characterization of Pt-doped $LiFePO_4$/C composites using the sol-gel method as the cathode material in lithium-ion batteries

5.1 Effects of palladium doping on the structure and electrochemical properties of $LiFePO_4$/C prepared using the sol-gel method

M. Talebi-Esfandarani and O. Savadogo*

Laboratory of New Materials for Electrochemistry and Energy
École Polytechnque de Montréal,
C.P. 6079, Succ. Centre Ville, Montréal, QC
Canada, H3C 3A7

*Corresponding author: osavadogo@polymtl.ca, Phone: +1 514 3404725

Submitted to Journal of New Materials for Electrochemical Systems, November 18, 2013

Abstract

$LiFePO_4$/C, $LiFe_{0.98}Pd_{0.02}PO_4$/C, and $LiFe_{0.96}Pd_{0.04}PO_4$/C composite cathode materials were synthesized using the sol-gel method. The effect of palladium on the structure and electrochemical properties of $LiFePO_4$/C were investigated by X-ray diffraction (XRD), X-ray photoelectron spectroscopy (XPS), scanning electron microscopy (SEM), surface area measurement (BET), charge/discharge testing, and cyclic voltammetry (CV). The results indicate that palladium doping facilitates the formation of Li_3PO_4 impurity. Also, the lattice parameters of the $LiFePO_4$ structure decrease in size as the palladium content increases. In addition, the particles become larger and agglomerated by palladium incorporation. The electrochemical results show that palladium doping decreases the electrochemical performance of $LiFePO_4$/C, owing to shrinking lattice parameters and the difficulty of achieving the diffusion of lithium ions into the structure during the intercalation/de-intercalation process. These results suggest that

palladium doping by sol-gel method changes the $LiFePO_4$ structure significantly which may impact it performances as cathode for the lithium ion battery applications.

Keywords: $LiFePO_4$/C, sol-gel method, palladium doping, lithium ion diffusion.

5.1.1 Introduction

Since 1997, $LiFePO_4$ has been considered a promising candidate as a cathode material in lithium ion battery applications, because of its excellent thermal stability, low cost, non toxicity, and abundance in nature [1-3]. However, pristine $LiFePO_4$ suffers from its diffusion limitation ($10^{-14}cm^2s^{-1}$) and low electrical conductivity (10^{-9} Scm^{-1}), which result in low current densities, limiting its application in large electronic devices [4, 5]. Various approaches have been proposed to solve these problems, such as decreasing particle size, carbon coating, and metal doping [6-12]. Experimental results and theoretical studies show that metal doping is more complex than carbon coating and particle size reduction. Moreover, the doping mechanism is not yet clearly understood. It has been demonstrated that small particles facilitate the passage of Li ions through the $LiFePO_4$ structure [10], that carbon coating improves the electronic properties on the surface of the $LiFePO_4$ particles [13], and that a doping agent can increase the intrinsic electrical conductivity of bulk $LiFePO_4$ particles [14-16]. A doping agent can also make a longer Li-O bond with a lower energy barrier in the $LiFePO_4$ structure, so that Li ion movement becomes easier, enhancing the ionic conductivity [17-19]. However, doping bulk $LiFePO_4$ material without a carbon coating is not enough to improve its electrochemical performance. As a result, researchers usually combine the doping and carbon coating elements in order to achieve this improvement.

To select an appropriate doping approach, many factors must be considered, including the site of the doping, the physicochemical properties of the dopant, and the amount of dopant required.

Theoretical studies have shown that $LiFePO_4$ has a one-dimensional Li ion diffusion pathway [21-23], and that a non mobile dopant at the Li site probably blocks the diffusion of Li ions [24, 25]. Also, a very large amount of dopant may block the diffusion channels for Li ions throughout the $LiFePO_4$ structure, and also collapse or destroy that structure [11, 25, 26]. However, it has been reported that various dopant elements enhance the electrochemical performance of $LiFePO_4$, including Sn [14], Mg [15], La [26], Na [27], Cu [28], V [29], Ti [30], Co [31], Ru [32], Mo [33], F [34], Cl [35], Zn [36], Cr [37], etc.

So far, to our knowledge, the effect of palladium (Pd) on $LiFePO_4$ has not been reported. In this paper, we introduce a method for synthesizing Pd-doped $LiFePO_4$ material using the sol-gel method, and investigate the effect of Pd doping on the physical and electrochemical properties of the prepared materials.

5.1.2 Experimental

5.1.2.1 Synthesis of materials

$LiFePO_4$, $LiFe_{0.98}Pd_{0.02}PO_4$, and $LiFe_{0.96}Pd_{0.04}PO_4$ samples were synthesized using the sol-gel method and a stoichiometric amount of $Li(CH_3COO)$ (lithium acetate, Alfa Aesar), $Fe(NO_3)_3.9H_2O$ (iron nitrate, Sigma Aldrich), $Pd(NO_3)_2.2H_2O$ (palladium nitrate, Sigma Aldrich), and H_3PO_4 (phosphoric acid, Anachemia). First, phosphoric acid was diluted in the distilled water, and then iron nitrate, palladium nitrate, and lithium acetate were added to the solution, which was mixed until the constituents were completely dissolved. The solution was combined with glycolic acid and the pH was adjusted to fall into the 8.5 to 9.5 range using ammonium hydroxide. The solution was heated at 90°C while stirring until a gel formed. After drying at 120°C in a vacuum oven, the sample was annealed at 500°C for 10 h to obtain $LiFePO_4$. Finally, the presynthesized $LiFePO_4$ was mixed with sucrose as a carbon source in a 70:30

weight ratio, followed by annealing at 700°C for 5 h to prepare a $LiFePO_4$/C composite. The procedure was performed under a nitrogen atmosphere.

5.1.2.2 Materials characterization

The phase purity and crystalline structure of the samples were investigated using an X-ray diffractometer (Philips X'pert) with CuKα radiation (λ=1.54056 A°). The oxidation states of the Fe and Pd ions were analyzed by X-ray photoelectron spectroscopy (VG ESCALAB 3 MKII) with an Al Kα radiation source (*hv*=1486.6 eV). The pressure in the analyzer chamber was around 8^{-9}Torr with a power of 216 W and a 2×3 mm analysis region. The data were calibrated with respect to a C1s peak at a value of 285.0 eV. Their morphology and particle size distributions were observed by scanning electron microscopy (JSM-7600TFE), and their specific surface area was determined using a BET measurement machine (Autosorb-1, Quantachrome instruments). The carbon content of the samples was measured by carbon analyzer (LECO Co., CS 400).

5.1.2.3 Electrochemical characterization

The composite cathodes for electrochemical measurement were prepared by mixing the $LiFePO_4$/C powders, carbon black (Super C65-Timcal), and polyvinylidene fluoride (PVDF) in a weight ratio of 80:10:10 in an N-methyl-2-pyrrolidone solvent for 3-6 h. Subsequently, the slurry was coated onto aluminum foil using the doctor blade technique and dried in a vacuum oven overnight. The cells (2032) were assembled in an argon-filled glove box with lithium metal as the anode, a Celgard 2400 as the separator, and 1 $molL^{-1}$ $LiPF_6$ in ethylene carbonate-dimethyl carbonate as the electrolyte. The charge/discharge test and cycling stability test were performed between 2.5 and 4.2V (vs. Li/Li^+) with a Solartron battery test analyzer. Cyclic voltammetry

(CV) was carried out using PAR273A in the potential range of 2.5-4.2V (vs. Li/Li^+) with scan rates of 0.1 mV/s. All the electrochemical measurements were carried out at room temperature.

5.1.3 Results and discussion

Figure 5-1 shows the XRD patterns for the $LiFePO_4$, $LiFe_{0.98}Pd_{0.02}PO_4$, and $LiFe_{0.96}Pd_{0.04}PO_4$ samples. For all the samples, the main diffraction peaks indexed a standard olivine $LiFePO_4$ phase with an orthorhombic structure, a space group of P_{mnb} (JCPDS 40-1499). The Pd-doped samples contain the Li_3PO_4 impurity phase. As the palladium content increases, the intensities of the Li_3PO_4 diffraction peaks are enhanced, indicating that palladium incorporation facilitates the formation of the Li_3PO_4 impurity. However, the Li_3PO_4 phase has usually been reported as an impurity in doped $LiFePO_4$ samples [27, 38]. At the same time, Li_3PO_4 might act as an inert and inactive mass, decreasing the electrochemical performance of $LiFePO_4$ material [39, 40].

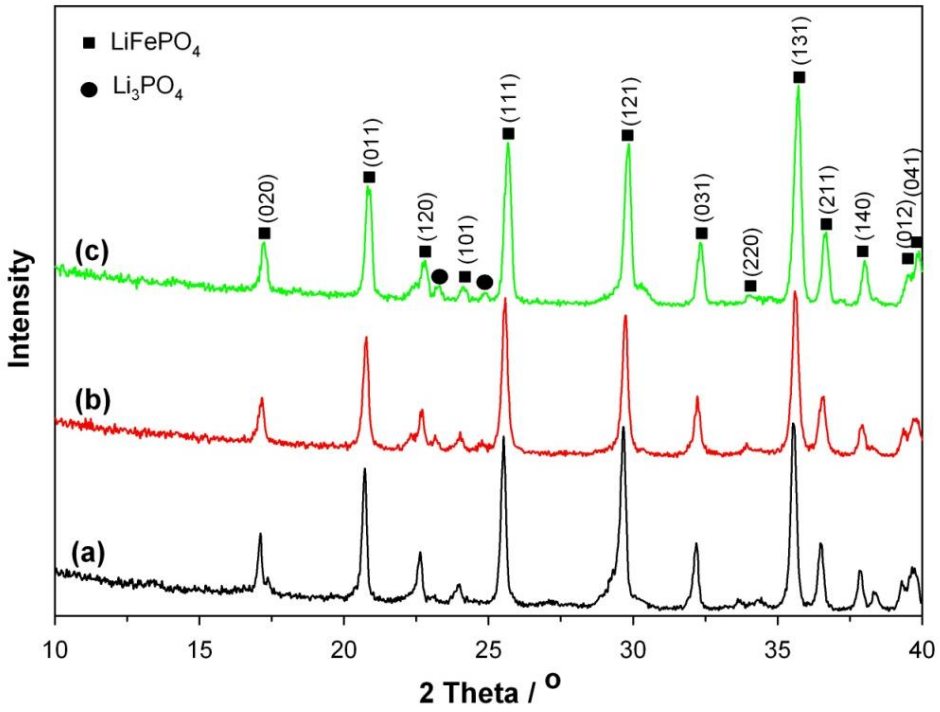

Figure 5-1: XRD patterns of (a) $LiFePO_4$, (b) $LiFe_{0.98}Pd_{0.02}PO_4$, and (c) $LiFe_{0.96}Pd_{0.04}PO_4$ samples

The lattice parameters of the samples were calculated using Topas software, and are listed in Table 5-1. These parameters demonstrate that palladium has been successfully doped into the $LiFePO_4$ phase. They decrease linearly, along with their cell volume, with an increasing amount of palladium. Therefore, the shrinkage in the lattice parameters delays Li ion insertion and extraction throughout the structure of the $LiFePO_4$, because there is less space available for diffusion [17, 19, 32,41]. This probably blocks channel diffusion, consequently decreasing the electrochemical performance of the cathode materials, especially under the high current rate, which is compatible with Islam's suggestion [23]. These results seem to be inconsistent with the expectation that the lattice parameters increase with an increasing amount of Pd^{2+} replacement of Fe^{2+} ions, since the ionic radius of Pd^{2+} (86Å) is larger than that of Fe^{2+} (78Å). The same unexpected result has been reported for Ti-doped $LiFePO_4$ [38].

Table 5-1: Lattice parameters of pristine and doped $LiFePO_4$ from XRD data

Sample	**a(Å)**	**b(Å)**	**c(Å)**	**V**
$LiFePO_4$	10.32408	6.00286	4.69050	290.689
$LiFe_{0.98}Pd_{0.02}PO_4$	10.31850	6.00157	4.69036	290.461
$LiFe_{0.96}Pd_{0.04}PO_4$	10.31470	5.99609	4.68602	289.820

The oxidation states of Fe and Pd for the $LiFePO_4$ and $LiFe_{0.96}Pd_{0.04}PO_4$ samples can be determined by XPS analysis. The XPS spectra within a wide range of binding energies for the $LiFePO_4$ and $LiFe_{0.96}Pd_{0.04}PO_4$ samples are illustrated in Figure 5-2. The peaks corresponding to Fe 2p, O 1s, P 2p, and C 1s were observed for both samples, as indicated in Figure 5-2. The binding energy for the Li 1s peak overlaps the Fe 3p peak (56 eV), and so it was not feasible to

determine its binding energy or approximate its element content. Note that the Pd 3d peak was observed for the doped sample, as shown in Figure 5-2(b), confirming the existence of Pd in the sample.

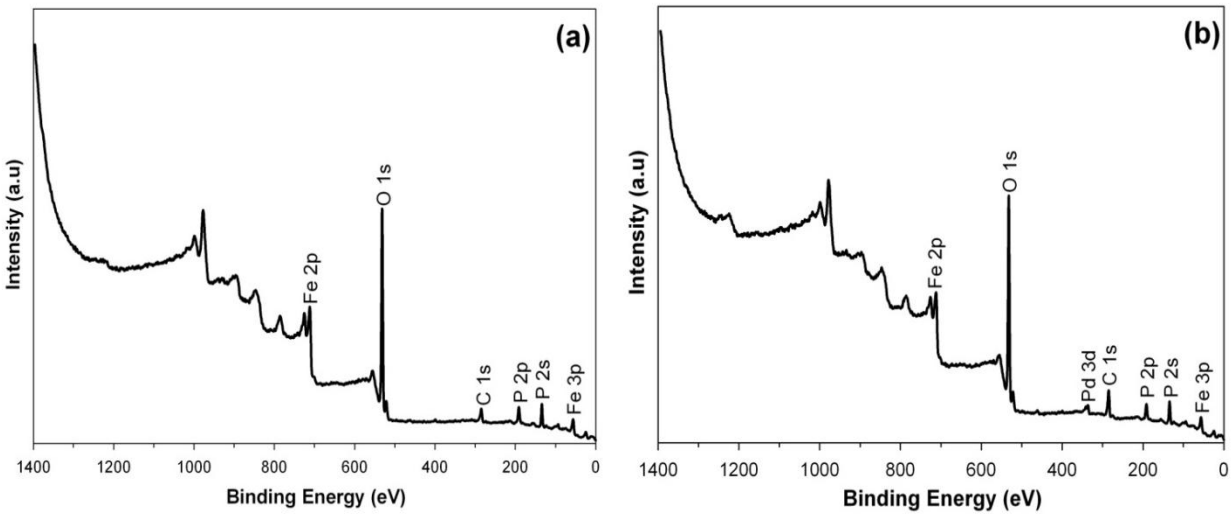

Figure 5-2: XPS spectra of the samples: (a) $LiFePO_4$; and (b) $LiFe_{0.96}Pd_{0.04}PO_4$

Figure 5-3(a) shows the high resolution spectrum for the Pd 3d peak in the doped sample. It contains a doublet with binding energies of 336 eV and 341 eV, corresponding to the Pd 3d5/2 and Pd 3d3/2 lines respectively, which determines that the oxidation state of Pd in the doped sample is +2 [42]. In order to examine the effect of Pd doping on the oxidation state and binding energy of Fe, the high-resolution spectra of the Fe 2p peak for the two samples were compared, as illustrated in Figure 5-3(b). $LiFePO_4$ samples contain the Fe 2p3/2 (710.9 eV) and Fe 2p1/2 (724 eV) peaks, indicating that the oxidation state of the Fe is +2, which is compatible with other reports [31, 41]. For the doped sample, no obvious changes were observed in comparison with the $LiFePO_4$ sample, indicating that the doping of Pd does not significantly change the valence of Fe^{2+}.

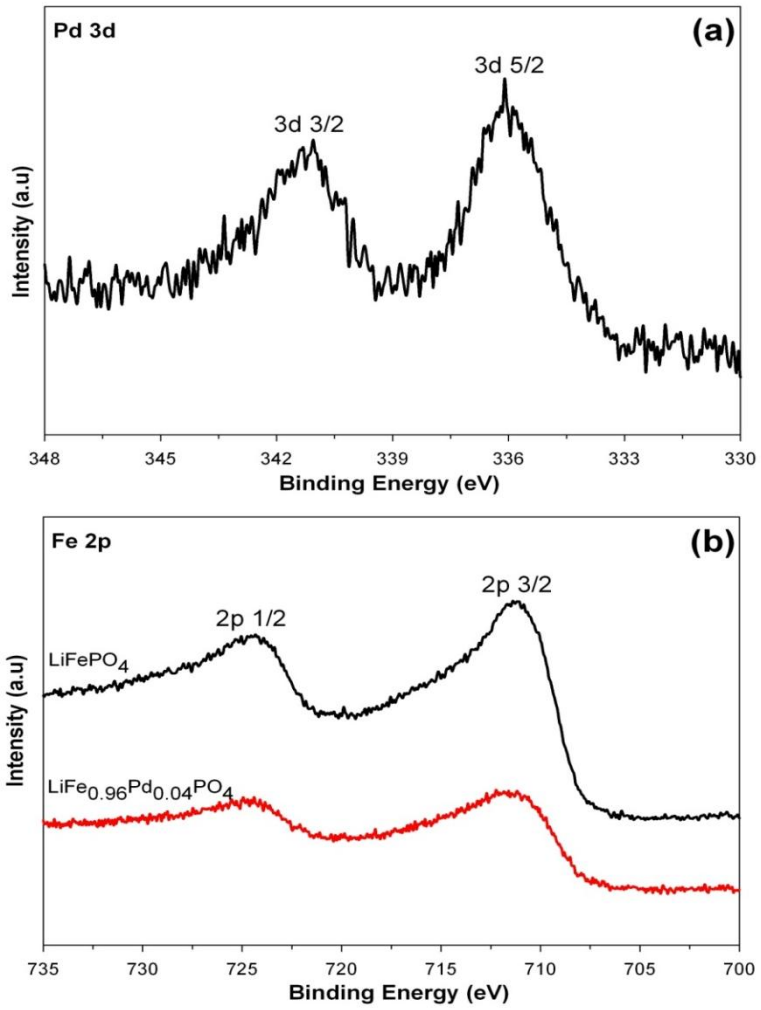

Figure 5-3: (a) XPS core levels of Pd 3d for the $LiFe_{0.96}Pd_{0.04}PO_4$ sample; (b) XPS core levels of Fe 2p for the $LiFePO_4$ and $LiFe_{0.96}Pd_{0.04}PO_4$ samples

Figure 5-4 shows the SEM images of the $LiFePO_4$, $LiFe_{0.98}Pd_{0.02}PO_4$, and $LiFe_{0.96}Pd_{0.04}PO_4$ samples. The $LiFePO_4$ material consists of small homogeneous particles 100-500 nm in size, as shown in Figure 5-4(b). However, palladium incorporation changes the morphology of this material completely, and the particles become larger and agglomerated. This explains its lower electrochemical capacity, as discussed later. However, agglomeration in the doped samples may be caused by the Li_3PO_4 phase, in which melting may have occurred during the calcination

process [31]. Also, the specific surface area of the samples decreases with increasing palladium content, as shown in Table 5-2. Therefore, the amount of surface area for the reaction reduces with palladium incorporation. It is believed that small, regular particles tend to reduce the length of the path of Li ions diffusing through the structure, resulting in fast reaction and diffusion kinetics for the intercalation/de-intercalation process, which can enhance the electrochemical performance of $LiFePO_4$ material.

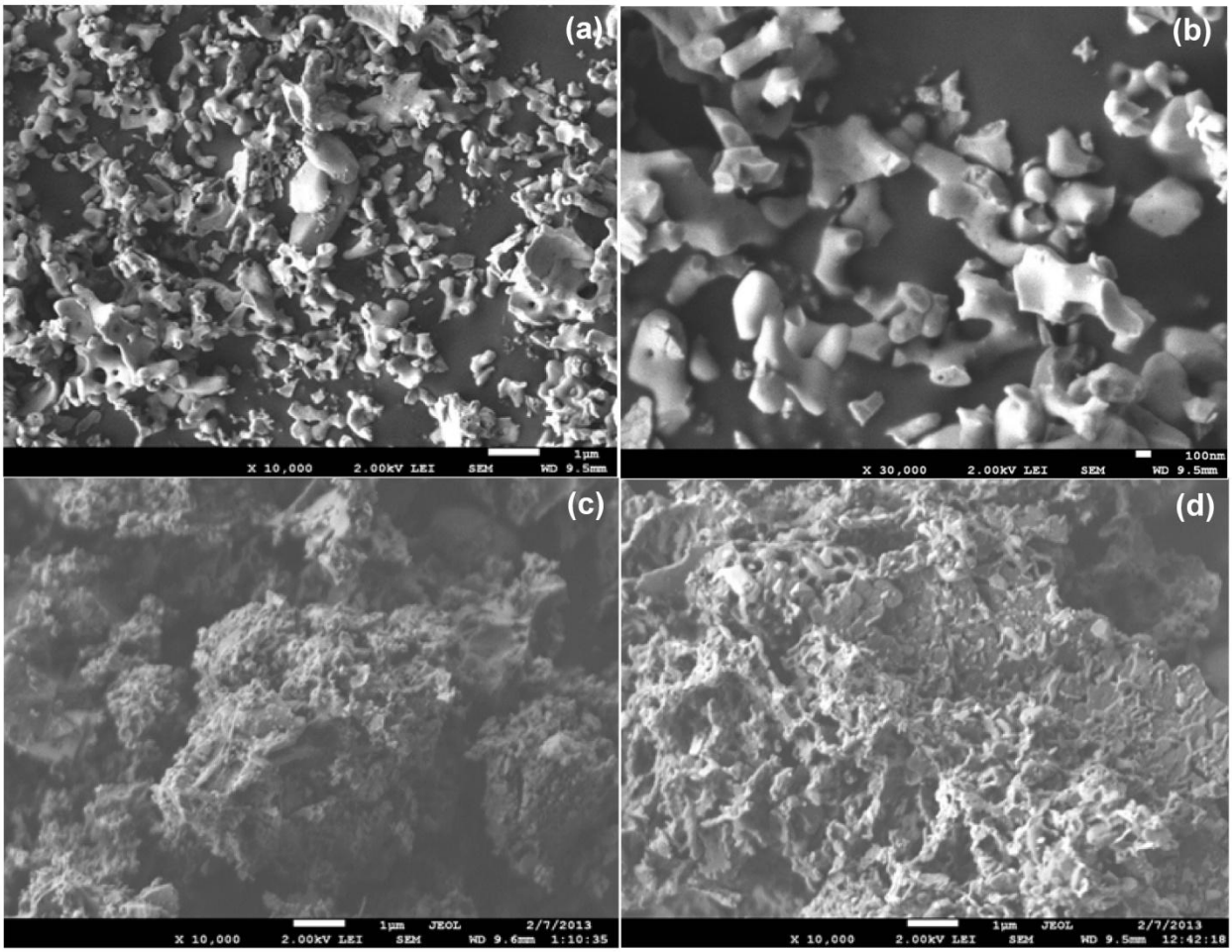

Figure 5-4: SEM images of (a) $LiFePO_4$, (b) High resolution $LiFePO_4$, (c) $LiFe_{0.98}Pd_{0.02}PO_4$, and (d) $LiFe_{0.96}Pd_{0.04}PO_4$

Table 5-2: BET result of the samples

Sample	Specific surface area(m^2/g)
$LiFePO_4$/C	43.7
$LiFe_{0.98}Pd_{0.02}PO_4$/C	40.7
$LiFe_{0.96}Pd_{0.04}PO_4$/C	33.5

Figure 5-5 shows the discharge curves of the $LiFePO_4$/C, $LiFe_{0.98}Pd_{0.02}PO_4$/C, and $LiFe_{0.96}Pd_{0.04}PO_4$/C samples at different current rates between 2.5 and 4.2 V. The $LiFePO_4$/C sample shows a flat voltage plateau at around 3.4 V, related to a two-phase Fe^{3+}/Fe^{2+} redox reaction process between $FePO_4$ and $LiFePO_4$. The $LiFePO_4$/C sample achieves the specific capacity of 164, 150, 120, and 105 mAh/g at rates of 0.2C, 1C, 5C, and 10C respectively. Palladium substitution decreases the discharge capacity of the samples, and a further decrease in the discharge capacity is observed when the palladium content is increased. This is partly due to the existence of the Li_3PO_4 phase which acts as an impurity, as palladium incorporation facilitates the formation of the Li_3PO_4. This impurity can act as an inert and inactive mass during the redox process, reducing electrochemical performance [39, 40]. Another possibility is that the lattice parameters decrease with an increasing palladium content, and parameter shrinkage makes it difficult for Li ions to diffuse into the structure of $LiFePO_4$. This is because there is less space available for diffusion of Li^+ ion by blocking the channel. Also, the large size and agglomeration of the particles, as shown in the SEM results, delay Li ion diffusion during the reaction process that the Pd-doped samples undergo. However, in the case of the $LiFe_{0.96}Pd_{0.04}PO_4$/C sample, a flat plateau is not observed, clearly confirming higher polarization, owing to the extra Li_3PO_4 impurity phase and the limitation of Li ion diffusion. The $LiFe_{0.96}Pd_{0.04}PO_4$/C sample achieves the low specific capacity of 107, 79, 58, and 42 mAh/g at rates of 0.2C, 1C, 5C, and 10C

respectively. Murugan et al. also report that cobalt doping does not have a positive effect on the electrochemical properties of $LiFePO_4/C$ [43].

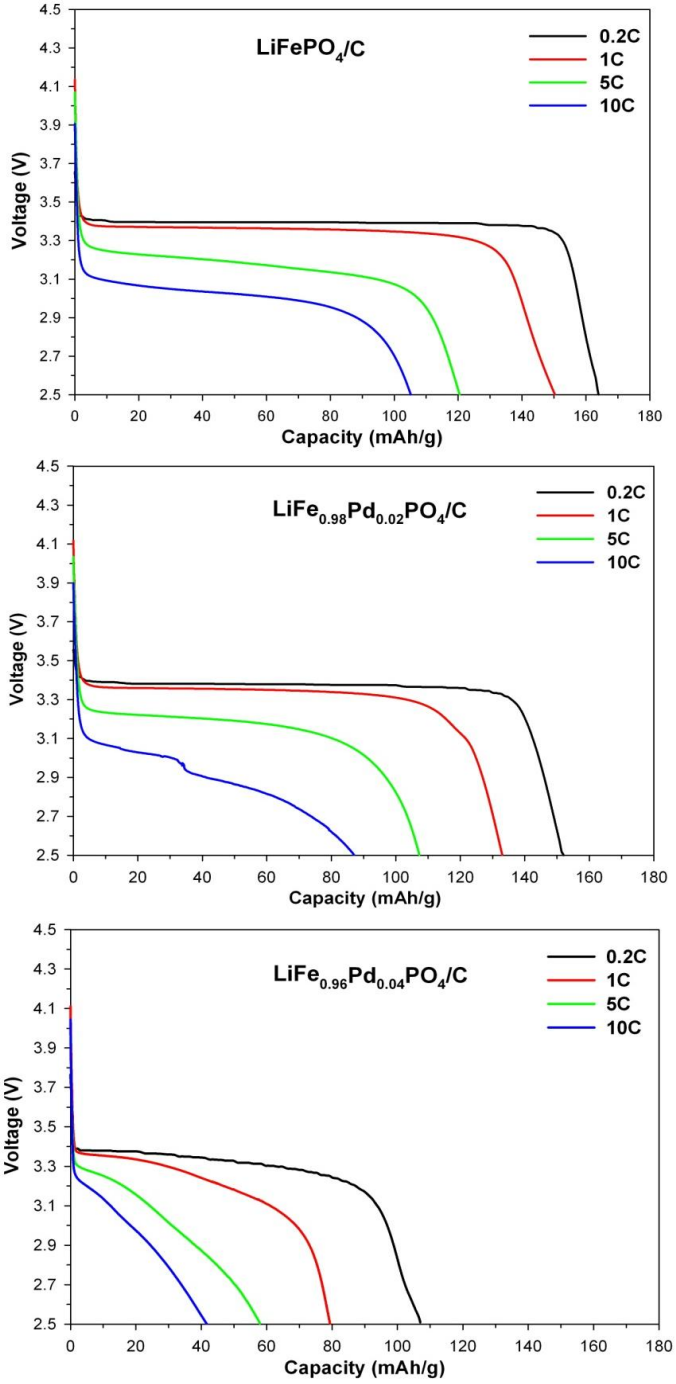

Figure 5-5: Discharge curves for the $LiFePO_4/C$, $LiFe_{0.98}Pd_{0.02}PO_4/C$, and $LiFe_{0.96}Pd_{0.04}PO_4/C$ samples at various rates

In all three samples, the carbon contents in the final cathode materials were around 6.8 wt%. The effects of palladium doping on the electrochemical properties of $LiFePO_4$/C materials can be further investigated by cyclic voltammograms. Figure 5-6 shows the CV curves of $LiFePO_4$/C, $LiFe_{0.98}Pd_{0.02}PO_4$/C, and $LiFe_{0.96}Pd_{0.04}PO_4$/C samples between 2.5 and 4.2V at a scan rate of 0.1 mV/s. For all the samples, the oxidation/reduction peaks, attributed to the reaction of the Fe^{2+}/Fe^{3+} redox couple, were clearly observed. However, the $LiFePO_4$/C sample shows more symmetry in its anodic/cathodic peaks, and the peaks are sharper, suggesting better electrochemical properties. Although the $LiFe_{0.96}Pd_{0.04}PO_4$/C sample shows less separation between its anodic/cathodic peaks, the amount of current is very low in comparison with that of other samples. The results indicate that Li ion insertion and extraction can be achieved more easily in the $LiFePO_4$/C sample.

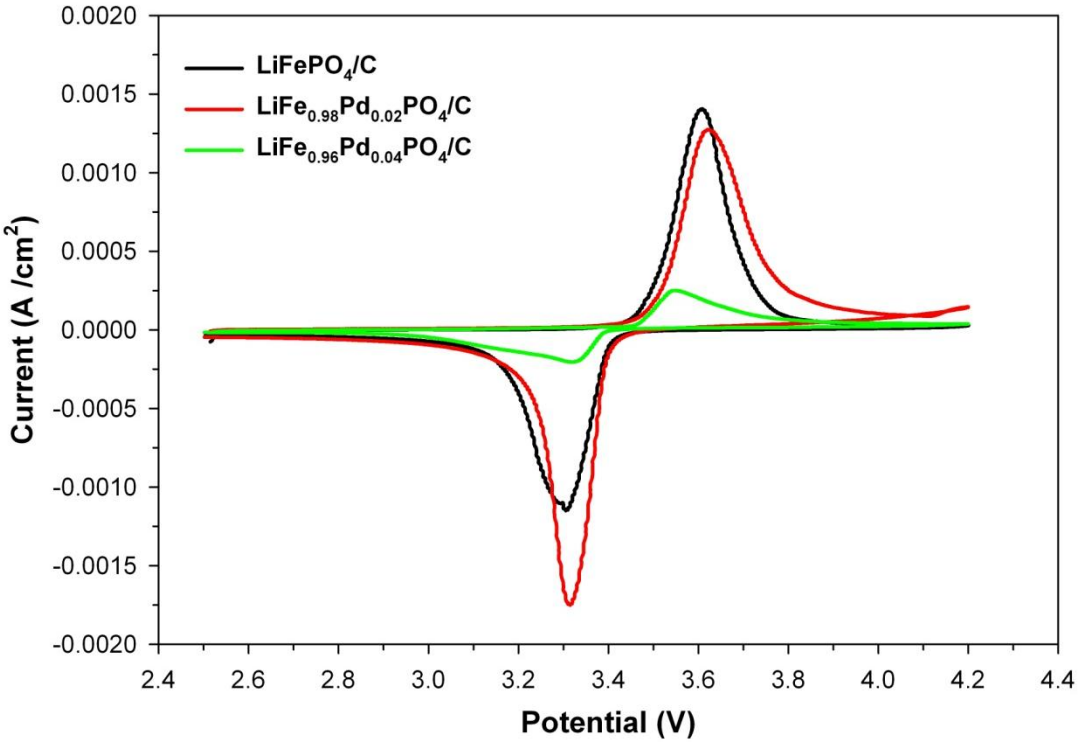

Figure 5-6: CV curves of the $LiFePO_4$/C, $LiFe_{0.98}Pd_{0.02}PO_4$/C, and $LiFe_{0.96}Pd_{0.04}PO_4$/C samples

The discharge cycling tests at various rates for the $LiFePO_4$/C, $LiFe_{0.98}Pd_{0.02}PO_4$/C, and $LiFe_{0.96}Pd_{0.04}PO_4$/C samples are shown in Figure 5-7. Here, the $LiFePO_4$/C sample can be seen to exhibit good capacity retention at various discharge rates. Moreover, its capacity can be completely recovered when the rate is decreased from 10 C to 0.2 C. However, capacity fading can be observed when the amount of palladium doping is increased, especially for the $LiFe_{0.96}Pd_{0.04}PO_4$/C sample in high-rate tests, which indicates poor cycling stability. The poor electrochemical performance and cycling of the Pd-doped samples, especially the $LiFe_{0.96}Pd_{0.04}PO_4$/C sample, can be attributed to the formation of the Li_3PO_4 impurity phase, shrinkage of the lattice parameters, agglomeration, and large particle size, which result in the difficulty of diffusing Li ions into the structure during the intercalation/de-intercalation process. However, this examination indicates that doping at the Fe site with Pd^{2+} does not improve the electrochemical properties of the $LiFePO_4$/C material for lithium ion battery applications.

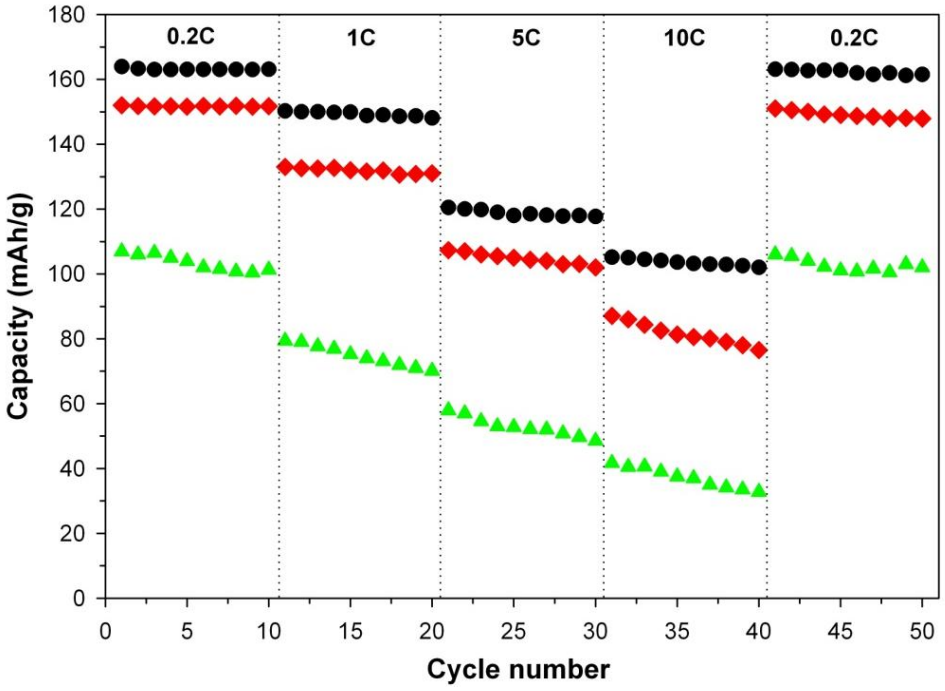

Figure 5-7: Cycling performance of the $LiFePO_4$/C (●), $LiFe_{0.98}Pd_{0.02}PO_4$/C (♦), and $LiFe_{0.96}Pd_{0.04}PO_4$/C (▲) samples at various discharge rates

5.1.4 Conclusions

$LiFePO_4$, $LiFe_{0.98}Pd_{0.02}PO_4$, and $LiFe_{0.96}Pd_{0.04}PO_4$ were synthesized using the sol-gel technique. XRD analysis indicates that the Li_3PO_4 impurity phase was detected for the Pd-doped samples, especially the $LiFe_{0.96}Pd_{0.04}PO_4$ sample, and that the lattice parameters of the Pd-doped samples decrease linearly as the amount of Pd^{2+} doping increases. Also, the particles become larger and they agglomerate following palladium incorporation, as shown in the SEM results. The electrochemical results show that the specific capacity of the $LiFePO_4$/C sample decreases with an increase in palladium content. The $LiFe_{0.96}Pd_{0.04}PO_4$/C sample show an unsuitable electrochemical performance and poor rate cycling between samples, which could be attributed to its shrinking lattice parameters, large particle size, and the Li_3PO_4 impurity phase. As a result, palladium doping using the sol-gel method has a negative impact in the chemical composition, structure and electrochemical behavior of the $LiFePO_4$/C cathode material.

References

[1] A.K. Padhi, K.S. Nanjundaswamy, J.B. Goodenough, Journal of The Electrochemical Society, 144, 1188 (1997).

[2] A. Yamada, S.C. Chung, K. Hinokuma Journal of The Electrochemical Society, 148, A224 (2001).

[3] Z.-R. Chang, H.-J. Lv, H.-W. Tang, H.-J. Li, X.-Z. Yuan, H. Wang, Electrochimica Acta, 54, 4595 (2009).

[4] S. Franger, F. Le Cras, C. Bourbon, H. Rouault Electrochemical and Solid-State Letters, 5, A231 (2002).

[5] Y.-N. Xu, S.-Y. Chung, J.T. Bloking, Y.-M. Chiang, W.Y. Ching, Electrochemical and Solid-State Letters, 7, A131 (2004).

[6] A. Kuwahara, S. Suzuki, M. Miyayama, Journal of Electroceramics, 24, 69 (2010).

[7] D.-H. Kim, J. Kim, Electrochemical and Solid-State Letters, 9, A439 (2006).

[8] N. Ravet, Y. Chouinard, J.F. Magnan, S. Besner, M. Gauthier, M. Armand, Journal of Power Sources, 97–98, 503 (2001).

[9] X. Zhou, F. Wang, Y. Zhu, Z. Liu, Journal of Materials Chemistry, 21, 3353 (2011).

[10] C.M. Doherty, R.A. Caruso, C.J. Drummond, Energy & Environmental Science, 3, 813 (2010).

[11] Z.-R. Chang, H.-J. Lv, H. Tang, X.-Z. Yuan, H. Wang, Journal of Alloys and Compounds, 501, 14 (2010).

[12] M. Wagemaker, B.L. Ellis, D. Lützenkirchen-Hecht, F.M. Mulder, L.F. Nazar, Chemistry of Materials, 20, 6313 (2008).

[13] W.L. Liu, J.P. Tu, Y.Q. Qiao, J.P. Zhou, S.J. Shi, X.L. Wang, C.D. Gu, Journal of Power Sources, 196, 7728 (2011).

[14] J. Ma, B. Li, H. Du, C. Xu, F. Kang, Journal of Solid State Electrochemistry, 16, 1 (2012).

[15] D. Arumugam, G. Paruthimal Kalaignan, P. Manisankar, Journal of Solid State Electrochemistry, 13, 301 (2009).

[16] X. Ou, G. Liang, L. Wang, S. Xu, X. Zhao, Journal of Power Sources, 184, 543 (2008).

[17] M.-R. Yang, W.-H. Ke, Journal of The Electrochemical Society, 155, A729 (2008).

[18] G.X. Wang, S. Bewlay, S.A. Needham, H.K. Liu, R.S. Liu, V.A. Drozd, J.-F. Lee, J.M. Chen, Journal of The Electrochemical Society, 153, A25 (2006).

[19] H. Liu, C. Li, Q. Cao, Y.P. Wu, R. Holze, Journal of Solid State Electrochemistry, 12, 1017 (2008).

[20] W.-J. Zhang, Journal of The Electrochemical Society, 157, A1040 (2010).

[21] D. Morgan, A. Van der Ven, G. Ceder, Electrochemical and Solid-State Letters, 7, A30 (2004).

[22] C. Ouyang, S. Shi, Z. Wang, X. Huang, L. Chen, Physical Review B, 69, 104303 (2004).

[23] M.S. Islam, D.J. Driscoll, C.A.J. Fisher, P.R. Slater, Chemistry of Materials, 17, 5085 (2005).

[24] S. Shi, L. Liu, C. Ouyang, D.-s. Wang, Z. Wang, L. Chen, X. Huang, Physical Review B, 68, 195108 (2003).

[25] C.Y. Ouyang, S.Q. Shi, Z.X. Wang, H. Li, X.J. Huang, L.Q. Chen, Journal of Physics: Condensed Matter, 16, 2265 (2004).

[26] D. Li, Y. Huang, D. Jia, Z. Guo, S.-J. Bao, Journal of Solid State Electrochemistry, 14, 889 (2010).

[27] Z.-H. Wang, L.-X. Yuan, J. Ma, L. Qie, L.-L. Zhang, Y.-H. Huang, Electrochimica Acta, 62, 416 (2012).

[28] J.B. Heo, S.B. Lee, S.H. Cho, J. Kim, S.H. Park, Y.S. Lee, Materials Letters, 63, 581 (2009).

[29] J. Hong, X.-L. Wang, Q. Wang, F. Omenya, N.A. Chernova, M.S. Whittingham, J. Graetz, The Journal of Physical Chemistry C, 116, 20787 (2012).

[30] Z.-H. Wang, Q.-Q. Pang, K.-J. Deng, L.-X. Yuan, F. Huang, Y.-L. Peng, Y.-H. Huang, Electrochimica Acta, 78, 576 (2012).

[31] R.-r. Zhao, I.M. Hung, Y.-T. Li, H.-y. Chen, C.-P. Lin, Journal of Alloys and Compounds, 513, 282 (2012).

[32] Y. Wang, Y. Yang, X. Hu, Y. Yang, H. Shao, Journal of Alloys and Compounds, 481, 590 (2009).

[33] H. Gao, L. Jiao, W. Peng, G. Liu, J. Yang, Q. Zhao, Z. Qi, Y. Si, Y. Wang, H. Yuan, Electrochimica Acta, 56, 9961 (2011).

[34] F. Lu, Y. Zhou, J. Liu, Y. Pan, Electrochimica Acta, 56, 8833 (2011).

[35] C.S. Sun, Y. Zhang, X.J. Zhang, Z. Zhou, Journal of Power Sources, 195, 3680 (2010).

[36] H. Liu, Q. Cao, L.J. Fu, C. Li, Y.P. Wu, H.Q. Wu, Electrochemistry Communications, 8, 1553 (2006).

[37] H.C. Shin, S.B. Park, H. Jang, K.Y. Chung, W.I. Cho, C.S. Kim, B.W. Cho, Electrochimica Acta, 53, 7946 (2008).

[38] S.-h. Wu, M.-S. Chen, C.-J. Chien, Y.-P. Fu, Journal of Power Sources, 189, 440 (2009).

[39] P. Axmann, C. Stinner, M. Wohlfahrt-Mehrens, A. Mauger, F. Gendron, C.M. Julien, Chemistry of Materials, 21, 1636 (2009).

[40] D.Y.W. Yu, K. Donoue, T. Kadohata, T. Murata, S. Matsuta, S. Fujitani, Journal of The Electrochemical Society, 155, A526 (2008).

[41] C.S. Sun, Z. Zhou, Z.G. Xu, D.G. Wang, J.P. Wei, X.K. Bian, J. Yan, Journal of Power Sources, 193, 841 (2009).

[42] G.A. Shafeev, J.-M. Themlin, L. Bellard, W. Marine, A. Cros, Journal of Vacuum Science & Technology A: Vacuum, Surfaces, and Films, 14, 319 (1996).

[43] D. Shanmukaraj, G.X. Wang, R. Murugan, H.K. Liu, Materials Science and Engineering: B, 149, 93 (2008).

5.2 Synthesis and characterization of Pt-doped $LiFePO_4$/C composites using the sol-gel method as the cathode material in lithium-ion batteries

M. Talebi-Esfandarani and O. Savadogo*

Laboratory of New Materials for Electrochemistry and Energy
École Polytechnque de Montréal,
C.P. 6079, Succ. Centre Ville, Montréal, QC
Canada, H3C 3A7

*Corresponding author: osavadogo@polymtl.ca, Phone: +1 514 3404725

Submitted to Journal of Applied Electrochemistry November 16, 2013

Abstract

$LiFePO_4$/C and $LiFe_{0.96}Pt_{0.04}PO_4$/C nanocomposite cathode materials were synthesised using the sol-gel method in a nitrogen atmosphere. The samples were characterised by x-ray diffraction (XRD), x-ray photoelectron spectroscopy (XPS), and scanning electron microscopy (SEM). Their electrochemical properties were investigated using galvanostatic charge/discharge tests, cyclic voltammetry (CV), and electrochemical impedance spectroscopy (EIS). The XRD results indicate that substituting iron with platinum does not destroy the structure of $LiFePO_4$, but expands the lattice parameters and enlarges the cell volume. The electrochemical results show that platinum doping improves the electrochemical performance of $LiFePO_4$/C particles owing to the expansion of the lattice structure, which provides more space for Li ion diffusion. The, larger lattice structure parameters of the $LiFe_{0.96}Pt_{0.04}PO_4$/C material result in a high discharge capacity

of 166, 156, 142, and 140 mAh/g at rates of 0.2C, 1C, 5C, and 10C respectively, as compared to 164, 150, 120, and 105 mAh/g for undoped $LiFePO_4$/C.

Keywords: $LiFePO_4$/C, sol-gel method, platinum doping.

5.2.1 Introduction

$LiFePO_4$ has been chosen as a promising candidate for cathode materials in lithium-ion battery applications because of features like low cost, abundance in nature, excellent thermal stability, non-toxicity, and high cyclability [1, 2]. However, pristine $LiFePO_4$ has its drawbacks as well: low intrinsic electrical conductivity and poor Li ion diffusion, which limit its application in large devices [3, 4]. Various strategies, including carbon coating, minimising the particle size, and element doping have been proposed to remedy these drawbacks [5-14].

Element doping has been confirmed to improve the intrinsic electrical conductivity of $LiFePO_4$ particles [13-15]. Moreover, a doped element causes lattice parameter expansion and enlargement of the cell volume, which induces lengthening and weakening of the Li–O bond with a lower energy barrier, and provide more space for Li ion diffusion. This facilitates Li ion movement in the $LiFePO_4$ structure, increases ionic conductivity, and improves the electrochemical performance of the $LiFePO_4$ material [16-18]. Furthermore, the doped element in the lattice structure can act as a pillar to prevent the collapse of the crystal structure during the charge/discharge process, which is indicative of good electrochemical performance [19, 20].

Generally speaking, there are two types of doping: at the lithium site (M_1), and at the iron site (M_2). However, in some cases, the exits of an immobile element doping at M_1 site probably block the diffusion channel of the Li ion [21]. Consequently, doping at the M_2 site might be a

better choice for enhancing Li ion diffusion. For some parameters, including physicoal-chemical properties, the amount of the doping element and the ionic radius must be taken into consideration. However, Nazar et al. report that the improved electrical conductivity is caused by the formation of a conductive film of Fe_2P on the doped samples, and not the doping element [22]. Also, theoretical studies indicate that element doping on $LiFePO_4$ is not useful [23], since $LiFePO_4$ has a one-dimensional Li ion diffusion pathway [24, 25] and also because the large amount of an unmoving doped element at the M_1 site may block the channel for Li ion diffusion and decrease electrochemical performance [26, 27]. However, various doping elements, such as Ti [9], Cu [10], La [18], Ru [19], Zn [20], Co [28], Na [29], V [30], Mg [31], etc, have been proposed to improve the electrochemical performance of $LiFePO_4$.

Up to now, the effect of platinum on the structure and electrochemical properties of $LiFePO_4$ has not been reported. In this paper, Pt-doped $LiFePO_4$ material is synthesised using the sol-gel method, and the effect of Pt doping on the structure and electrochemical properties of $LiFePO_4$/C is investigated.

5.2.2 Experimental

5.2.2.1 Synthesis of materials

The $LiFePO_4$ and $LiFe_{0.96}Pt_{0.04}PO_4$ samples were synthesised using the sol-gel method. The precursor materials were $Li(CH_3COO)$ (lithium acetate, Alfa Aesar), $Fe(NO_3)_3.9H_2O$ (iron nitrate, Sigma Aldrich), $H_2PtCl_6.6H_2O$ (hexachloroplatine, Alfa Aesar), H_3PO_4 (phosphoric acid, Anachemia), and $C_2H_4O_3$ (glycolic acid, Sigma Aldrich). For the synthesis of the $LiFePO_4$ sample, phosphoric acid was diluted in distilled water and metal precursors were added to the solution while stirring, until completely dissolved. The solution was mixed slowly with glycolic acid and the pH was adjusted to fall in the 8.5 to 9.5 range using ammonium hydroxide. The

solution was heated at 90°C while stirring, until a gel formed under a nitrogen atmosphere. After drying at 120°C in a vacuum oven for 48 h, the sample was annealed at 500°C for 10 h in a nitrogen flow to obtain $LiFePO_4$ powders. For the synthesis of the $LiFe_{0.96}Pt_{0.04}PO_4$ sample, 4 mol % of the iron nitrate was replaced by 4 mol % of hexachloroplatine. Finally, the pre-synthesised $LiFePO_4$ and $LiFe_{0.96}Pt_{0.04}PO_4$ samples were mixed with sucrose as the carbon source in a 70:30 weight ratio, followed by calcination at 700°C for 5 h in a nitrogen atmosphere to obtain a $LiFePO_4$/C and $LiFe_{0.96}Pt_{0.04}PO_4$/C composite.

5.2.2.2 Materials characterisation

The crystal structure and cell parameters of the samples were identified using an X-ray diffractometer (Philips X'pert) with CuKα radiation (λ=1.54056 A°). The oxidation states of the Fe and Pt ions were analysed by X-ray photoelectron spectroscopy (VG ESCALAB 3 MKII) with an Al Kα radiation source ($h\nu$=1486.6 eV). The data were calibrated with respect to the C Celgard 2400 1s peak at a fixed value of 285.0 eV. The morphology and particle size were examined by scanning electron microscopy (JSM-7600TFE). The carbon content of the samples was measured by carbon analyzer (LECO Co., CS 400).

5.2.2.3 Electrochemical characterisation

The composite cathode materials for the electrochemical tests were prepared by mixing 80% active material, 10% carbon black (Super C65-Timcal), and 10% poly vinylidene fluoride (PVDF) in N-methyl-2-pyrrolidone solvent. Then, the slurry was used to coat an aluminium foil current collector using the doctor blade technique and dried in vacuum oven overnight. The dried electrodes, with an area of 1.77 cm^2 and containing 2-4 mg of active materials, were used as the cathode material in the cells. The cells (2032) were assembled in an argon-filled glove box with lithium metal as the anode (as the counter and reference electrodes), and a Celgard 2400

separator. $LiPF_6$ (1M) in a 1:1 volume ratio of ethylene carbonate to dimethyl carbonate (LP30 from Merck) was used as the electrolyte. The charge/discharge test and cycling stability test were performed at different current rates over a 2.5-4.2V voltage range with the Solartron battery test analyser. Cyclic voltammetry (CV) was carried out using PAR273A in the potential ranges of 2.5-4.2V (vs. Li/Li^+) with scan rates of 0.1 mVs^{-1}. The electrochemical impedance spectrum (EIS) measurements were taken using the Solartron 1260 in a frequency range of 0.01Hz-1mHz at the discharge status of the cells.

5.2.3 Results and discussion

The XRD patterns for the $LiFePO_4$ and $LiFe_{0.96}Pt_{0.04}PO_4$ samples are shown in Figure 5-8. For both samples, the main diffraction peaks identify a single phase of $LiFePO_4$ olivine structure indexed by an orthorhombic space group of P_{mnb} (JCPDS 40-1499). The impurity phases, such as Li_3PO_4 and Fe_2P, were not detected for either sample. Li_3PO_4 has usually been reported as an

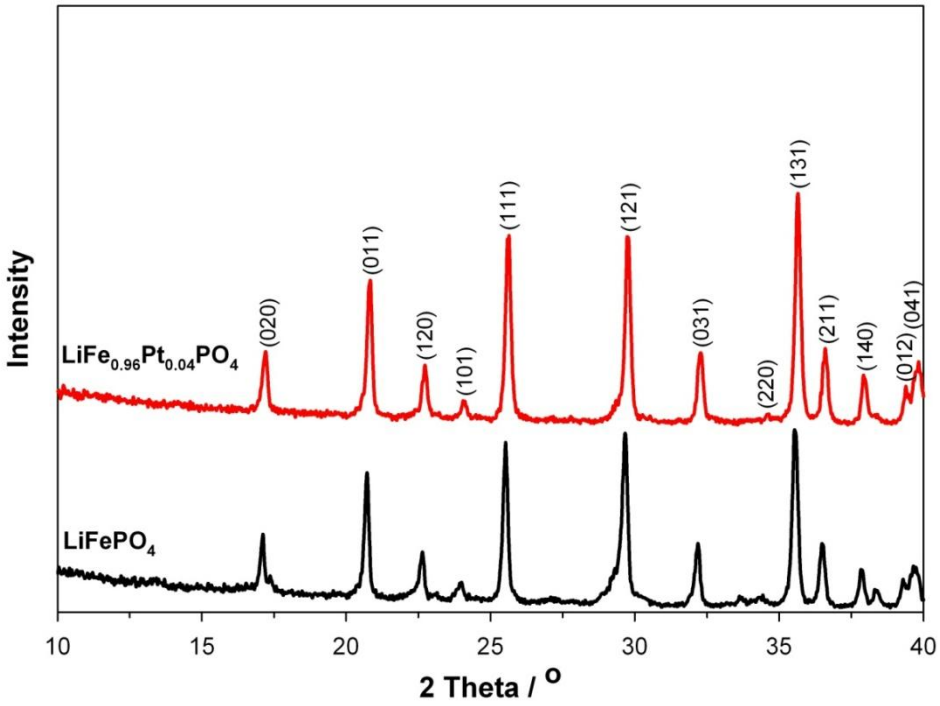

Figure 5-8: XRD patterns of $LiFePO_4$ and doped $LiFe_{0.96}Pt_{0.04}PO_4$ samples

impurity in doped $LiFePO_4$ samples, which reduces electrochemical performance [9, 14, 32]. For the $LiFe_{0.96}Pt_{0.04}PO_4$ samples, we observe an increase in the intensities of the diffraction peaks, indicating that platinum doping enhances the degree of crystallinity. Particles with well-shaped crystallinity are essential for enhancing the electrochemical performance of $LiFePO_4$ materials [2]. Considering the proper degree of crystallinity, the $LiFe_{0.96}Pt_{0.04}PO_4$ sample is expected to show enhanced electrochemical performances compared with $LiFePO_4$, which we explain in the electrochemical results section.

The lattice parameters of the samples, which were calculated from XRD patterns using Topas software, are summarized in Table 5-3. Owing to the Pt doping, the lattice parameters expand and the cell volume increases, indicating that the Pt has been successfully doped into the $LiFePO_4$ phase. Since the ionic radius of Pt^{2+} is larger than that of Fe^{2+}, it is reasonable that the lattice parameters increase with the doping of Pt^{2+} at the Fe^{2+} site. The expansion of the lattice parameters provides more space for Li ion diffusion and facilitates the movement of Li ions through the structure of the $LiFePO_4$ material during the intercalation and de-intercalation process. As a result, the electrochemical performance of the $LiFePO_4$ material is enhanced [9, 16, 17].

Table 5-3: The lattice parameters of both samples from XRD data

Sample	**a(Å)**	**b(Å)**	**c(Å)**	**V(Å^3)**
$LiFePO_4$	10.32408	6.00286	4.69050	290.689
$LiFe_{0.96}Pt_{0.04}PO_4$	10.32643	6.00533	4.69210	290.974

XPS analysis is a powerful technique for investigating the oxidation states of Fe and Pt for the $LiFePO_4$ and $LiFe_{0.96}Pt_{0.04}PO_4$ samples. XPS spectra in a wide range of binding energies are

shown for the two samples in Figure 5-9. The peaks corresponding to Fe 2p, O 1s, P 2p, and C 1s were detected for both samples, and are labeled as such in Figure 5-9. The binding energy for the Li 1s peak is overlapped by the Fe 3p peak (56 eV), which indicates that its binding energy and the approximation of the content of the element were prevented. It is worth noting that the Pt 4f peak was observed for the $LiFe_{0.96}Pt_{0.04}PO_4$ sample, as illustrated in Figure 5-9, confirming the presence of Pt in the doped sample.

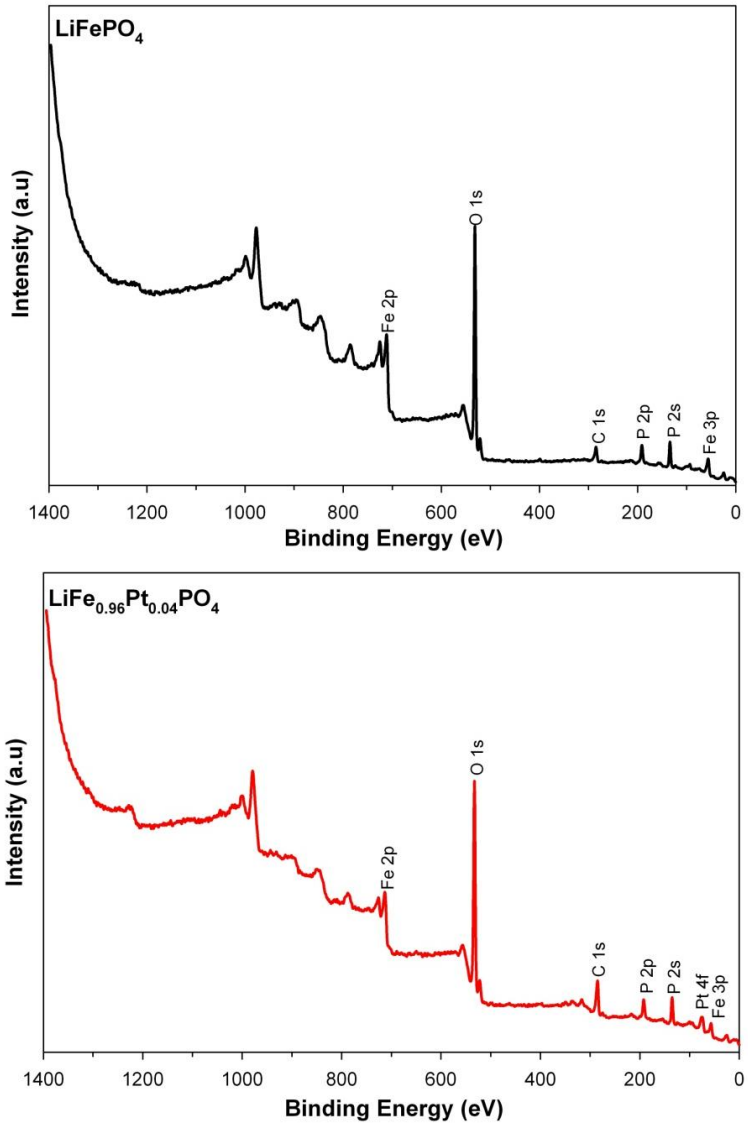

Figure 5-9: XPS spectra of $LiFePO_4$ and $LiFe_{0.96}Pt_{0.04}PO_4$ samples

Figure 5-10(a) shows the high resolution spectrum for the Pt 4f peak for the $LiFe_{0.96}Pt_{0.04}PO_4$ sample. It contains a doublet with binding energies of 72.4 eV and 75.5 eV, corresponding to the Pt 4f7/2 and Pt 4f5/2 lines respectively, and determining that the oxidation state of Pt in the doped sample is +2 [33]. This reveals that Pt^{4+} ions are partly changed into Pt^{2+} during the synthesis of the material, since the Pt precursor was in Pt^{4+} status. However, the ionic radius of Pt^{2+} (80Å) is larger than that of Pt^{4+} (62.5Å). Owing to the reduction of Pt^{4+} to Pt^{2+} with its larger ionic radius, it can expand the lattice parameters and enlarge the cell volume, which is compatible with the XRD result. In order to investigate the effect of Pt doping on the binding energy and oxidation state of Fe, the high resolution spectra of the Fe 2p peak for the two samples were compared, as shown in Figure 5-10(b). The $LiFePO_4$ samples contain Fe 2p3/2 (710.9 eV) and Fe 2p1/2 (724 eV) peaks, indicating that the oxidation state of the Fe is +2 [28, 34]. For the doped sample, the Fe 2p3/2 (710.6 eV) and the Fe 2p1/2 (724 eV) peaks show a little shift in comparison with those of the $LiFePO_4$ sample, but Pt doping does not significantly change the valence of Fe^{2+}.

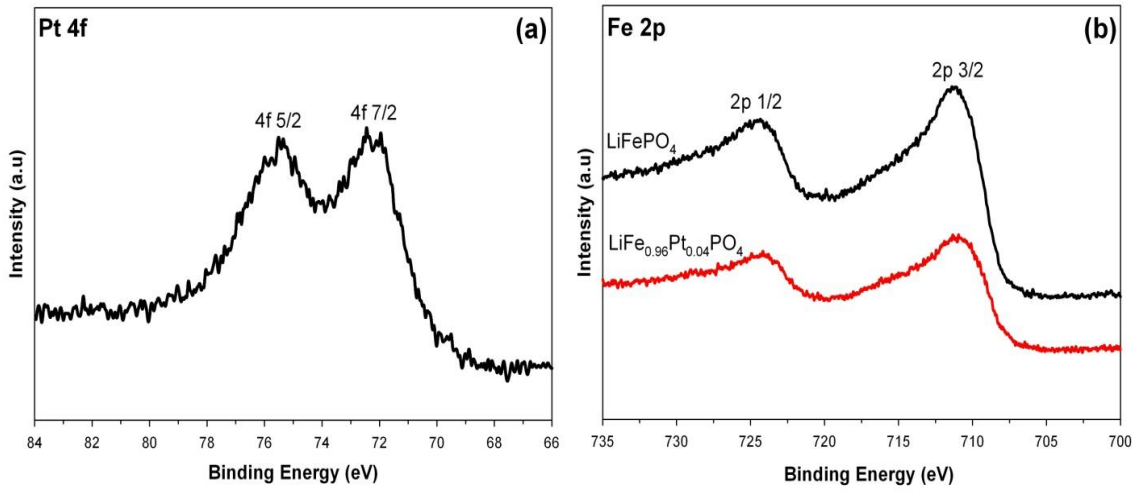

Figure 5-10: (a) XPS core level of Pt 4f for $LiFe_{0.96}Pt_{0.04}PO_4$ sample. (b) XPS core levels of Fe 2p for both samples

Figure 5-11 illustrates the SEM images of the $LiFePO_4$ and $LiFe_{0.96}Pt_{0.04}PO_4$ samples. The $LiFePO_4$ materials consist of small homogenous particles 100-500 nm in size, as shown in Fig. 5-11(a,b). As can be seen in Figure 5-11(c,d), the $LiFe_{0.96}Pt_{0.04}PO_4$ particles are more homogeneous, and a more uniform particle in terms of size distribution is achieved for the doped samples. The size of the particles for the doped sample is in the 100-200 nm range. The noticeable change in terms of refining and homogenising the size of the particles could be related to the presence of Pt during synthesis in the doped sample. The use of small, homogeneous particles is a known strategy for improving the electrochemical properties of the $LiFePO_4$ material, because of the short diffusion path of the Li ions during the redox reaction [8, 11, 35, 36]. Therefore, an excellent electrochemical performance for the doped sample is expected.

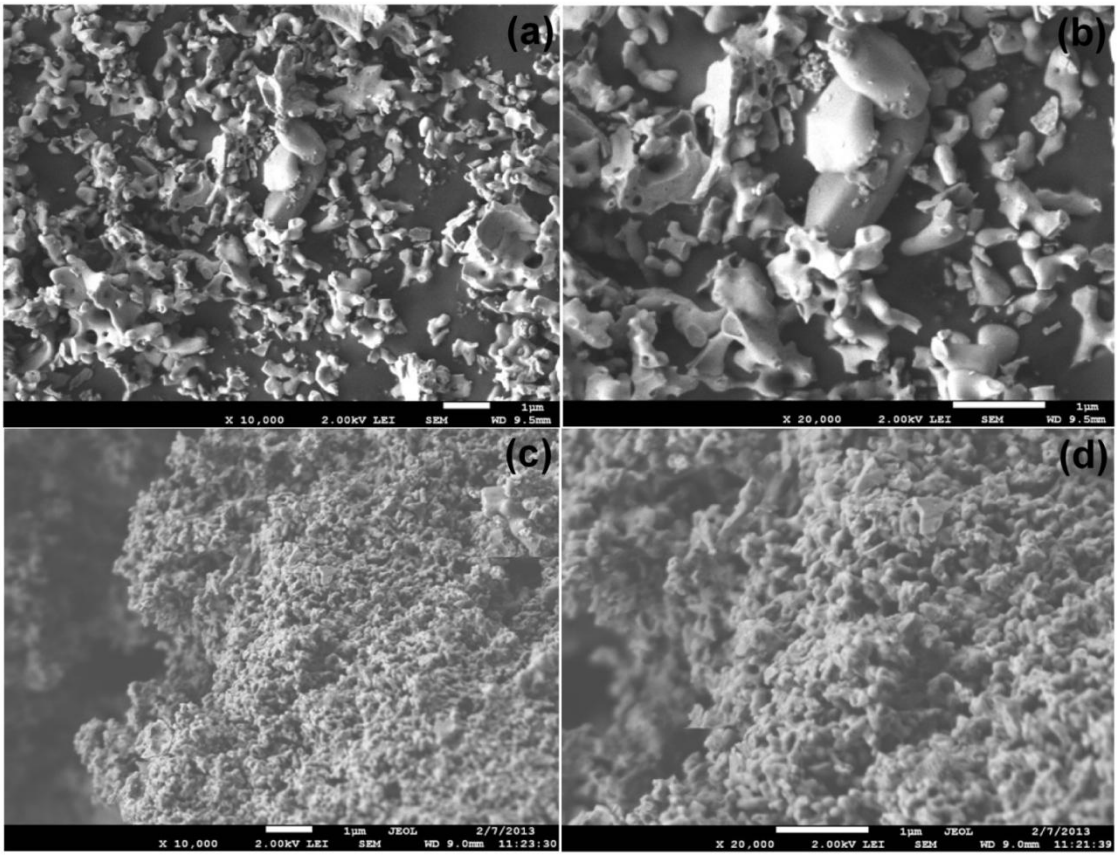

Figure 5-11: Low magnification and high magnification SEM images of $LiFePO_4$ (a,b), and $LiFe_{0.96}Pt_{0.06}PO_4$ (c,d) samples

Figure 5-12 compares the discharge curves of the $LiFePO_4$/C and $LiFe_{0.96}Pt_{0.04}PO_4$/C samples at different C-rates. The $LiFePO_4$/C sample shows a flat voltage plateau at around 3.4 V at low rates, which can be attributed to a two phase Fe^{3+}/Fe^{2+} redox process between $FePO_4$ and $LiFePO_4$ [1].

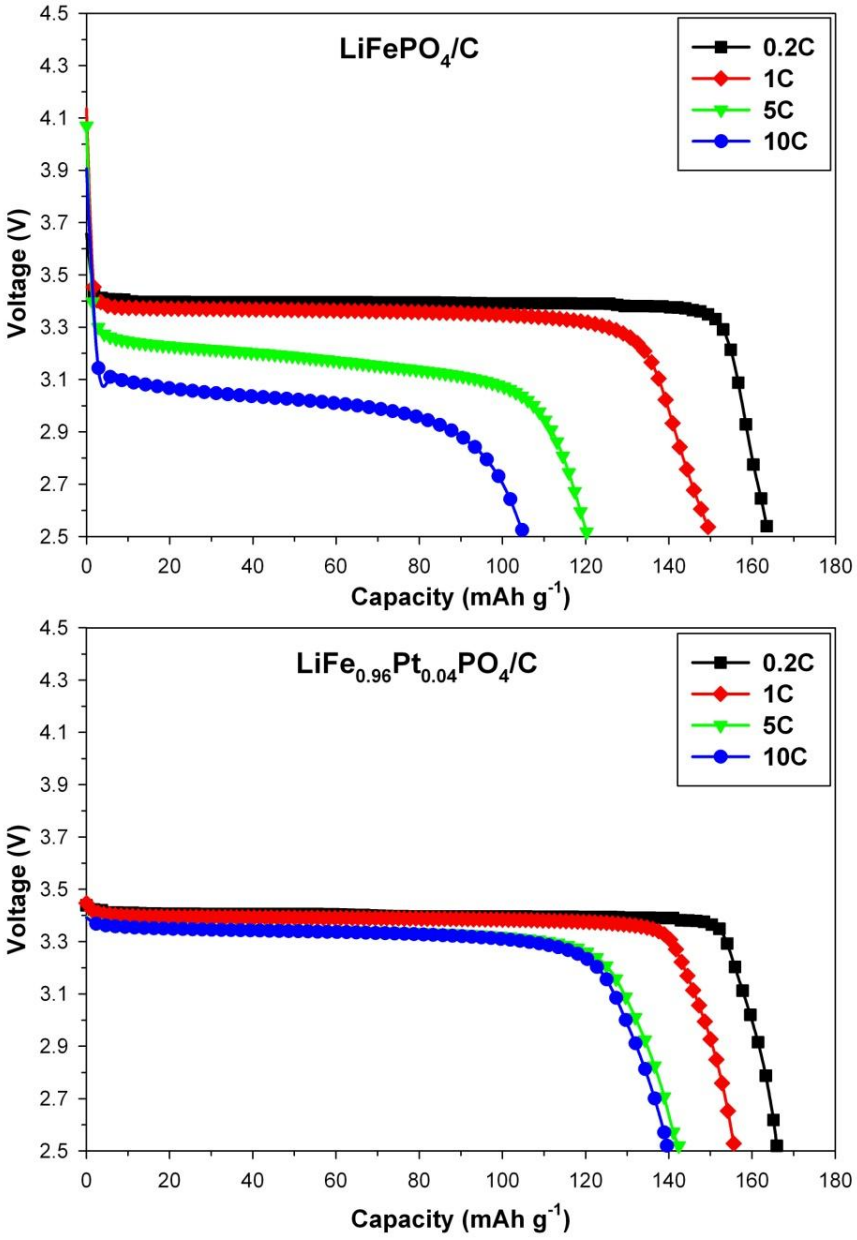

Figure 5-12: The discharge curves of $LiFePO_4$/C and $LiFe_{0.96}Pt_{0.04}PO_4$/C samples at various current rates

We can see that the discharge capacity of the $LiFePO_4$/C sample was strongly affected by the C-rate. The $LiFePO_4$/C sample achieves the specific capacity of 164, 150, 120, and 105 mAh/g at the rates of 0.2C, 1C, 5C, and 10C respectively. The discharge capacity for the $LiFe_{0.96}Pt_{0.04}PO_4$/C sample increases to 166, 156, 142, and 140 mAh/g at rates of 0.2C, 1C, 5C, and 10C, respectively. Furthermore, the $LiFe_{0.98}Pt_{0.02}PO_4$/C sample shows flatter plateaus than the $LiFePO_4$/C sample at high current rates, which confirms the lower polarization for the doped sample. The content of the remaining carbon for both samples was around 6.8 wt % which measured by carbon analyzer (LECO). The increase in specific capacity can be related to the enhanced mobility of the Li ion for the doped sample. As shown in Table 5-3, Pt doping causes enlargement and expansion of the lattice parameters, providing more space for the transfer of Li ions and facilitating Li ion diffusion into the $LiFePO_4$ structure, which is consistent with other reports [9, 16, 29]. Therefore, the Li ion movement in the $LiFePO_4$ structure is faster, resulting in increased discharge capacities. Also, the uniform particle size distribution could offset the barrier to the sluggish charge transport of phosphate [2] and would enhance the utilisation ratio of the active materials, improving electrochemical performance. This is attributed to the refinement of the particle size of $LiFePO_4$ materials and which we observed in the SEM results for the doped sample.

Figure 5-13 shows the CV curves of the $LiFePO_4$/C and $LiFe_{0.96}Pt_{0.04}PO_4$/C samples at a scanning rate of 0.1 mV/s over a voltage range of 2.5-4.2 V. For both samples, the clear oxidation-reduction peaks consist of a two phase redox reaction of Fe^{2+}/Fe^{3+} in $LiFePO_4$ [10]. However, the $LiFe_{0.96}Pt_{0.04}PO_4$/C sample shows sharper and larger redox peaks with higher current, which can be attributed to an improvement in the Li ion's diffusion velocity. Also, the potential separation between the oxidation-reduction peaks in the $LiFe_{0.96}Pt_{0.04}PO_4$/C sample is

smaller than that in the $LiFePO_4$/C sample, suggesting lower polarization and better reversibility for the electrochemical reaction.

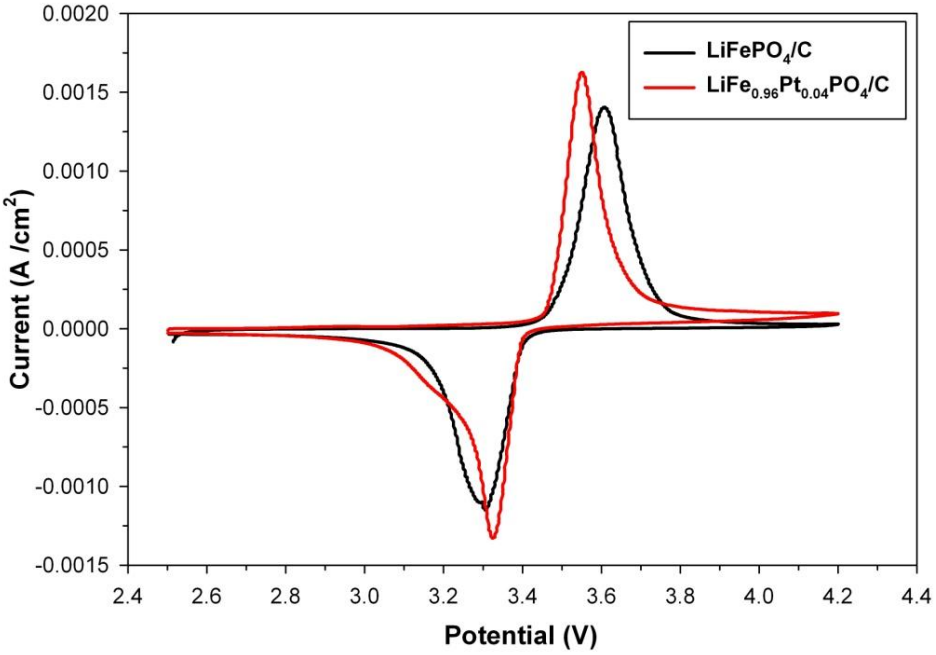

Figure 5-13: The CV curves of $LiFePO_4$/C and $LiFe_{0.96}Pt_{0.04}PO_4$/C samples at the scanning rate 0.1 mV/s

The details of the potential values and the peak current density of the redox reactions from the CV results are listed in Table 5-4. The well-defined peaks and the potential separation of the smaller peaks suggest that the electrochemical properties are improved by Pt doping.

Table 5-4: The oxidation peak potential (Eox), the reduction peak potential (Ered), potential separation (ΔE) and current density of redox reactions for the CV result in Figure 5-13

Sample	**E_{ox} (V)**	**E_{red} (V)**	**ΔE(V)**	**i_p(Ox) (mA/cm^2)**	**i_p(Red) (mA/cm^2)**
$LiFePO_4$/C	3.60	3.30	0.30	1.40	1.15
$LiFe_{0.96}Pt_{0.04}PO_4$/C	3.55	3.32	0.22	1.63	1.33

For further electrochemical investigation, EIS was carried out for the two samples in the full discharge state of the cells, as shown in Figure 5-14. Both samples exhibit a depressed semicircle in the high frequency region and a straight line in the low frequency region. An intercept at high frequency at the Z' axis corresponds to the resistance of the electrolyte (R_e). The numerical value of the diameter of the semicircle on the Z' axis in the middle frequency range is attributed to the charge transfer resistance (R_{ct}). The straight line in the low frequency range indicates the presence of Warburg impedance (Z_w), which is associated with Li ion diffusion. The CPE represents the double layer capacitance and passivation film capacitance. An equivalent circuit is used to fit the impedance spectra, as shown in the inset in Figure 5-14.

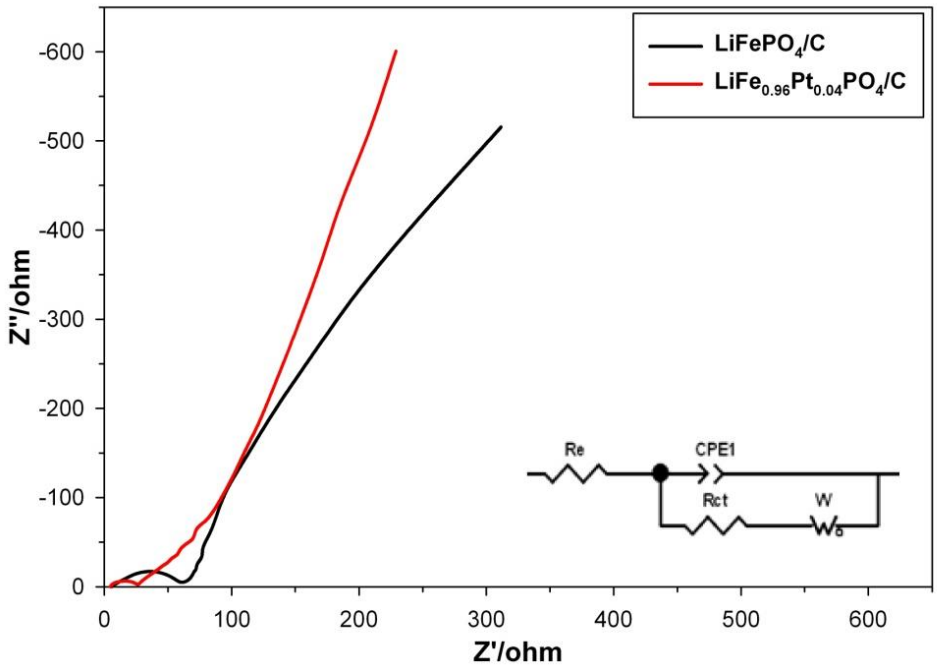

Figure 5-14: EIS spectra of $LiFePO_4/C$ and $LiFe_{0.96}Pt_{0.04}PO_4/C$ samples. The inset shows an equivalent circuit of the electrode

The fitted impedance parameters are listed in Table 5-5. The charge transfer resistances (Rct) of the $LiFePO_4$/C and $LiFe_{0.96}Pt_{0.04}PO_4$/C samples are 52.27 Ω and 15.00 Ω respectively. The charge transfer resistance correlates to the reaction between the active materials and the electrolyte [37, 38]. The smaller resistance shows a greater possibility of Li ion movement and electron transfer on the electrode materials, so that a decrease in charge transfer resistance is beneficial during the intercalation/de-intercalation process, and enhances electrochemical performance [39]. Therefore, the electrochemical properties of $LiFePO_4$/C can be improved by Pt doping, which is consistent with the CV results.

Table 5-5: Impedance parameters of samples based on the equivalent circuit as inset in the Figure 5-14

Sample	$\mathbf{R_e(\Omega)}$	$\mathbf{R_{ct}(\Omega)}$	$\boldsymbol{CPE_1}$
$LiFePO_4$/C	5.67	52.27	0.6
$LiFe_{0.96}Pt_{0.04}PO_4$/C	4.68	15.00	0.7

The cycling stability of the $LiFePO_4$/C and $LiFe_{0.96}Pt_{0.04}PO_4$/C samples at different C-rates is shown in Figure 5-15. The cells for both samples were charged at a constant current of 1C between 2.5-4.2 V, and discharged at different C-rates. For the $LiFe_{0.96}Pt_{0.04}PO_4$/C sample, we observed no obvious capacity fading over cycling at different rates, even at 10 C, which indicates good cycling performance and rate capability. But, for the $LiFePO_4$/C sample, a little capacity loss is observed at a high rate. Globally, the better electrochemical properties and cycling performance for the doped sample is attributed to good crystallinity, expansion of the lattice parameters, uniform particle distribution, and improved Li ion diffusion as a result of platinum doping.

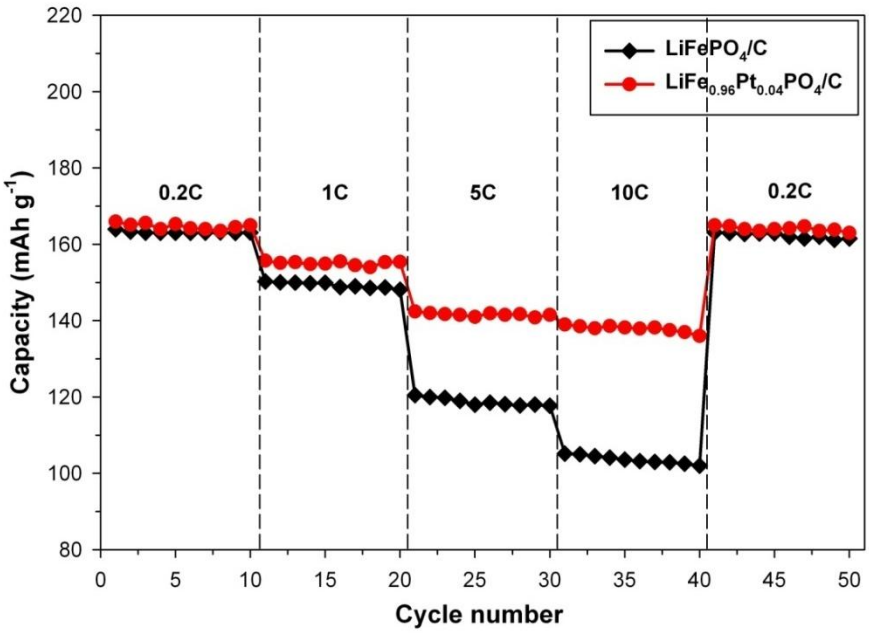

Figure 5-15: Cycling performance of $LiFePO_4/C$ and $LiFe_{0.96}Pt_{0.04}PO_4/C$ samples at different discharge rates

5.2.4 Conclusions

The structural and electrochemical properties $LiFePO_4$/C and $LiFe_{0.96}Pt_{0.04}PO_4$/C nanocomposite cathode materials prepared using the sol-gel method were investigated. Pt doping caused lattice expansion and cell volume enlargement, providing more space for the movement of Li ions and facilitating Li ion diffusion into the $LiFePO_4$ crystal structure. In addition, a uniform particle size distribution was observed for the Pt-doped sample. The improvement in electrochemical performance can be attributed to lattice parameter expansion, uniform particle distribution, and Li ion diffusion enhancement brought about by platinum doping.

References

1. Padhi AK, Nanjundaswamy KS, Goodenough JB (1997) Journal of The Electrochemical Society 144:1188
2. Yamada A, Chung SC, Hinokuma K (2001) Journal of The Electrochemical Society 148:A224
3. Franger S, Le Cras F, Bourbon C, Rouault H (2002) Electrochemical and Solid-State Letters 5:A231
4. Xu Y-N, Chung S-Y, Bloking JT, Chiang Y-M, Ching WY (2004) Electrochemical and Solid-State Letters 7:A131
5. Zhou X, Wang F, Zhu Y, Liu Z (2011) Journal of Materials Chemistry 21:3353
6. Su F-Y, You C, He Y-B, Lv W, Cui W, Jin F, Li B, Yang Q-H, Kang F (2010) Journal of Materials Chemistry 20:9644
7. Doherty CM, Caruso RA, Drummond CJ (2010) Energy & Environmental Science 3:813
8. Kim D-H, Kim J (2006) Electrochemical and Solid-State Letters 9:A439
9. Wu S-h, Chen M-S, Chien C-J, Fu Y-P (2009) Journal of Power Sources 189:440
10. Heo JB, Lee SB, Cho SH, Kim J, Park SH, Lee YS (2009) Materials Letters 63:581
11. Yang J, Xu JJ (2006) Journal of The Electrochemical Society 153:A716
12. Kuwahara A, Suzuki S, Miyayama M (2010) Journal of Electroceramics 24:69
13. Ravet N, Chouinard Y, Magnan JF, Besner S, Gauthier M, Armand M (2001) Journal of Power Sources 97–98:503
14. Chung S-Y, Bloking JT, Chiang Y-M (2002) Nat Mater 1:123
15. Chen J, Vacchio MJ, Wang S, Chernova N, Zavalij PY, Whittingham MS (2008) Solid State Ionics 178:1676
16. Yang M-R, Ke W-H (2008) Journal of The Electrochemical Society 155:A729
17. Liu H, Li C, Cao Q, Wu YP, Holze R (2008) J Solid State Electrochem 12:1017
18. Luo S, Tian Y, Li H, Shi K, Tang Z, Zhang Z (2010) Journal of Rare Earths 28:439
19. Wang Y, Yang Y, Hu X, Yang Y, Shao H (2009) Journal of Alloys and Compounds 481:590
20. Shenouda AY, Liu HK (2009) Journal of Alloys and Compounds 477:498
21. Ellis BL, Lee KT, Nazar LF (2010) Chemistry of Materials 22:691
22. Herle PS, Ellis B, Coombs N, Nazar LF (2004) Nat Mater 3:147
23. Islam MS, Driscoll DJ, Fisher CAJ, Slater PR (2005) Chemistry of Materials 17:5085
24. Morgan D, Van der Ven A, Ceder G (2004) Electrochemical and Solid-State Letters 7:A30
25. Ouyang C, Shi S, Wang Z, Huang X, Chen L (2004) Physical Review B 69:104303

26. Ouyang CY, Shi SQ, Wang ZX, Li H, Huang XJ, Chen LQ (2004) Journal of Physics: Condensed Matter 16:2265

27. Li D, Huang Y, Jia D, Guo Z, Bao S-J (2010) J Solid State Electrochem 14:889

28. Zhao R-r, Hung IM, Li Y-T, Chen H-y, Lin C-P (2012) Journal of Alloys and Compounds 513:282

29. Yin X, Huang K, Liu S, Wang H, Wang H (2010) Journal of Power Sources 195:4308

30. Hong J, Wang X-L, Wang Q, Omenya F, Chernova NA, Whittingham MS, Graetz J (2012) The Journal of Physical Chemistry C 116:20787

31. Liu Z, Zhang X, Hong L (2009) J Appl Electrochem 39:2433

32. Axmann P, Stinner C, Wohlfahrt-Mehrens M, Mauger A, Gendron F, Julien CM (2009) Chemistry of Materials 21:1636

33. Bancroft GM, Adams I, Coatsworth LL, Bennewitz CD, Brown JD, Westwood WD (1975) Analytical Chemistry 47:586

34. Sun CS, Zhou Z, Xu ZG, Wang DG, Wei JP, Bian XK, Yan J (2009) Journal of Power Sources 193:841

35. Sanchez MAE, Brito GES, Fantini MCA, Goya GF, Matos JR (2006) Solid State Ionics 177:497

36. Guo ZP, Liu H, Bewlay S, Liu HK, Dou SX (2003) J. New. Mat. Electrochem. Systems 6:259

37. Liu J, Jiang R, Wang X, Huang T, Yu A (2009) Journal of Power Sources 194:536

38. Molenda J, Ojczyk W, Marzec J (2007) Journal of Power Sources 174:689

39. Kim J-K, Choi J-W, Chauhan GS, Ahn J-H, Hwang G-C, Choi J-B, Ahn H-J (2008) Electrochimica Acta 53:8258

CHAPTER 6 ARTICLES 4 AND 5: SUMMARY OF DOPING WITH HYDROTHERMAL METHOD

This chapter consists of the following two publications;

1. Synthesis and characterization of palladium doped $LiFePO_4/C$ nano composites using hydrothermal method for Li-ion batteries application

2. Enhancement of electrochemical properties of Platinum doped $LiFePO_4/C$ cathode material synthesized using hydrothermal method

6.1 Synthesis and characterization of palladium doped $LiFePO_4$/C nano composites using hydrothermal method for Li-ion batteries applications

M. Talebi-Esfandarani and O. Savadogo*

Laboratory of New Materials for Electrochemistry and Energy

École Polytechnque de Montréal,

C.P. 6079, Succ. Centre Ville, Montréal, QC, Canada, H3C 3A7

*Corresponding author: osavadogo@polymtl.ca, Phone: +1 514 3404725

Submitted in Electrochimica Acta, November 19, 2013

Abstract

$LiFe_{1-x}Pd_xPO_4$ (x = 0.00, 0.02, 0.04) nano-composite cathode materials were synthesized using hydrothermal method. The samples were characterized by XRD, SEM, BET, XPS, and their electrochemical properties were investigated using discharge capability, cyclic voltammetry (CV) and electrochemical impedance spectroscopy (EIS). The XRD and XPS results indicate that the palladium has been successfully doped into the $LiFePO_4$ structure. The results indicate that the optimized palladium doping reduces the particle size and facilitates the Li-ion diffusion, improving the electrochemical properties of $LiFePO_4$. Electrochemical results show that the $LiFe_{0.98}Pd_{0.02}PO_4$/C sample delivers the discharge capacity of 167, 159, 130, 93, 70 mAh/g at 0.1C, 0.2C, 1C, 5C and 10C rates, respectively. In comparison the discharge capacity of the non-Pd-doped $LiFePO_4$/C sample is smaller and is respectively 117, 104, 83, 63 and 47 mAh/g for the corresponding rates. However, by increasing the palladium content, the electrochemical

performances decrease due to the formation of Li_3PO_4 impurity and the difficulty of the Li-ion diffusion during the redox reaction.

Keywords: $LiFePO_4$/C, hydrothermal method, palladium doping, lithium ion diffusion.

6.1.1 Introduction

Since the first paper on the utilization of $LiFePO_4$ as cathode material Li-batteries in 1997[1], it has attracted much attention as a candidate for new generation of Li-ion batteries due to its good thermal stability, being environmentally friendly and inexpensive [1-3]. However, $LiFePO_4$ suffers from its low electronic conductivity and poor Li^+ diffusion mobility, resulting in a low rate capability [1]. Various efforts have been proposed to solve its drawbacks such as coating with conductive carbon layer [4, 5], decreasing the size of particles [6, 7] and doping with some elements [8, 9]. It has been proved that a uniform carbon coating and the particles size minimizing are effective methods for improving the electrochemical performance of $LiFePO_4$ materials [3-5, 10]. However, there are controversial results about the effect of element doping [3, 11]. Nazar et al. reported that increasing the electrical conductivity is due to the Fe_2P conductive film for the doped samples and is not because of the doping element [11]. Theoretical studies reported by Islam's group [12, 13] and Cedar's group [14] showed that element doping is not favorable since one-dimensional Li diffusion channel might be blocked by dopant element at Li site, reducing the Li-ion diffusion rates [15, 16]. Therefore, doping at Fe site can be an alternative option to avoid blocking of diffusion channel [17, 18].

Despite of these arguments, many studies have reported the improvement of electrochemical properties of $LiFePO_4$ by different element doping [18-26]. Doped agent has been confirmed to enhance the intrinsic electrical conductivity of $LiFePO_4$ bulk particles [20, 21]. Furthermore,

doped element causes lengthening and weakening of Li–O bond with a lower energy barrier due to the lattice parameters expansion and enlargement of the cell volume in the $LiFePO_4$ structure, facilitating Li ion diffusion and enhancing electrochemical performance [22-24]. In addition, Liu and other researchers reported that the doped element in the structure can act as a pillar and protect the crystal structure of $LiFePO_4$ material from shrinking and collapsing during charge/discharge process, indicating good cycling capability [25-27].

However, in order to prepare the $LiFePO_4$ material, various methods have been employed such as hydrothermal, solid state, sol-gel, solvothermal and etc [28-34]. In addition, many parameters including the phase purity, crystal structure, morphology and particle sizes must be controlled during the preparation which can affect the electrochemical properties of $LiFePO_4$ material [29-35].

We have recently reported the doping of palladium on the $LiFePO_4$ material prepared with sol-gel method. Nevertheless, the electrochemical performance of $LiFePO_4$ material reduces due to the formation of Li_3PO_4 in the doped samples. In this work, for a comparison, the Pd-doped $LiFePO_4$ samples synthesized with hydrothermal method and the effect of palladium on the structure and electrochemical properties of materials were examined.

6.1.2 Experimental

6.1.2.1 Synthesis of materials

The starting materials were $FeSO_4 \cdot 7H_2O$, H_3PO_4 (85 wt. %), $LiOH \cdot H_2O$ and Pd $(NO_3)_2.2H_2O$. To synthesize $LiFePO_4$, $LiFe_{0.98}Pd_{0.02}PO_4$ and $LiFe_{0.96}Pd_{0.04}PO_4$ materials via a hydrothermal method, a stoichiometric amounts of H_3PO_4, $FeSO_4 \cdot 7H_2O$ and Pd $(NO_3)_2.2H_2O$ were dissolved in the mixture of ethylene glycol and deionized water (50/50, v/v) as a reaction medium under

magnetic stirring in a nitrogen atmosphere. Hydrazine was added to the mixture as reducing agent to minimize the oxidation of Fe^{2+} to Fe^{3+}. $LiOH{\cdot}H_2O$ was separately dissolved in the deionized water and then added to the above mixture dropwise under magnetic stirring in a nitrogen atmosphere. The pH of the solution was adjusted to 6 by adding H_3PO_4. The dissolved solutions were mixed together homogeneously with strong stirring. The resulting mixture was quickly transferred to a Teflon-lined stainless steel autoclave and sealed and heated at 190 °C for 6 h. Afterward, it was cooled down to room temperature. The precipitate was obtained by suction filtration and washing several times with deionized water and acetone, followed by drying at 70 °C in a vacuum oven for overnight to obtain product. For electrochemical properties evaluation, the pre-synthesized samples were mixed with sucrose as carbon source, and annealed at 700 °C for 5 h under a nitrogen atmosphere to obtain the $LiFePO_4$/C, $LiFe_{0.98}Pd_{0.02}PO_4$/C and $LiFe_{0.96}Pd_{0.04}PO_4$/C composites. Annealing were done in order to carbonize the sucrose completely and to increase the crystallinity of the samples.

6.1.2.2 Material characterization

The crystal structure of samples was analyzed using x-ray diffractometer (Philips X'pert) with CuKα radiation source (λ=1.54056 A°). The oxidation state information of Fe and Pd ions was investigated using x-ray photoelectron spectroscopy (VG ESCALAB 3 MKII) with Al Kα radiation source (*hv*=1486.6 eV). The data were calibrated using P2p3/2 peak at value of 133.8 eV. The morphology of samples was observed by scanning electron microscope (JSM-7600TFE). The specific surface area of samples was obtained by Brunauer-Emmett-Teller (BET) technique (Autosorb-1, Quantachrome instruments) with nitrogen as adsorption gas. The carbon content of the samples was determined using C-detctor (LECO Co., CS 400).

6.1.2.3 Electrochemical characterization

The cathode electrodes were prepared by mixing active material with carbon black (Super C65-Timcal) and poly vinylidene fluoride (PVDF) in a weight ratio of 80:10:10 in N-methyl-2-pyrrolidone solvent to obtain homogeneous slurry and then the slurry was coated onto aluminum foil using Doctor-blade technique. Then, the coated film was dried in a vacuum oven for overnight and cut into circles with diameter of 15 mm as cathode side. The electrochemical measurements were carried out with CR2032 cells. The lithium metal was used as anode; and electrolyte was 1 $molL^{-1}$ $LiPF_6$ in ethylene carbonate-dimethyl carbonate (EC/DMC, 1:1 by vol) and a microporous monolayer polypropylene (Celgard 2400) as separator. The cells were assembled in the argon-filled glove box. Charge/discharge test at various rates were performed between 2.5 and 4.2V (vs. Li/Li^+) on Solartron battery test analyzer and Cell test software. Cyclic voltammetry (CV) studies were carried out using PAR273A in the potential ranges of 2.5-4.2V (vs. Li/Li^+) at scan rates of 0.1 mV/s. The electrochemical impedance spectrum (EIS) measurements were performed in frequency range of 0.01 Hz-1 mHz at discharge status of all the cells. All the electrochemical measurements were performed at ambient temperature.

6.1.3 Results and discussion

The XRD patterns of the $LiFePO_4$, $LiFe_{0.98}Pd_{0.02}PO_4$ and $LiFe_{0.96}Pd_{0.04}PO_4$ samples are shown in Figure 6-1(a). For all the samples, the main diffraction peaks can be indexed to a $LiFePO_4$ phase with an orthorhombic structure, space group of P_{mnb} according to JCPDS #40-1499. However, as shown in Figure 6-1(b), the $LiFe_{0.96}Pd_{0.04}PO_4$ sample contains unwanted phase of Li_3PO_4 impurity because of high Pd concentration and unfavorable results appear as reported in our previous work [36]. Li_3PO_4 is usually reported as impurity phase in doped $LiFePO_4$ samples [3, 9] and reduces the electrochemical performance of $LiFePO_4$ because of acting as inactive and

inert mass [37, 38]. The refined lattice parameters were calculated and are shown in Figure 6-2. As show in Figure 6-2, the b and c lattice parameters and the cell volume decrease linearly when the Pd content in the sample increases. In contrary the a parameter increases with the Pd content.

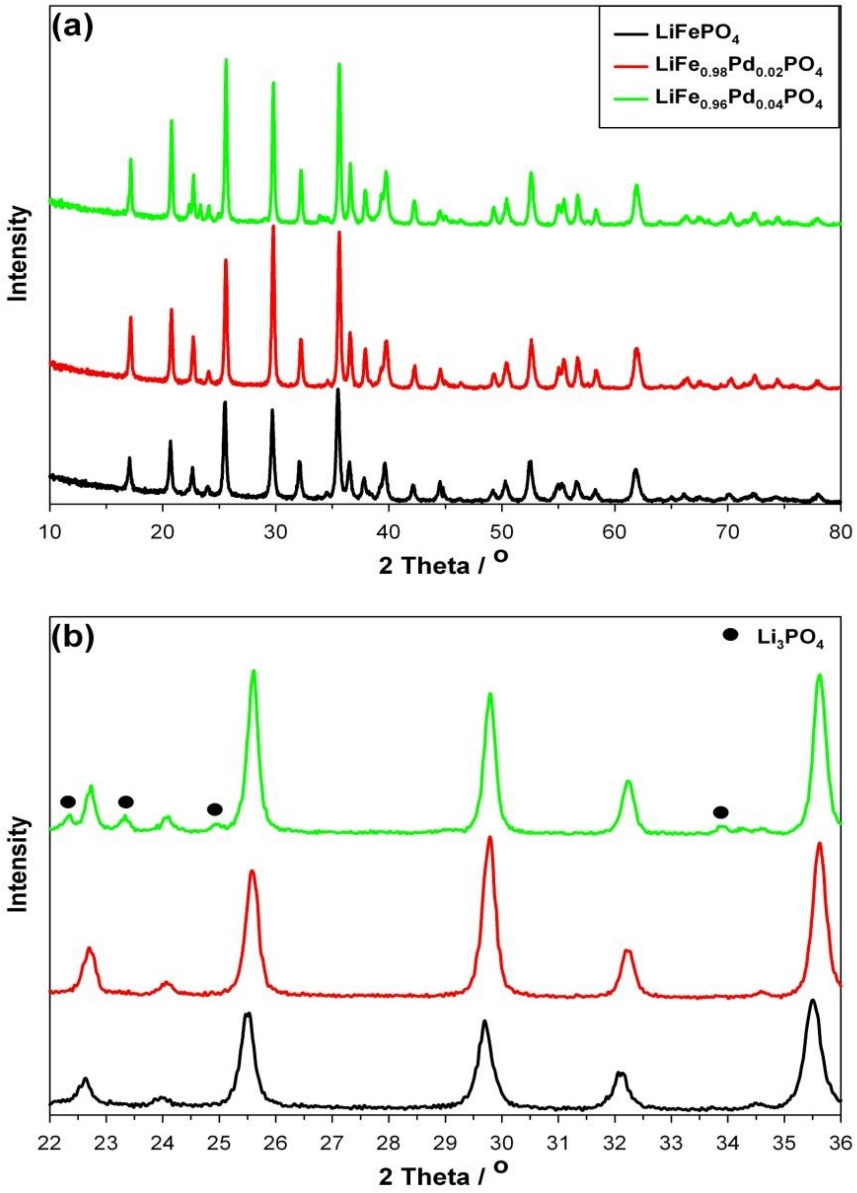

Figure 6-1: (a) XRD patterns of $LiFePO_4$, $LiFe_{0.98}Pd_{0.02}PO_4$ and $LiFe_{0.96}Pd_{0.04}PO_4$ samples, and (b) partial magnified patterns of samples

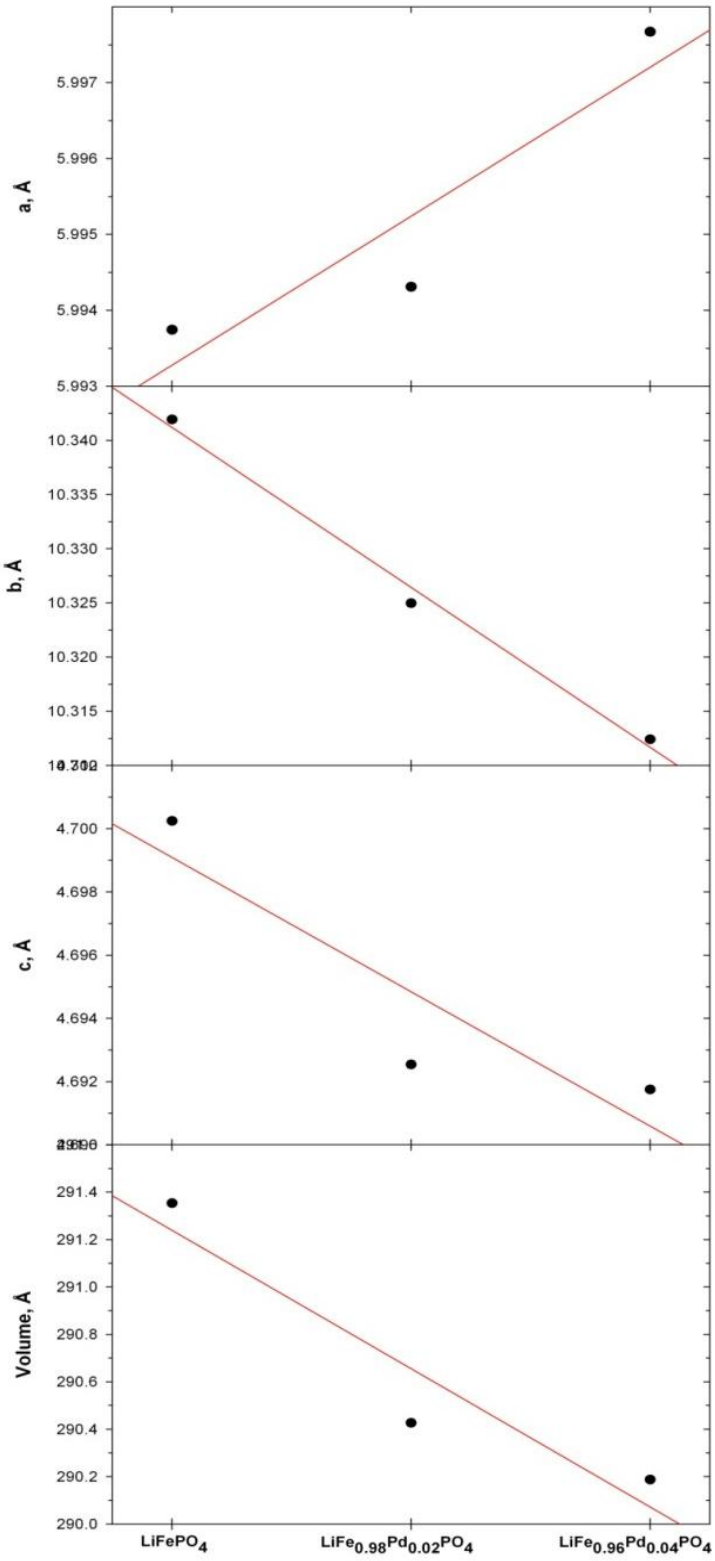

Figure 6-2: Lattice parameters and cell volume of $LiFePO_4$, $LiFe_{0.98}Pd_{0.02}PO_4$, and $LiFe_{0.96}Pd_{0.04}PO_4$ samples

The comparison of the lattice parameters of the $LiFePO_4$ nano composites to those of $LiFe_{1-x}Pd_xPO_4$ based electrodes indicates that palladium has been successfully doped into the $LiFePO_4$ structure. Two possibilities may appear to the structure of the Pd-doped LiFePO4. The Fe^{2+} changes to Fe^{3+} during the de-intercalation process of Pd and shrinks the structure, consequently, collapsing the lattice parameters and limiting Li-ions diffusion [27]. However, the lattice parameters might be also prevented from shrinking by Pd-doped due to the unchangeable radius of Pd^{2+}. Therefore, the Pd-doped in the structure may act as a pillar to prevent the shrinking and collapse, stabilizing the crystal structure during the intercalation/ de-intercalation process of Li^+ ions [25-27]. Getting one of these two types of structures of the doped samples may depend on their Pd content.

Figure 6-3 shows the XPS spectrum within a wide range of binding energy for various samples. The peaks related to Fe 2p, O 1s, P 2p and C 1s were detected for all samples, as labeled in the Figure 6-3. The binding energy for the Li 1s peak is overlapped with Fe 3p peak (56 eV). Therefore, the investigation of its binding energy and estimation of the element content were not allowed. It is worthy to note that the Pd 3d peak was observed for the Pd-doped samples as illustrated in Fig 6-3(b,c), confirming the existence of Pd in the samples.

Figure 6-4(a) presents the high resolution Pd 3d spectra for both Pd-doped samples. As shown, the intensity of Pd 3d spectrum of $LiFe_{0.96}Pd_{0.04}PO_4$ sample is almost two times larger than the $LiFe_{0.98}Pd_{0.02}PO_4$ sample, indicating that Pd^{2+} ions exist in the samples. In both samples, Pd 3d contains a doublet with binding energies of 336.1 eV and 341.1 eV which are ascribed to the Pd 3d5/2 and Pd 3d3/2 lines, respectively, indicating that the oxidation state of Pd in the doped samples is +2 [39]. In order to study the effect of Pd doping on the oxidation state and binding

energy of Fe, the high resolution Fe 2p spectra for all the samples were compared, as shown in Figure 6-4(b).

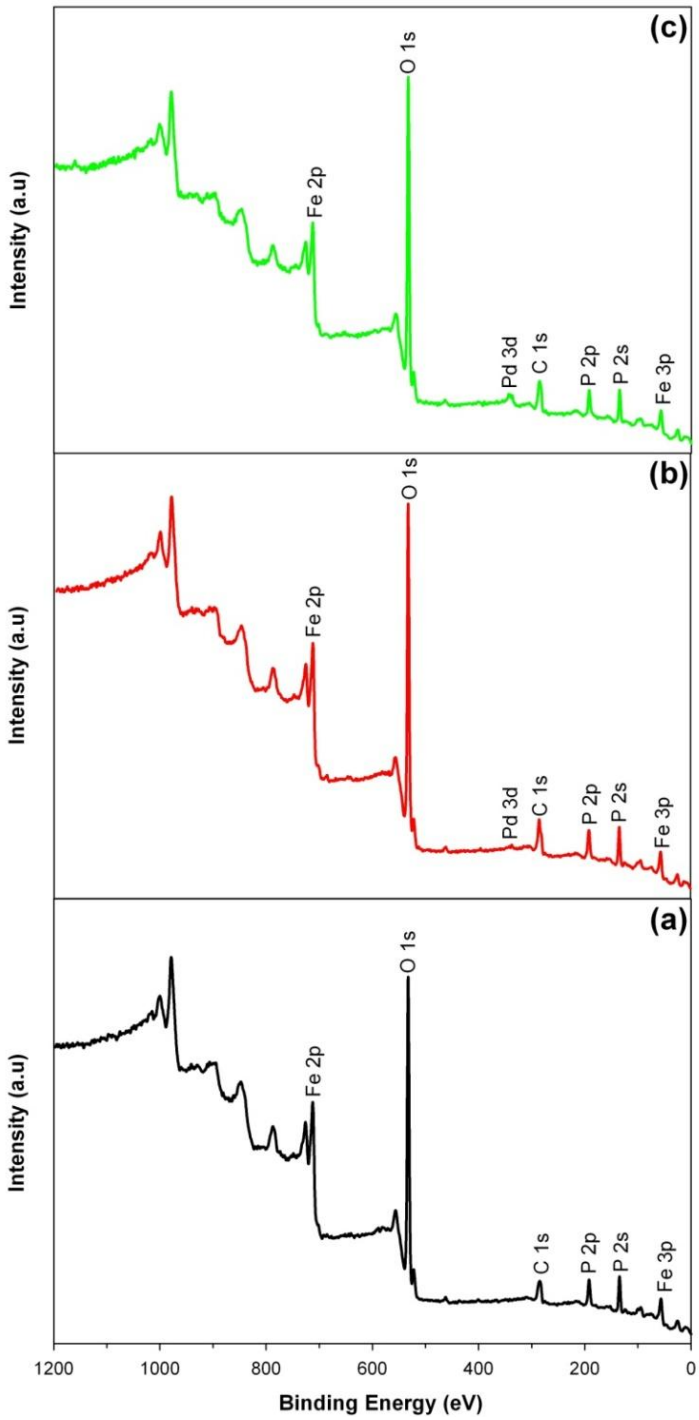

Figure 6-3: XPS spectrum of (a) $LiFePO_4$, (b) $LiFe_{0.98}Pd_{0.02}PO_4$ and (c) $LiFe_{0.96}Pd_{0.04}PO_4$ samples

All the samples have two doublet peaks of Fe 2p3/2 and Fe 2p1/2 with binding energies of 711 eV and 724.6 eV, indicating that the oxidation state of the Fe is +2. These results are in agreement with other reports [9, 36]. The comparison of the binding energies of Fe in $LiFePO_4$ based electrode and in Pd-doped samples shows no noticeable change in the binding energies of the main peaks of Fe. For the Pd-doped samples Figure 6-4(a) shows no change in the binding energies of Pd. These results show that the Pd doping does not considerably change the chemical valence of Fe^{2+} which is in consistence with our previous work [36].

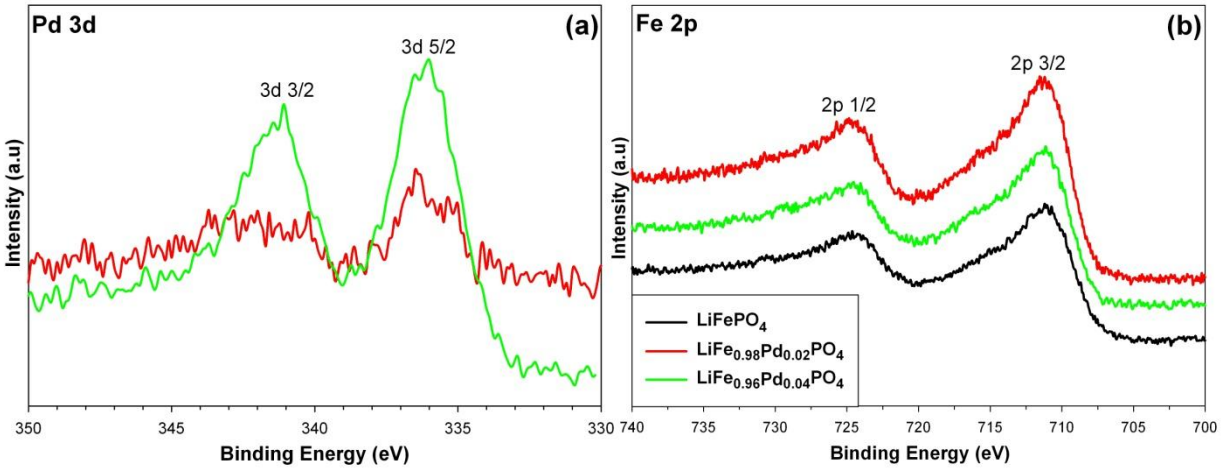

Figure 6-4: (a) XPS core level of Pd 3d for Pd-doped samples and (b) XPS core level of Fe 2p for all samples

Figure 6-5 illustrates the SEM images of the samples. The particle size of $LiFePO_4$ powder was around 1-5 μm in length and 400-900 nm in width. $LiFe_{0.98}Pd_{0.02}PO_4$ sample consists of uniform and homogeneous individual particles with sizes of around 1-3 μm in length and 200-600 nm in width as shown in Figure 6-5(b). However, by increasing the Pd concentration, the particles became irregular flake shape with the similar sizes of around 1-5 μm in length, 200-600 nm in

width and a little agglomerated, as shown in Figure 6-5(c). However, the surface area of the $LiFe_{0.98}Pd_{0.02}PO_4$ powder was larger than that of the $LiFePO_4$ powder, as listed in Table 6-1.

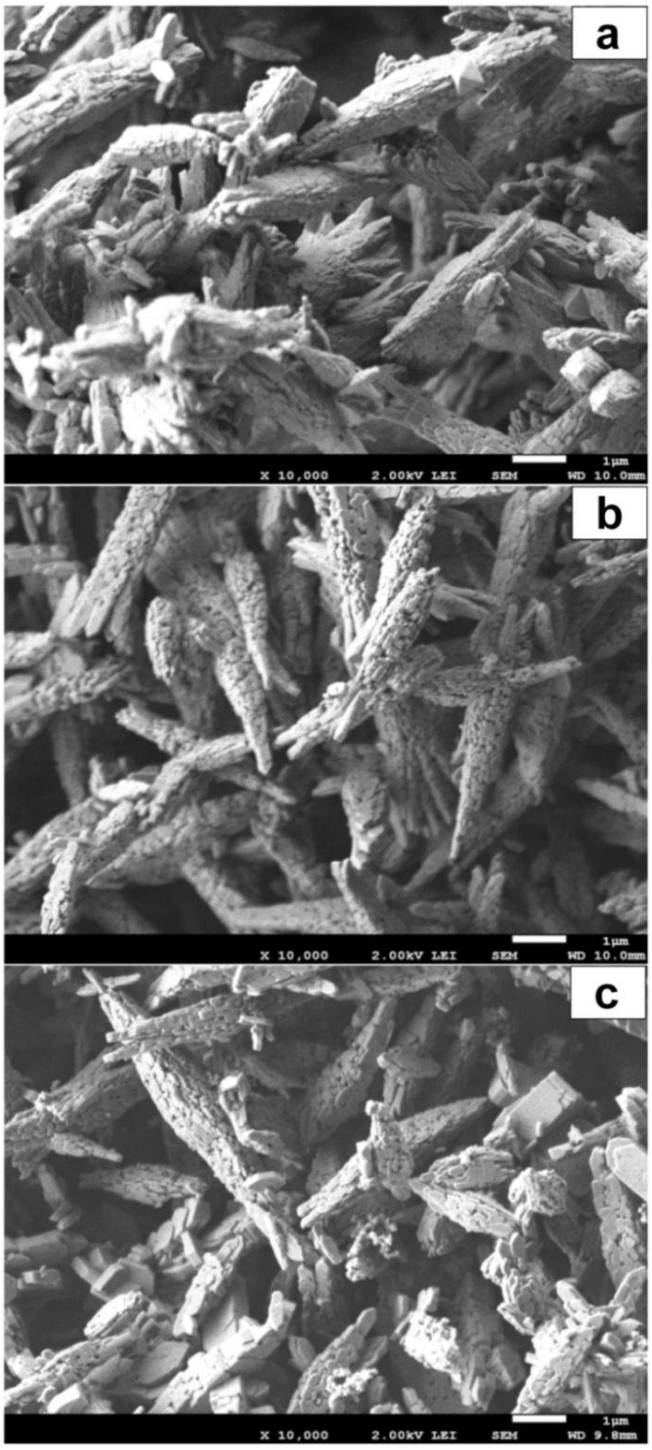

Figure 6-5: SEM image of a) $LiFePO_4$, b) $LiFe_{0.98}Pd_{0.02}PO_4$ and c) $LiFe_{0.96}Pd_{0.04}PO_4$ samples

But, for $LiFe_{0.96}Pd_{0.04}PO_4$ sample which has a higher Pd content than $LiFe_{0.98}Pd_{0.02}PO_4$, its BET surface area is lower. This is probably due to the presence of Li_3PO_4 impurity in the $LiFe_{0.96}Pd_{0.04}PO_4$ sample as indicated above from XRD results shown in Figure 6-1. Normally, the particles should have the morphologic features of uniform dispersion, regular particles with small size, homogeneity and large surface area to obtain an excellent electrochemical discharge performance [13, 30-32]. A decrease in particle size leads to an increase in specific surface area for more reaction and reduces the Li-ion diffusion distance during the intercalation/de-intercalation process [13, 32]. Therefore, a better electrochemical discharge performance is expected for the $LiFe_{0.98}Pd_{0.02}PO_4$ sample which exhibited small and uniform particle sizes.

Table 6-1: BET results of $LiFePO_4$, $LiFe_{0.98}Pd_{0.02}PO_4$ and $LiFe_{0.96}Pd_{0.04}PO_4$

Sample	**Specific surface area(m^2/g)**
$LiFePO_4$	5
$LiFe_{0.98}Pd_{0.02}PO_4$	7
$LiFe_{0.96}Pd_{0.04}PO_4$	5

Figure 6-6 illustrates the discharge capacity curves of $LiFePO_4$/C, $LiFe_{0.98}Pd_{0.02}PO_4$/C and $LiFe_{0.96}Pd_{0.04}PO_4$/C samples at various C-rates between 2.5 and 4.2 V. Both of $LiFePO_4$/C and $LiFe_{0.98}Pd_{0.02}PO_4$/C samples show a wide and flat voltage plateau around 3.4 V at 0.1C rate, indicating two phase redox reactions between $FePO_4$ and $LiFePO_4$ [1]. However, in the case of $LiFe_{0.96}Pd_{0.04}PO_4$/C sample, the flat voltage plateau becomes sloping, probably due to the presence of some Li_3PO_4 impurity phase. $LiFePO_4$/C sample delivers the specific capacities of 117, 104, 83, 63 and 47 mAh/g at 0.1C, 0.2C, 1C, 5C and 10C rates, respectively.

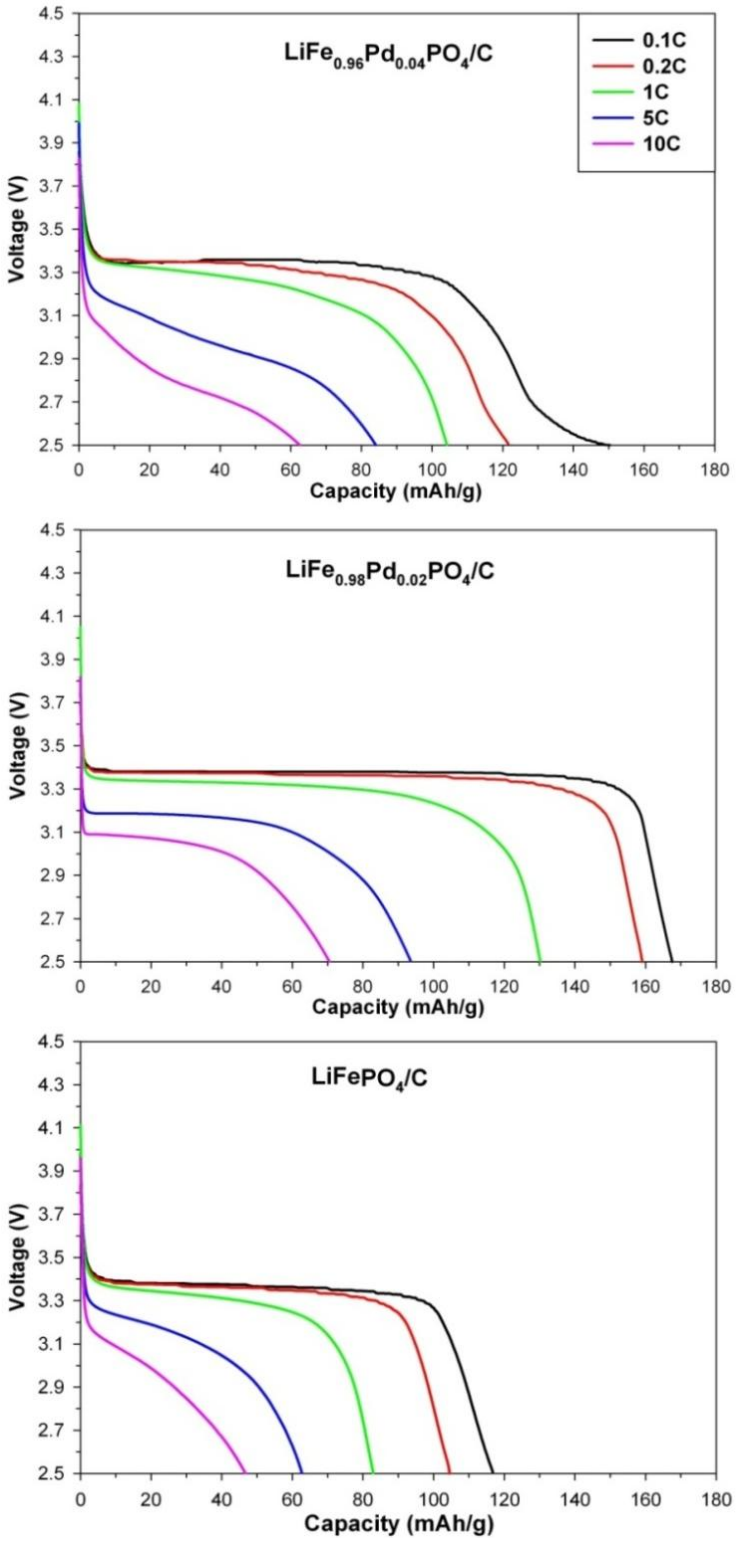

Figure 6-6: Discharge curves of $LiFePO_4/C$, $LiFe_{0.98}Pd_{0.02}PO_4/C$ and $LiFe_{0.96}Pd_{0.04}PO_4/C$ samples at various rates

In contrary, from Figure 6-6, we can determine that $LiFe_{0.98}Pd_{0.02}PO_4$/C sample exhibits the best discharge performance than $LiFePO_4$/C sample. The discharge capacities of $LiFe_{0.98}Pd_{0.02}PO_4$/C are 168, 159, 130, 93 and 70 mAh/g at 0.1C, 0.2C, 1C, 5C and 10C, respectively. However, by increasing the Pd content in the sample $LiFe_{0.96}Pd_{0.04}PO_4$/C, the discharge capacity decreased to 150, 122, 104, 84 and 63 mAh/g at 0.1C, 0.2C, 1C, 5C and 10C, respectively. This is probably due to the presence of Li_3PO_4 impurity in the $LiFe_{0.96}Pd_{0.04}PO_4$/C sample. Li_3PO_4 impurity may act as inert and inactive mass to prevent the transfer of electrons and Li^+ ions during the redox process of $LiFePO_4$, consequently, reducing the electrochemical performance [37, 38]. It is obvious that the $LiFe_{0.98}Pd_{0.02}PO_4$/C sample exhibits good electrochemical properties, which can be interpreted as the enhancement of Li-ion diffusion due to the appropriate amount of Pd doping of this sample. The optimized Pd-doped might act as a pillar to prevent the shrinking and collapse of lattice structure, stabilizing the crystal structure during the intercalation /de-intercalation process of Li^+ [25, 27]. Another possibility can be related to small and uniform particle sizes and/or high surface area of of $LiFe_{0.98}Pd_{0.02}PO_4$/C sample. These characteristics may favor the Li ion diffusion during the redox reaction and the increase of the electrochemical rate [29-31]. In all three samples, the carbon contents in the final cathode materials were ~ 6.5 wt%.

Cyclic voltammetry measurements were carried out to study the characteristics of the redox reactions for the various samples as shown in Figure 6-7. For each sample, both of oxidation and reduction current peaks were observed, corresponding to the reaction of the Fe^{2+}/Fe^{3+} redox couple during the Li^+ insertion/extraction process. Among the samples, $LiFe_{0.98}Pd_{0.02}PO_4$/C illustrates the best electrochemical properties, with the highest peak current and the narrowest potential separation (0.265 V) between the anodic and the cathodic current peaks. The potential

separation between the anodic and the cathodic peaks for the $LiFePO_4$/C and $LiFe_{0.96}Pd_{0.04}PO_4$/C samples are 0.288 V and 0.273 V, respectively. This is in agreement of the report in [40] which has shown clearly that the potential separation demonstrates potential polarization of the active material during charge and discharge process. Therefore the lower potential separation obtained with the $LiFe_{0.98}Pd_{0.02}PO_4$/C sample support a better reversibility in the electrochemical reaction during the charge-discharge process of the cell in comparison to those of $LiFePO_4$/C and $LiFe_{0.96}Pd_{0.04}PO_4$/the based electrodes.

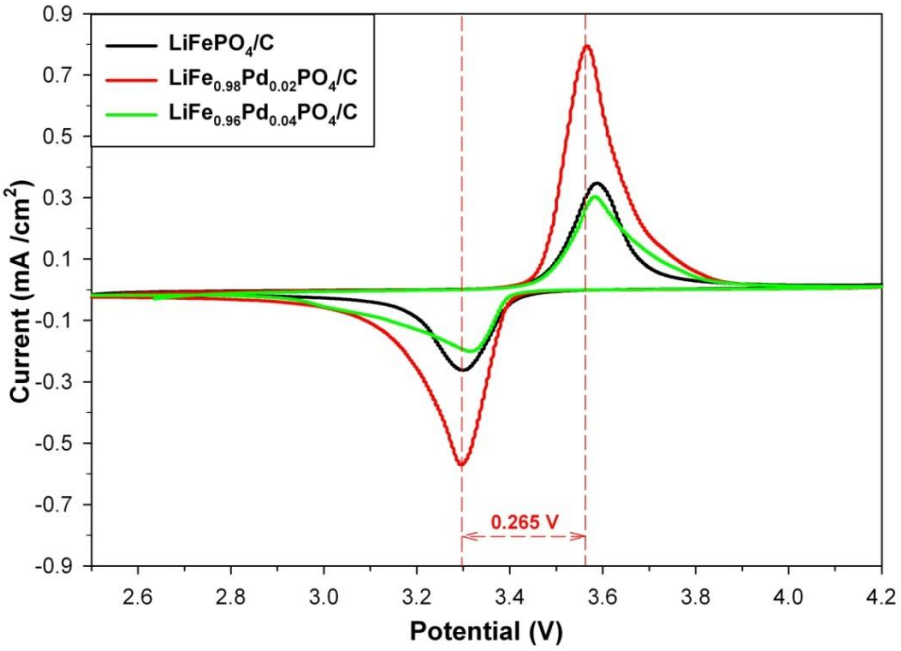

Figure 6-7: CV curves of $LiFePO_4$/C, $LiFe_{0.98}Pd_{0.02}PO_4$/C and $LiFe_{0.96}Pd_{0.04}PO_4$/C samples at scanning rate of 0.1 mV/s

EIS was carried out for further investigation of effect of Pd doping on the electrochemical properties of the samples. Before EIS tests, all the cells were discharged from 4.2 to 2.5V. Figure 6-8 shows the Nyquist plots of samples at room temperature. All the samples have a depressed semicircle in the high frequency region and an inclined line in the low frequency region. An

intercept on the Z' axis at the high frequency indicates the resistance between the electrolyte and electrode (R_e). The numerical value of diameter of the semicircle on the Z' axis represents the charge transfer resistance (R_{ct}). The straight line at lower frequency is associated with the Li^+ diffusion resistance into the bulk of the materials, namely the Warburg impedance [40]. The interpretation of the impedance spectra is based on a simplified equivalent circuit model as shown in the inset of Figure 6-8. The constant phase element represents the double layer capacitance (CPE). As shown in Figure 6-8, the R_{ct} values of $LiFePO_4$/C, $LiFe_{0.98}Pd_{0.02}PO_4$/C and $LiFe_{0.96}Pd_{0.04}PO_4$/C are 74.67, 35.78 and 147.92 Ω, respectively. It is obvious that there is a significant decrease in R_{ct} after optimized Pd doping. The smaller R_{ct} is beneficial to get a fast kinetic reaction during the redox process, and helps to get a better electrochemical performance [9]. It is well known that the slope of the straight line of the EIS curve is proportional to the Li^+ diffusion coefficient [40]. Accordingly from the slope of the straight lines of these curves shown in Figure 6-8, the Li^+ diffusion coefficient for the $LiFe_{0.98}Pd_{0.02}PO_4$/C is higher than those of $LiFePO_4$/C and $LiFe_{0.96}Pd_{0.04}PO_4$/C samples. This might be due to the pillar effect of optimized Pd^{2+} doping in the crystal structure during the intercalation/ de-intercalation process. Therefore, the $LiFe_{0.98}Pd_{0.02}PO_4$/C sample provides better kinetic response and electrochemical performance, which is compatible with the CV results.

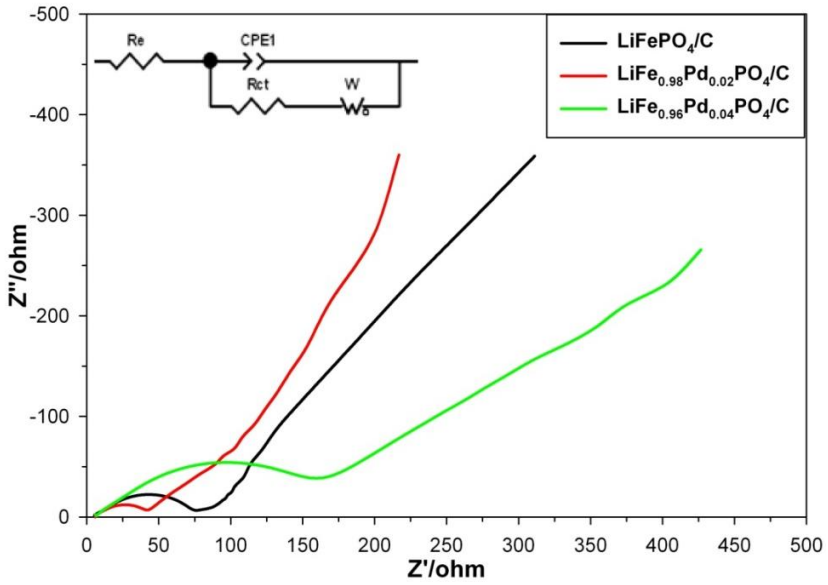

Figure 6-8: The Nyquist plots of $LiFePO_4$/C, $LiFe_{0.98}Pd_{0.02}PO_4$/C and $LiFe_{0.96}Pd_{0.04}PO_4$/C samples in the frequency range of 0.01 Hz-1 mHz

Figure 6-9 shows the cycling capability of $LiFePO_4$/C, $LiFe_{0.98}Pd_{0.02}PO_4$/C and $LiFe_{0.96}Pd_{0.04}PO_4$/C samples in various discharge current rates. All the cells were charged at constant current rate of 1C between 2.5 and 4.2V and discharged at various current rates. It can be observed from Figure 6-9 that no obvious capacity fading is observed for the $LiFePO_4$/C and $LiFe_{0.98}Pd_{0.02}PO_4$/C samples at various discharge current rates. The good cycling behavior for the $LiFe_{0.98}Pd_{0.02}PO_4$/C sample might be attributed to the pillar effect of optimized Pd^{2+} doping, stabilizing the crystal structure during the cycling process. However, a large capacity loss is observed in the $LiFe_{0.96}Pd_{0.04}PO_4$/C sample in all the current rates due to existence of Li_3PO_4 impurity phase and difficulty of Li^+ ions diffusion.

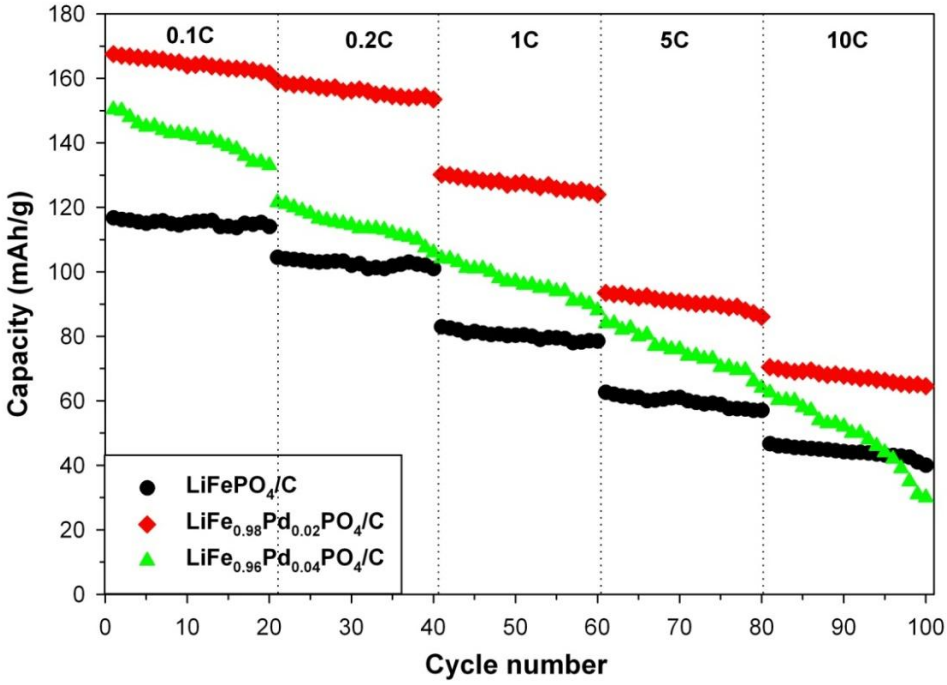

Figure 6-9: Cycling performance of $LiFePO_4/C$, $LiFe_{0.98}Pd_{0.02}PO_4/C$ and $LiFe_{0.96}Pd_{0.04}PO_4/C$ samples at various discharge rates

6.1.4 Conclusions

$LiFePO_4$/C and Pd-doped $LiFePO_4$/C were successfully synthesized via hydrothermal method and the effect of Pd content on the structure and electrochemical properties of $LiFePO_4$/C were investigated. Among the samples, $LiFe_{0.98}Pd_{0.02}PO_4$/C demonstrates the best electrochemical performance with discharge capacities of 168, 159, 130, 93 and 70 mAh/g at 0.1C, 0.2C, 1C, 5C and 10C, respectively. However, by increasing the Pd content, the electrochemical performance reduces due to the existence of Li_3PO_4 impurity phase in the $LiFe_{0.96}Pd_{0.04}PO_4$/C sample. The optimized Pd doping exhibits uniform particles. This improves the reversibility of lithium intercalation and de-intercalation. The charge transfer resistance decrease and the rate of the Li-ion diffusion increases for sample $LiFe_{0.98}Pd_{0.02}PO_4$/C. This is attributed to the small uniform particles and the pillar effect of Pd in this sample which prevents the shrinking and collapse of structure. This helps to stabilize the crystal structure during cycling.

References

[1] A.K. Padhi, K.S. Nanjundaswamy, J.B. Goodenough, Journal of The Electrochemical Society, 144 (1997) 1188-1194.

[2] A. Yamada, S.C. Chung, K. Hinokuma Journal of The Electrochemical Society, 148 (2001) A224-A229.

[3] S.-Y. Chung, J.T. Bloking, Y.-M. Chiang, Nat Mater, 1 (2002) 123-128.

[4] N. Ravet, Y. Chouinard, J.F. Magnan, S. Besner, M. Gauthier, M. Armand, Journal of Power Sources, 97–98 (2001) 503-507.

[5] X. Zhou, F. Wang, Y. Zhu, Z. Liu, Journal of Materials Chemistry, 21 (2011) 3353-3358.

[6] L. Wang, X. He, W. Sun, J. Wang, Y. Li, S. Fan, Nano Letters, 12 (2012) 5632-5636.

[7] R. Malik, D. Burch, M. Bazant, G. Ceder, Nano Letters, 10 (2010) 4123-4127.

[8] J. Hong, X.-L. Wang, Q. Wang, F. Omenya, N.A. Chernova, M.S. Whittingham, J. Graetz, The Journal of Physical Chemistry C, 116 (2012) 20787-20793.

[9] Z.-H. Wang, L.-X. Yuan, J. Ma, L. Qie, L.-L. Zhang, Y.-H. Huang, Electrochimica Acta, 62 (2012) 416-423.

[10] J. Chen, M.J. Vacchio, S. Wang, N. Chernova, P.Y. Zavalij, M.S. Whittingham, Solid State Ionics, 178 (2008) 1676-1693.

[11] P.S. Herle, B. Ellis, N. Coombs, L.F. Nazar, Nat Mater, 3 (2004) 147-152.

[12] M.S. Islam, D.J. Driscoll, C.A.J. Fisher, P.R. Slater, Chemistry of Materials, 17 (2005) 5085-5092.

[13] C.A.J. Fisher, M.S. Islam, Journal of Materials Chemistry, 18 (2008) 1209-1215.

[14] D. Morgan, A. Van der Ven, G. Ceder, Electrochemical and Solid-State Letters, 7 (2004) A30-A32.

[15] C.Y. Ouyang, S.Q. Shi, Z.X. Wang, H. Li, X.J. Huang, L.Q. Chen, Journal of Physics: Condensed Matter, 16 (2004) 2265.

[16] C. Ouyang, S. Shi, Z. Wang, X. Huang, L. Chen, Physical Review B, 69 (2004) 104303.

[17] J. Lee, W. Zhou, J.C. Idrobo, S.J. Pennycook, S.T. Pantelides, Physical Review Letters, 107 (2011) 085507.

[18] H. Gao, L. Jiao, W. Peng, G. Liu, J. Yang, Q. Zhao, Z. Qi, Y. Si, Y. Wang, H. Yuan, Electrochimica Acta, 56 (2011) 9961-9967.

[19] K.L. Harrison, C.A. Bridges, M.P. Paranthaman, C.U. Segre, J. Katsoudas, V.A. Maroni, J.C. Idrobo, J.B. Goodenough, A. Manthiram, Chemistry of Materials, 25 (2013) 768-781.

[20] D. Arumugam, G. Paruthimal Kalaignan, P. Manisankar, J Solid State Electrochem, 13 (2009) 301-307.

[21] J. Ma, B. Li, H. Du, C. Xu, F. Kang, J Solid State Electrochem, 16 (2012) 1-8.

[22] M.-R. Yang, W.-H. Ke, Journal of The Electrochemical Society, 155 (2008) A729-A732.

[23] C.S. Sun, Z. Zhou, Z.G. Xu, D.G. Wang, J.P. Wei, X.K. Bian, J. Yan, Journal of Power Sources, 193 (2009) 841-845.

[24] H. Liu, C. Li, Q. Cao, Y.P. Wu, R. Holze, J Solid State Electrochem, 12 (2008) 1017-1020.

[25] A.Y. Shenouda, H.K. Liu, Journal of Alloys and Compounds, 477 (2009) 498-503.

[26] Y. Wang, Y. Yang, X. Hu, Y. Yang, H. Shao, Journal of Alloys and Compounds, 481 (2009) 590-594.

[27] H. Liu, Q. Cao, L.J. Fu, C. Li, Y.P. Wu, H.Q. Wu, Electrochemistry Communications, 8 (2006) 1553-1557.

[28] Y. Hu, J. Yao, Z. Zhao, M. Zhu, L. Ying, H. Jin, H. Zhao, J. Wang, Materials Chemistry and Physics.

[29] L. Li, X. Tang, H. Liu, Y. Qu, Z. Lu, Electrochimica Acta, 56 (2010) 995-999.

[30] Q. Song, X. Ou, L. Wang, G. Liang, Z. Wang, Materials Research Bulletin, 46 (2011) 1398-1402.

[31] L.-X. Yuan, Z.-H. Wang, W.-X. Zhang, X.-L. Hu, J.-T. Chen, Y.-H. Huang, J.B. Goodenough, Energy & Environmental Science, 4 (2011) 269-284.

[32] G. Chen, X. Song, T.J. Richardson, Electrochemical and Solid-State Letters, 9 (2006) A295-A298.

[33] D. Jugović, D. Uskoković, Journal of Power Sources, 190 (2009) 538-544.

[34] M. Talebi Esfandarani, O. Savadogo, Submitted to Journal of Alloys and Compounds, (2013).

[35] X. Ou, H. Gu, Y. Wu, J. Lu, Y. Zheng, Electrochimica Acta, 96 (2013) 230-236.

[36] M. Talebi Esfandarani, O. Savadogo, Submitted to Journal of New Materials for Electrochemical Systems, (2013).

[37] P. Axmann, C. Stinner, M. Wohlfahrt-Mehrens, A. Mauger, F. Gendron, C.M. Julien, Chemistry of Materials, 21 (2009) 1636-1644.

[38] D.Y.W. Yu, K. Donoue, T. Kadohata, T. Murata, S. Matsuta, S. Fujitani, Journal of The Electrochemical Society, 155 (2008) A526-A530.

[39] K.S. Kim, A.F. Gossmann, N. Winograd, Analytical Chemistry, 46 (1974) 197-200.

[40] Bard a.J., F. L.R, Electrochemical Methods. Fundamentals and Applications., in, Wiley, 2001.

6.2 Enhancement of electrochemical properties of Platinum doped $LiFePO_4$/C cathode material synthesized using hydrothermal method

M. Talebi-Esfandarani and O. Savadogo*

Laboratory of New Materials for Electrochemistry and Energy

École Polytechnique de Montréal,

C.P. 6079, Succ. Centre Ville, Montréal, QC, Canada, H3C 3A7

*Corresponding author: osavadogo@polymtl.ca, Phone: +1 514 3404725

Submitted at Solid State Ionics, November 18, 2013

Abstract

The Pt-doped $LiFePO_4$/C cathode material synthesized for the first time. $LiFePO_4$ and $LiFe_{0.96}Pt_{0.04}PO_4$ composites were synthesized using hydrothermal method. The physical and chemical properties of samples were characterized by XRD, XPS, SEM and BET. For electrochemical properties investigation, the samples were mixed with sucrose as carbon source, and calcined at 700 °C for 5 h. The XRD results showed that the platinum has been successfully doped into the $LiFePO_4$ bulk structure. The XPS results indicated that platinum doping does not change the chemical state of Fe (II). The SEM and BET results showed that platinum doping reduces the size of the particles. The electrochemical characterization of the electrodes using discharge capacity, cyclic voltammetry (CV) and electrochemical impedance spectroscopy (EIS) showed that the Li-ion cell based on $LiFe_{0.96}Pt_{0.04}PO_4$/C electrode exhibited better charge /discharge performance than those of $LiFePO_4$/C sample. The $LiFe_{0.96}Pt_{0.04}PO_4$/C based cell

delivered the specific capacity of 168, 162, 135, 120 and 102 mAh/g at 0.1C, 0.2C, 1C, 5C and 10C, respectively, in comparison with 117, 104, 83, 63 and 47 mAh/g for the $LiFePO_4$/C cell.

Keywords: $LiFePO_4$, hydrothermal method, platinum doping.

6.2.1 Introduction

For the past two decades, Li-ion battery has attracted much attention for powering portable electronic devices considering its combination of high power and energy density, long cyclic life, and stability [1, 2]. Conventionally, $LiCoO_2$ with capacity of 140 mAh/g is being used as cathode material in commercial Li-ion batteries. However, $LiCoO_2$ has its own drawbacks such as the limited abundance in nature, the toxicity issue and the high cost [2]. $LiFePO_4$ has been suggested as a promising candidate to replace $LiCoO_2$ as a cathode material for the next generation Li-ion batteries. $LiFePO_4$ has distinctive features of high theoretical capacity (170 mAh/g), high discharge potential (~3.45 V vs Li^+/Li), excellent thermal stability, low cost and being environmentally friendly [3, 4]. However, pristine $LiFePO_4$ suffers from its poor ion diffusion coefficient (10^{-14} cm^2s^{-1}) and low electrical conductivity (10^{-9} Scm^{-1}), limiting its application in large devices [5, 6]. To solve these drawbacks, progressive strategies have been employed such as coating particles with a conductive carbon layer [7, 8], reducing the particle sizes [9, 10], and doping with guest elements [11-13].

Among these strategies, particle size reduction and carbon coating have proven to be effective methods for improving the electrochemical performance of $LiFePO_4$ material, due to their contribution to decreasing the diffusion path length with a larger surface area for more reaction and the enhancement of electronic conductivity of surface of $LiFePO_4$ material [8, 9, 14, 15]. However, there are controversial results about the doping element strategy [16-18]. The

enhancement in the intrinsic electrical conductivity of bulk of $LiFePO_4$ material through doping has been reported [16, 19-21]. Nevertheless, incorporation of element doping causes formation of impurities and influences the electrochemical features of $LiFePO_4$ material. Some impurities such as Fe_2P conductive film and $Li_4P_2O_7$ improve the electrochemical performance while some impurities likes insulating Li_3PO_4 deteriorate the performance drastically. [14, 17, 22-24]. In addition, the theoretical studies proposed that doping is not favorable [25]. Despite of these arguments, many reports indicate enhancement of electrical conductivity and electrochemical performance of $LiFePO_4$ by different doped elements [11-13, 19-21, 26-29].

$LiFePO_4$ can be synthesized by various methods including solid-state reaction, microwave, sol-gel, co-precipitation, hydrothermal, solvothermal and etc [30-33]. Among these methods, the hydrothermal synthesis, which has some advantages such as simple synthesis process, low energy consumption, and morphology controllability, is a useful and efficient method to obtain well-crystallized uniform $LiFePO_4$ particles [34-36]. In general, the synthesis method can affect the morphology, size of particles, specific surface area, purity and crystal structure of $LiFePO_4$ material, resulting in different electrochemical properties [15, 33, 36-38].

We have already reported that the Pt-doped $LiFePO_4$ prepared by sol-gel method can improve the electrochemical performance [39]. The effect of the method of preparation was not shown. This work reports for the first time the effects of platinum doping on the structure and electrochemical properties of $LiFePO_4$ prepared with hydrothermal method. How the Pt doping affects the materials properties are investigated in detail.

6.2.2 Experimental

6.2.2.1 Synthesis of materials

The $LiFePO_4$ and $LiFe_{0.96}Pt_{0.04}PO_4$ samples were prepared by hydrothermal method. $FeSO_4 \cdot 7H_2O$, H_3PO_4 (85 wt. %), $LiOH \cdot H_2O$ and $H_2PtCl_6.6H_2O$ were used as raw materials and sucrose as carbon source. A stoichiometric amount H_3PO_4, $FeSO_4 \cdot 7H_2O$ and $H_2PtCl_6.6H_2O$ were dissolved in the mixture of ethylene glycol and deionized water under magnetic stirring in a nitrogen atmosphere. Certain amount of hydrazine as reducing agent was added into the mixture to inhibit the oxidation of Fe^{2+} to Fe^{3+}. Separately, $LiOH \cdot H_2O$ was dissolved in the deionized water and then added to the above mixture drop wise under magnetic stirring in a nitrogen atmosphere until it was completely dissolved. The pH of the solution was adjusted to 6 by adding H_3PO_4. The resulting homogenous mixture was swiftly transferred to a Teflon-lined stainless steel autoclave. The sealed autoclave was then heated at 190 °C for 6 h. Afterwards, the solution was cooled down to room temperature. The precipitate was filtered and washed several times with deionized water and acetone, followed by drying at 70 °C in a vacuum oven for overnight to obtain product. For electrochemical properties investigation, the pre-synthesized sample was mixed with sucrose in weight ratio of (70:30) and sintered at 700 °C for 5 h in a nitrogen atmosphere to obtain the $LiFe_{0.96}Pt_{0.04}PO_4$/C composite. $LiFePO_4$/C was prepared following the same procedure without the addition of $H_2PtCl_6.6H_2O$ precursor.

6.2.2.2 Material characterization

The phase purity and crystal structure of the synthesized samples were analyzed using X-ray diffractometer (Philips X'pert) with CuKα radiation (λ=1.54056 A°) in 2θ range of 10° to 80°. The chemical valence states of Fe and Pt were determined using x-ray photoelectron spectroscopy (VG ESCALAB 3 MKII) with Al Kα radiation source (*hv*=1486.6 eV). The data

were calibrated by P2p3/2 peak at value of 133.8 eV. The morphology and particle size of samples were observed by scanning electron microscope (JSM-7600TFE). The specific surface area of samples was measured by Brunauer-Emmett-Teller (BET) technique (Autosorb-1, Quantachrome instruments). The carbon content of the samples was determined using carbon analyzer (LECO Co., CS 400).

6.2.2.3 Electrochemical characterization

The cathode electrodes were fabricated by mixing of active material, carbon black (Super C65-Timcal) and poly vinylidene fluoride (PVDF) (weight ratio 80:10:10) in N-methyl-2-pyrrolidone to form a slurry. Afterwards, the slurry was coated onto aluminum foil and dried in vacuum oven for overnight. The cells (2032) for electrochemical measurement were assembled in the argon-filled glove box. The lithium metal was used as anode; a microporous polypropylene sheet (Celgard 2400, Celgard Inc., USA) was employed as separator, and 1 $molL^{-1}$ $LiPF_6$ in mixture of ethylene carbonate-dimethyl carbonate (volume ratio 1:1) was served as the electrolyte. Charge/discharge test and cycling properties at different current rates were carried out between 2.5 and 4.2V (vs. Li/Li^+) using Solartron battery test analyzer and Cell test software. Cyclic voltammetry (CV) was conducted using PAR273A in the potential ranges of 2.5-4.2V (vs. Li/Li^+) with the scan rates of 0.1 mV/s. The electrochemical impedance spectrum (EIS) measurement was performed on in frequency range of 0.01 Hz-1 mHz at discharge status of the cells. All the electrochemical measurements were carried out at room temperature.

6.2.3 Results and discussion

Figure 6-10 shows the XRD patterns of $LiFePO_4$ and $LiFe_{0.96}Pt_{0.04}PO_4$ samples. The main diffraction peaks for both samples can be indexed to an orthorhombic olivine-type structure, with

a space group of P_{mnb}, indicating a standard $LiFePO_4$ phase (JCPDS No. 40-1499). No observable peaks for impurities phase such as Li_3PO_4 and Fe_2P were detected for the both samples. However, the intensity of main diffraction peaks for the $LiFe_{0.96}Pt_{0.04}PO_4$ sample is higher and sharper than $LiFePO_4$ sample, indicating better crystallinity for the doped sample which might imply crystal growth by platinum contribution.

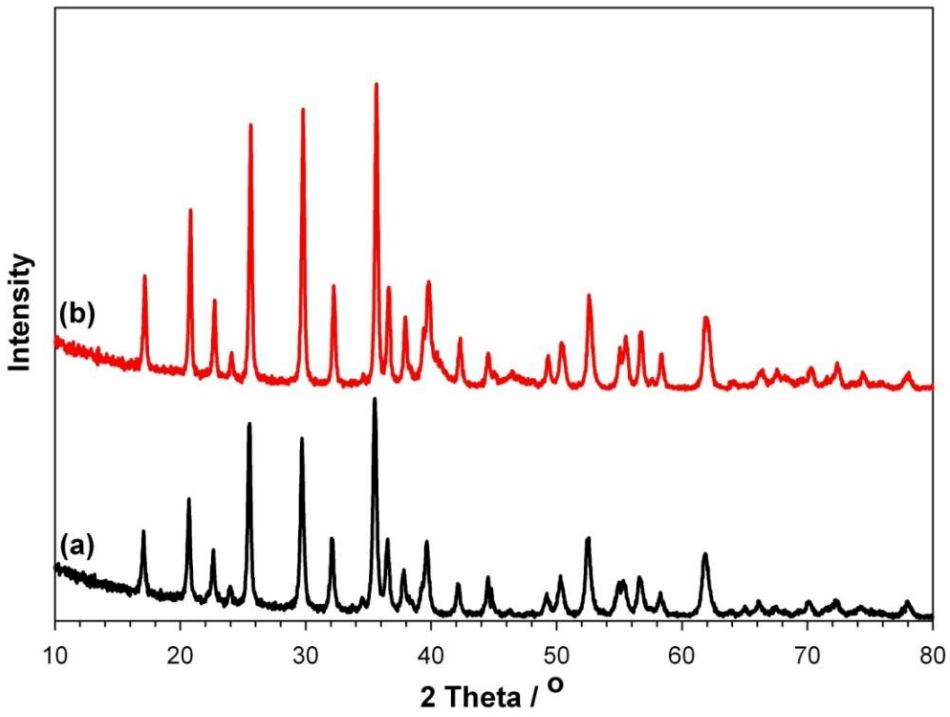

Figure 6-10: XRD patterns of $LiFePO_4$ (a) and $LiFe_{0.96}Pt_{0.04}PO_4$ (b) samples

The lattice parameters and cell volume of samples were calculated and listed in Table 6-2. These results reveal a decrease in the a and c lattice parameters and an increase in the b parameter. This results to an overall decrease in the cell volume. The same trend was observed in our previous report by palladium doping [24]. The results confirm that platinum has been successfully incorporated into the crystal structure of $LiFePO_4$ phase. This increase in the b parameter suggests that this doping may provide more space for the Li^+ ion movement and improves the Li-

ion diffusion rate. This is in agreement with the results obtained elsewhere with the vanadium doped in the bulk of $LiFePO_4$ structure [11]. The Pt doping element may also act as a pillar to prevent the shrinking and collapse of the $LiFePO_4$ crystal structure during the intercalation/de-intercalation process of Li^+ ions, stabilizing the crystal structure and indicating good cycling capability as it has been show previously for other doping agents [28, 29].

Table 6-2: The lattice parameters of $LiFePO_4$ and $LiFe_{0.96}Pt_{0.04}PO_4$ samples from XRD data

Sample	**a(Å)**	**b(Å)**	**c(Å)**	**V(Å^3)**
$LiFePO_4$	10.3419	5.9937	4.7002	291.3533
$LiFe_{0.96}Pt_{0.04}PO_4$	10.3251	5.9968	4.6923	290.5426

The XPS spectrum within a wide range of binding energy for $LiFePO_4$ and $LiFe_{0.96}Pt_{0.04}PO_4$ samples is shown in Figure 6-11. The peaks related to Fe 2p, O 1s, P 2p and C 1s were clearly observed for both samples, as labeled in Figure 6-11. The binding energy for the Li 1s peak is overlapped with Fe 3p peak (56 eV). Therefore, determination of its binding energy and estimation of the element content were not allowed. The XPS spectra are generally the same, except that the Pt 4f peak was observed for the doped sample, indicating the existence of Pt in the $LiFe_{0.96}Pt_{0.04}PO_4$ sample. Therefore, it can be confirmed that Pt ions are successfully incorporated into the $LiFePO_4$ structure.

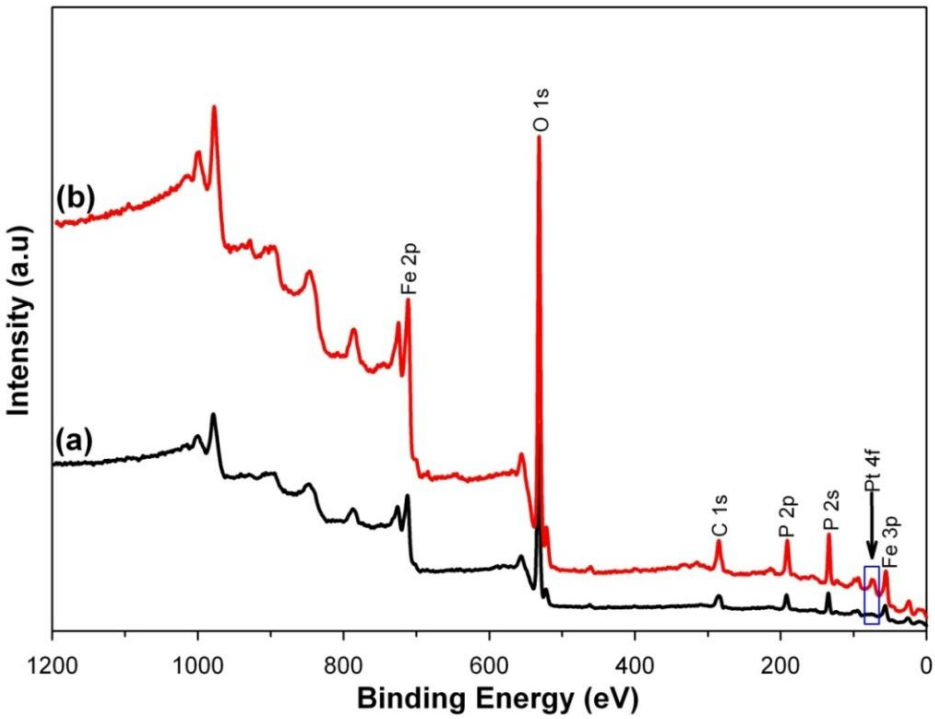

Figure 6-11: XPS spectrum of $LiFePO_4$ (a) and $LiFe_{0.96}Pt_{0.04}PO_4$ (b) samples

Further investigation of the oxidation states of Fe and Pt for the samples was carried out by high resolution XPS technique. Figure 6-12(a) shows the high resolution Pt 4f spectra for the Pt-doped sample which contains a doublet of Pt 4f7/2 and Pt 4f5/2 peaks with binding energies of 72.1 eV and 75.4 eV, respectively, suggesting that the oxidation state of Pt in the doped sample is +2. Effect of Pt doping on the oxidation state and binding energy of Fe is shown in Figure 6-12(b). $LiFe_{0.96}Pt_{0.04}PO_4$ sample contains two doublet peaks of Fe 2p3/2 (711.5 eV) and Fe 2p1/2 (724.8 eV), demonstrating that the oxidation state of the Fe is +2. It is worthy to note that no noticeable change in the binding energies of the main peaks for the $LiFe_{0.96}Pt_{0.04}PO_4$ sample is observed in comparison with $LiFePO_4$ sample, indicating that the Pt doping does not considerably change the chemical valence of Fe^{2+}.

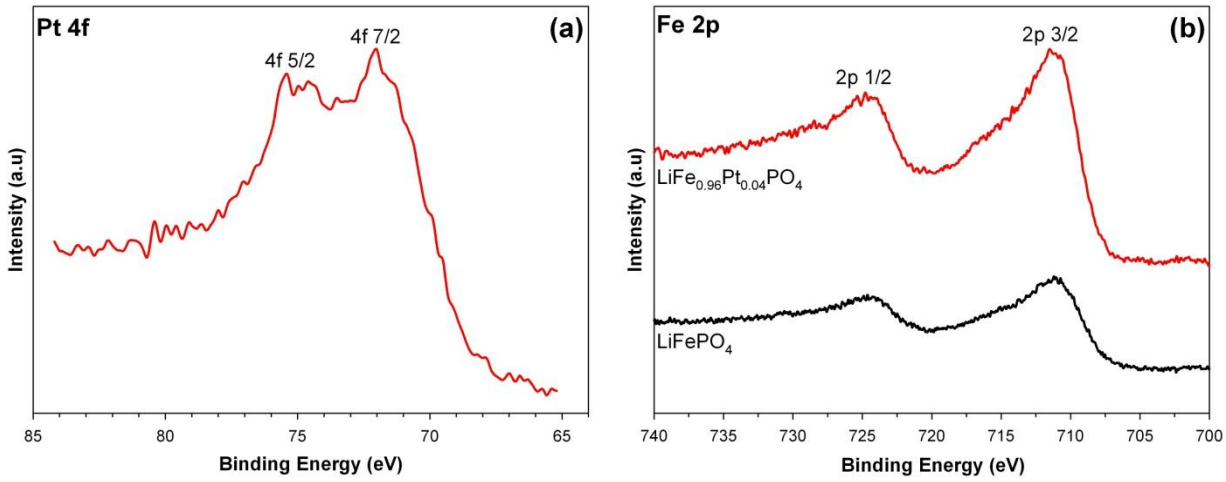

Figure 6-12: XPS core levels of Pt 4f for $LiFe_{0.96}Pt_{0.04}PO_4$ sample (a). XPS core levels of Fe 2p for $LiFePO_4$ and $LiFe_{0.96}Pt_{0.04}PO_4$ samples (b)

The SEM images of the samples are illustrated in Figure 6-13. It can be observed that the average particle size of the $LiFe_{0.96}Pt_{0.04}PO_4$ sample is smaller than $LiFePO_4$. The particle size of $LiFePO_4$ powder was around 1-5 μm in length and 400-900 nm in width. However, the Pt-doped sample shows more homogeneous and smaller particles with the size of around 1-3 μm in length and 100-600 nm in width. Such reductions in particle sizes can be related to the contribution of platinum during the particle growth process in the Pt-doped sample. In addition, the specific BET surface areas of sample increase from 5 to 7 m^2/g after Pt doping. Consequently, the amount of surface area for more reaction increases by platinum incorporation. The SEM images of the morphology of $LiFe_{0.96}Pt_{0.04}PO_4$ in Figure 6-13 (c; d) shows homogeneous particles with smaller size than those of $LiFePO_4$ material (Figure 6-13 (a; b)). The surface area of $LiFe_{0.96}Pt_{0.04}PO_4$ is then higher than those of $LiFePO_4$ might be the key point in the improvement of the electrochemical properties of this material. Therefore, a better electrochemical performance is

expected for $LiFe_{0.96}Pt_{0.04}PO_4$ sample with homogeneous and small particle sizes as it has reported elsewhere on other $LiFePO_4$ cathode materials [9].

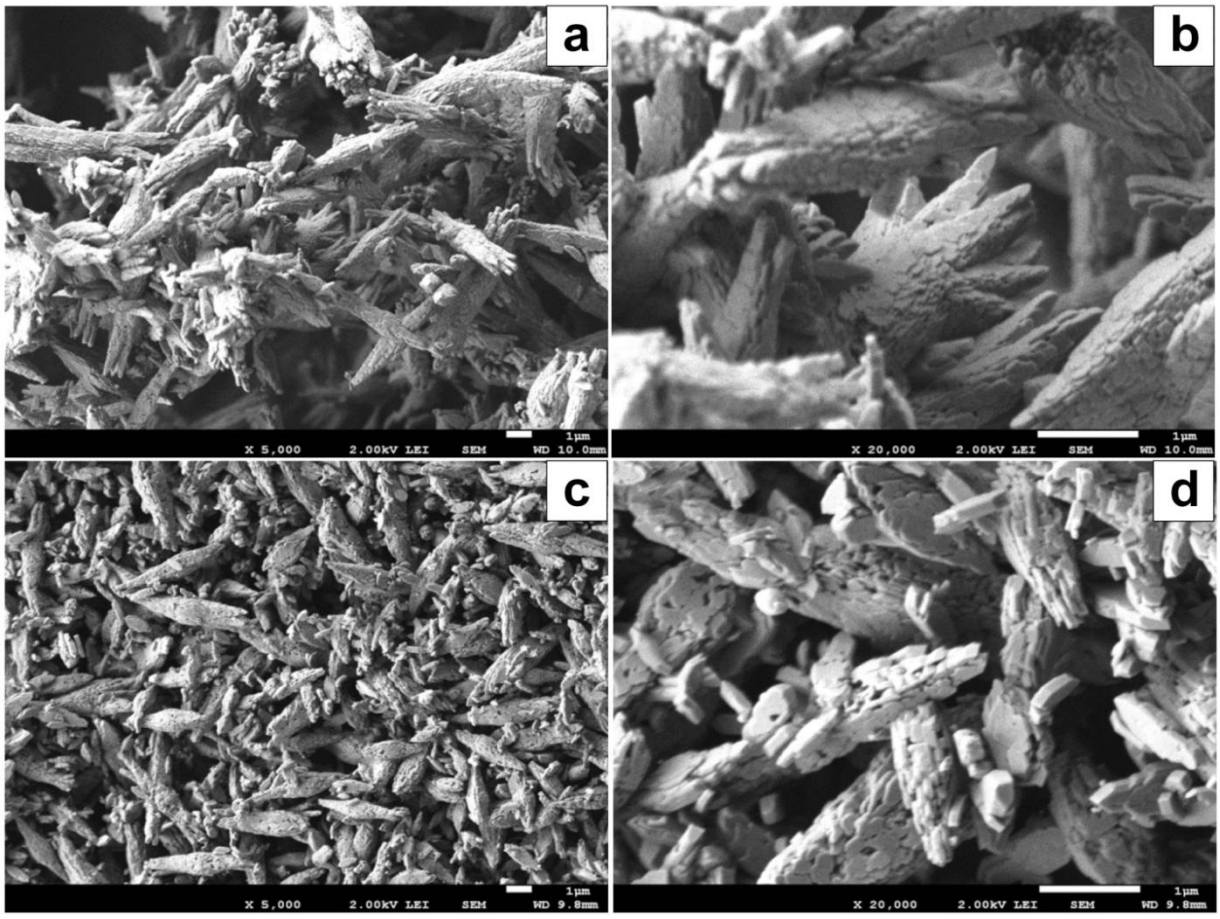

Figure 6-13: Low and high magnification SEM images of $LiFPO_4$ (a: x5000; b: x20000) and $LiFe_{0.96}Pt_{0.04}PO_4$ (c: x5000; d: x20000) samples

Figure 6-14 shows the discharge capacities at different rates for $LiFePO_4$/C and $LiFe_{0.96}Pt_{0.04}PO_4$/C samples. Both samples exhibit the typical flat voltage plateaus around 3.4V, indicating the two-phase reaction of $LiFePO_4$ and $FePO_4$ [3]. However, the voltage plateau for the doped sample is wider with smaller polarization part (oblique part) as compared to the $LiFePO_4$/C sample, implying better reaction kinetics for the doped sample. The

$LiFe_{0.96}Pt_{0.04}PO_4/C$ sample exhibited the discharge capacities of 168, 162, 135, 120 and 102 mAh/g at 0.1C, 0.2C, 1C, 5C and 10C, respectively, while $LiFePO_4/C$ sample delivers the discharge capacities of 117, 104, 83, 63 and 47 mAh/g.

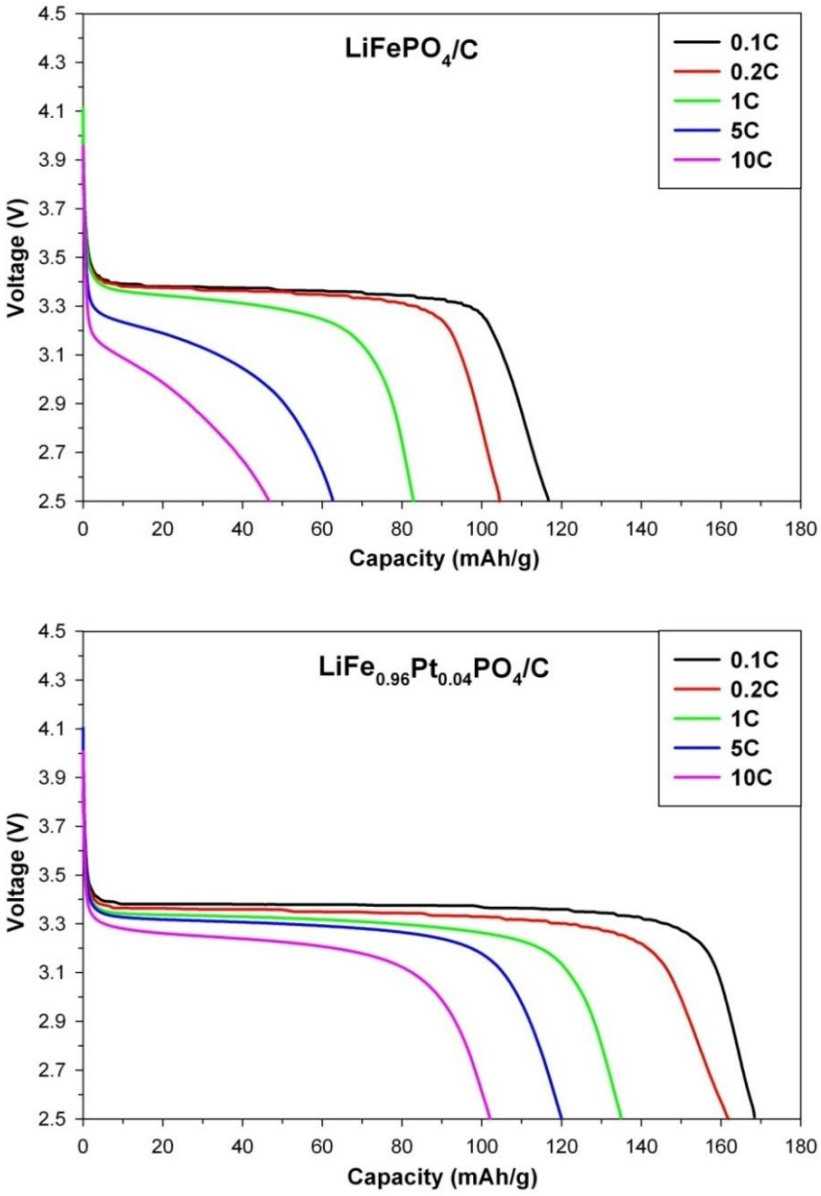

Figure 6-14: Discharge capacities of $LiFePO_4/C$ and $LiFe_{0.96}Pt_{0.04}PO_4/C$ samples at different C-rates

The results reveal that the Pt doping improves the discharge capacities of $LiFePO_4$/C at all discharge current rates (0.1C, 0.2C, 1C, 5C, 10C). This is probably due to the Pt element which might act as a pillar to prevent the shrinking and collapse of lattice structure, stabilizing the crystal structure during the intercalation/de-intercalation process of Li^+ ion. Similar phenomenon is reported in other studies using Zn-doping [28, 29, 40]. Another possibility can be ascribed to the homogeneous and smaller particle sizes of $LiFe_{0.96}Pt_{0.04}PO_4$/C sample with large surface area for more reaction and short distance for the fast Li-ion diffusion during the redox reaction. Therefore, Pt doping can improve the electrochemical performance of $LiFePO_4$/C material. These assumptions can be further examined by the CV and EIS test below. The carbon content of the both samples were around 6.6 wt% which measured by carbon analyzer (LECO).

The effect of Pt doping on the electrochemical properties of $LiFePO_4$/C material are further investigated by cyclic voltammetry (CV). Figure 6-15 illustrates the CV curves of the $LiFePO_4$/C and $LiFe_{0.96}Pt_{0.04}PO_4$/C samples at scan rate of 0.1 mV/s. For both samples, a pair oxidation/ reduction peaks, corresponding to the Fe^{2+}/Fe^{3+} redox reaction is clearly observed. However, the Pt-doped sample shows much higher oxidation/ reduction peaks with smaller potential separation between the oxidation and reduction peaks (0.225 V). The potential separation for the $LiFePO_4$/C sample is around 0.288 V. Sharper oxidation/reduction peaks with smaller potential separation support the faster ion diffusion and better reversibility for material during redox reaction [41]. Therefore, the result demonstrates that the electrochemical performance of $LiFePO_4$/C material is enhanced by Pt-doping.

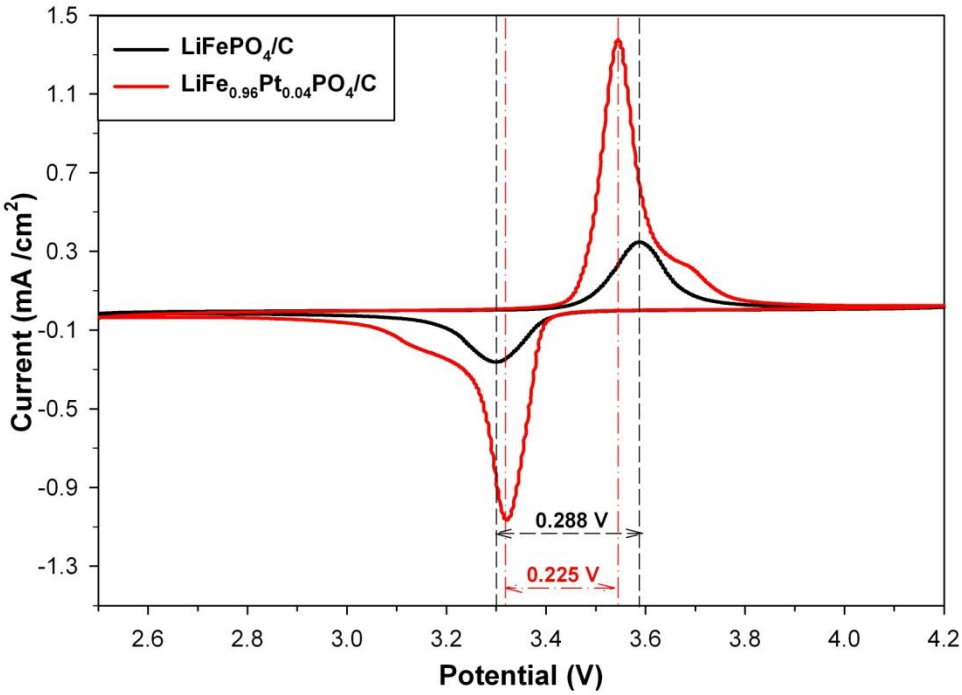

Figure 6-15: CV curves of the $LiFePO_4/C$ and $LiFe_{0.96}Pt_{0.04}PO_4/C$ samples at scan rate of 0.1 mV/s

Figure 6-16(a) shows the electrochemical impedance spectroscopy (EIS) curves of the $LiFePO_4/C$ and $LiFe_{0.96}Pt_{0.04}PO_4/C$ samples in the full discharged state of cells in frequency range of 0.01 Hz-1 mHz. Both EIS profiles contain a depressed semicircle and a straight line. The intercept of the depressed semicircle at high frequency region on the Z_{real} axis is attributed to the electrolyte resistance (R_e). The numerical value of the diameter of the depressed semicircle on the Z_{real} axis in the high to medium frequency is mainly related to charge transfer resistance (R_{ct}). The inclined line in the lower frequency is corresponded to the Warburg impedance (σ_w), which is associated with Li-ion diffusion in the $LiFePO_4$ electrode. The constant phase element (CPE) represents the double layer capacitance. The impedance data can be interpreted on the basis of an equivalent circuit as shown in inset of Figure 6-16(a). The fitted impedance

parameters are summarized in Table 6-3. It is observed that the R_{ct} value decreases after Pt doping. The smaller R_{ct} is favorable to the kinetic behavior during the redox reaction, enhancing the electrochemical properties [13].

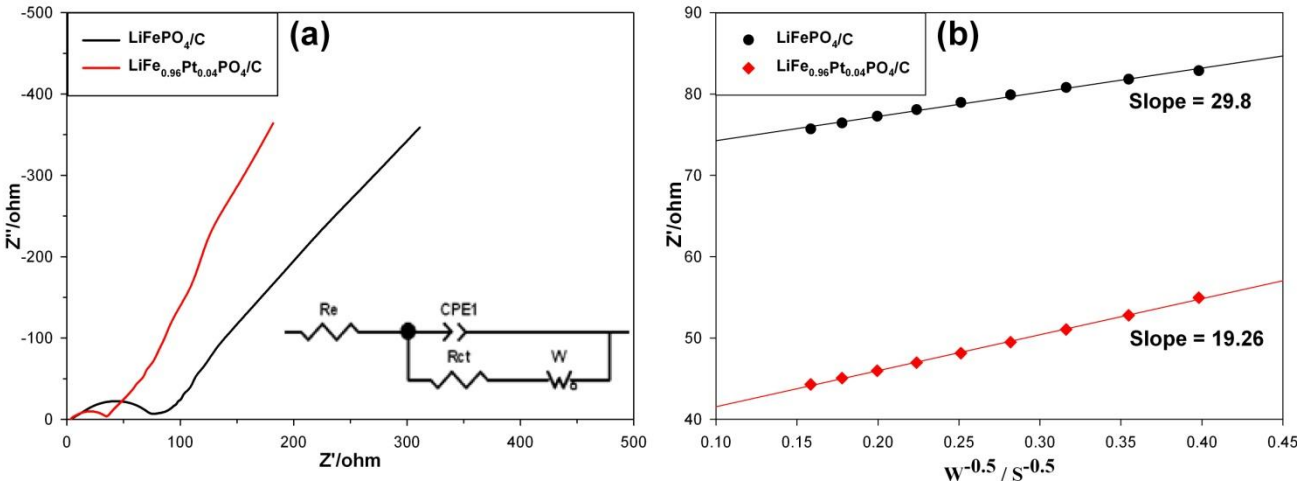

Figure 6-16: (a) EIS profiles of the $LiFePO_4$/C and $LiFe_{0.96}Pt_{0.04}PO_4$/C samples in the frequency range of 0.01 Hz-1 mHz. (b) The relationship between Zreal and $\omega^{-0.5}$ at low frequency. The inset of (a) shows an equivalent circuit

Based on the Eq (1), the Warburg impedance coefficient (σ_w) can be obtained from plot of Z_{re} vs. reciprocal root square of frequency ($\omega^{-0.5}$) in the low frequency region as shown in Figure 6-16(b). In addition, the lithium ion diffusion coefficient (D) could be calculated using Eq (2): [41]

$$Z_{re} = R_e + R_{ct} + \sigma_w \omega^{-0.5} \qquad (1)$$

$$D = R^2T^2 / 2A^2F^4n^4C^2\sigma_w^2 \qquad (2)$$

Where *D* is Li-ion diffusion coefficient (cm^2s^{-1}), R is the gas constant (8.314 J mol^{-1} K^{-1}), T is the absolute temperature (298 K), A is the surface area of cathode (cm^2), F is the Faraday constant (96486 C mol^{-1}), n is the number of electron involved in the redox reaction (1 in our

case), and C is the molar concentration of Li^+ ions. The obtained Warburg coefficient and calculated lithium ion diffusion coefficient are listed in Table 6-3. The results imply that the $LiFe_{0.96}Pt_{0.04}PO_4/C$ sample has higher lithium ion diffusion coefficient of 5.91×10^{-14} cm^2/s, compared with $LiFePO_4/C$ sample which is in consistent with the discharge capacities and CV results. The enhancement of Li-ion diffusion coefficient may be attributed to the following reasons. Firstly, Pt-doped in $LiFePO_4/C$ can act as a pillar to prevent the shrinking and collapse of crystal structure during the redox reaction, stabilizing crystal structure of $LiFePO_4/C$ material. Secondly, the $LiFe_{0.96}Pt_{0.04}PO_4/C$ sample contains more homogeneous particles with smaller size for more reaction. Therefore, the distance pathway for the Li-ion diffusion decreases and shorter diffusion path facilitates faster Li^+ intercalation/de-intercalation, improving Li-ion diffusion rate.

Table 6-3: Impedance parameters obtained from the EIS data

Sample	$\mathbf{R_e(\Omega)}$	$\mathbf{R_{ct}(\Omega)}$	$\boldsymbol{CPE_P}$	$\mathbf{\sigma_w(\Omega cm^2/s^{0.5})}$	$\mathbf{D(cm^2/s)}$
$LiFePO_4/C$	4.51	74.67	0.59	29.80	2.47×10^{-14}
$LiFe_{0.96}Pt_{0.04}PO_4/C$	3.29	29.56	0.64	19.26	5.91×10^{-14}

Cycling behaviors of the $LiFePO_4/C$ and $LiFe_{0.96}Pt_{0.04}PO_4/C$ samples are illustrated in Figure 6-17. All the cells were charged at fixed rate of 1C and discharged at various current rates. It is obvious that $LiFe_{0.96}Pt_{0.04}PO_4/C$ sample shows higher discharge capacities than $LiFePO_4/C$ sample. However, a small amount of capacity fading is observed specially at high current rates, indicating good cycling capability for the both samples. Moreover, for both samples, it can be observed that the capacities decreased when the current rates increased, because in higher current rates large amount of Li^+ must be extracted and inserted into the structure during relatively short

time. But this decrease is less important for $LiFe_{0.96}Pt_{0.04}PO_4/C$ (about 50 mAh/g) than those of $LiFePO_4/C$ (80 mAh/g). Therefore, this aspect must be significantly improved using an appropriate and optimized doping agent as Pt.

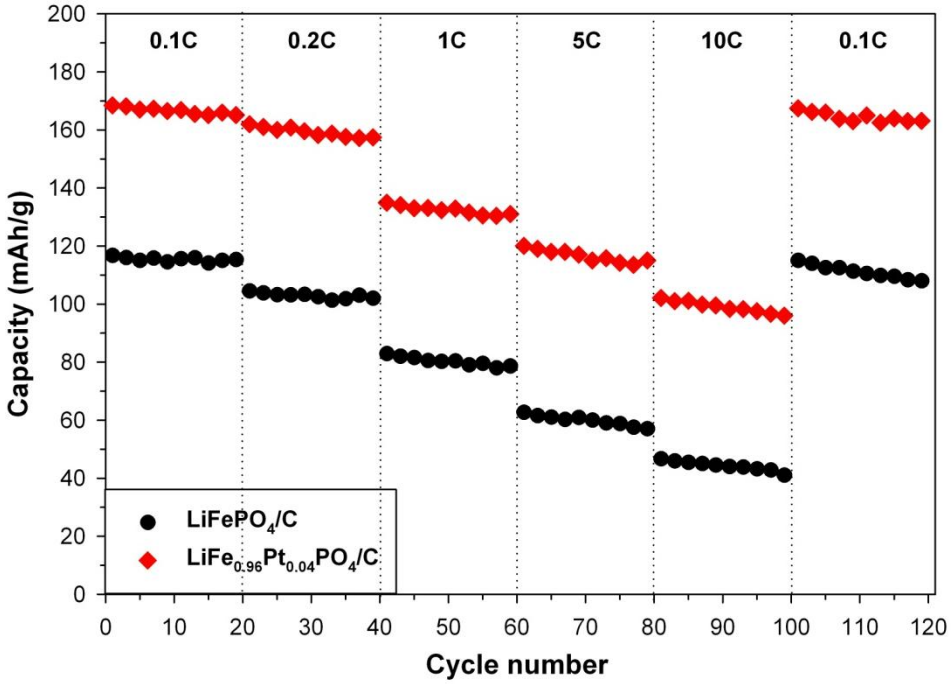

Figure 6-17: The cycling behaviors of the $LiFePO_4/C$ and $LiFe_{0.96}Pt_{0.04}PO_4/C$ samples at various current rates

6.2.4 Conclusions

$LiFePO_4$/C and $LiFe_{0.96}Pt_{0.04}PO_4$/C materials were synthesized by hydrothermal method and the effect of platinum doping on the structure and electrochemical properties of $LiFePO_4$/C was investigated for the first time by XRD, XPS, SEM, BET and electrochemical tests. The XRD and XPS results indicate that the platinum has been successfully incorporated into the $LiFePO_4$ material. The SEM results show that platinum doping helps to form homogeneous particles with smaller size than those of $LiFePO_4$/C. $LiFe_{0.96}Pt_{0.04}PO_4$/C sample exhibits superior electrochemical performances with specific capacities of 168, 162, 135, 120 and 102 mAh/g at 0.1C, 0.2C, 1C, 5C and 10C, respectively, in comparison with 117, 104, 83, 63 and 47 mAh/g for $LiFePO_4$/C sample. The improvement in electrochemical performances was attributed to the combination of pillar effect of platinum element for stabilizing the crystal structure and the homogeneous smaller particles for facilitating Li-ion movement, enhancing Li-ion diffusion rate caused by platinum doping.

References

[1] J.M. Tarascon, M. Armand, *Nature* **414** (2001) (6861) 359.

[2] J.B. Goodenough, Y. Kim, *Chemistry of Materials* **22** (2009) (3) 587.

[3] A.K. Padhi, K.S. Nanjundaswamy, J.B. Goodenough, *Journal of The Electrochemical Society* **144** (1997) (4) 1188.

[4] A. Yamada, S.C. Chung, K. Hinokuma *Journal of The Electrochemical Society* **148** (2001) (3) A224.

[5] P.P. Prosini, M. Lisi, D. Zane, M. Pasquali, *Solid State Ionics* **148** (2002) (1–2) 45.

[6] S.L. Bewlay, K. Konstantinov, G.X. Wang, S.X. Dou, H.K. Liu, *Materials Letters* **58** (2004) (11) 1788.

[7] N. Ravet, Y. Chouinard, J.F. Magnan, S. Besner, M. Gauthier, M. Armand, *Journal of Power Sources* **97–98** (2001) (0) 503.

[8] W.-J. Zhang, *Journal of Power Sources* **196** (2011) (6) 2962.

[9] R. Malik, D. Burch, M. Bazant, G. Ceder, *Nano Letters* **10** (2010) (10) 4123.

[10] X. Ou, H. Gu, Y. Wu, J. Lu, Y. Zheng, *Electrochimica Acta* **96** (2013) (0) 230.

[11] J. Hong, X.-L. Wang, Q. Wang, F. Omenya, N.A. Chernova, M.S. Whittingham, J. Graetz, *The Journal of Physical Chemistry C* **116** (2012) (39) 20787.

[12] H. Gao, L. Jiao, W. Peng, G. Liu, J. Yang, Q. Zhao, Z. Qi, Y. Si, Y. Wang, H. Yuan, *Electrochimica Acta* **56** (2011) (27) 9961.

[13] Z.-H. Wang, L.-X. Yuan, J. Ma, L. Qie, L.-L. Zhang, Y.-H. Huang, *Electrochimica Acta* **62** (2012) (0) 416.

[14] B. Kang, G. Ceder, *Nature* **458** (2009) (7235) 190.

[15] L. Wang, X. He, W. Sun, J. Wang, Y. Li, S. Fan, *Nano Letters* **12** (2012) (11) 5632.

[16] S.-Y. Chung, J.T. Bloking, Y.-M. Chiang, *Nat Mater* **1** (2002) (2) 123.

[17] P.S. Herle, B. Ellis, N. Coombs, L.F. Nazar, *Nat Mater* **3** (2004) (3) 147.

[18] N. Meethong, Y.-H. Kao, S.A. Speakman, Y.-M. Chiang, *Advanced Functional Materials* **19** (2009) (7) 1060.

[19] Z.-H. Wang, Q.-Q. Pang, K.-J. Deng, L.-X. Yuan, F. Huang, Y.-L. Peng, Y.-H. Huang, *Electrochimica Acta* **78** (2012) (0) 576.

[20] Y. Ge, X. Yan, J. Liu, X. Zhang, J. Wang, X. He, R. Wang, H. Xie, *Electrochimica Acta* **55** (2010) (20) 5886.

[21] J. Ma, B. Li, H. Du, C. Xu, F. Kang, *J Solid State Electrochem* **16** (2012) (1) 1.

[22] C. Hu, H. Yi, H. Fang, B. Yang, Y. Yao, W. Ma, Y. Dai, *Materials Letters* **65** (2011) (9) 1323.

[23] D.Y.W. Yu, K. Donoue, T. Kadohata, T. Murata, S. Matsuta, S. Fujitani, *Journal of The Electrochemical Society* **155** (2008) (7) A526.

[24] M. Talebi-Esfandarani, O. Savadogo, *Submitted to Journal of New Materials for Electrochemical Systems* (2013).

[25] M.S. Islam, D.J. Driscoll, C.A.J. Fisher, P.R. Slater, *Chemistry of Materials* **17** (2005) (20) 5085.

[26] D. Li, Y. Huang, D. Jia, Z. Guo, S.-J. Bao, *J Solid State Electrochem* **14** (2010) (5) 889.

[27] M.-R. Yang, W.-H. Ke, *Journal of The Electrochemical Society* **155** (2008) (10) A729.

[28] A.Y. Shenouda, H.K. Liu, *Journal of Alloys and Compounds* **477** (2009) (1–2) 498.

[29] H. Liu, Q. Cao, L.J. Fu, C. Li, Y.P. Wu, H.Q. Wu, *Electrochemistry Communications* **8** (2006) (10) 1553.

[30] M.-Y. Cho, K.-B. Kim, J.-W. Lee, H. Kim, H. Kim, K. Kang, K. Chul Roh, *RSC Advances* **3** (2013) (10) 3421.

[31] S.-A. Hong, S.J. Kim, J. Kim, B.G. Lee, K.Y. Chung, Y.-W. Lee, *Chemical Engineering Journal* **198–199** (2012) (0) 318.

[32] Z. Gong, Y. Yang, *Energy & Environmental Science* **4** (2011) (9) 3223.

[33] D. Jugović, D. Uskoković, *Journal of Power Sources* **190** (2009) (2) 538.

[34] J. Qian, M. Zhou, Y. Cao, X. Ai, H. Yang, *The Journal of Physical Chemistry C* **114** (2010) (8) 3477.

[35] B. Ellis, W.H. Kan, W.R.M. Makahnouk, L.F. Nazar, *Journal of Materials Chemistry* **17** (2007) (30) 3248.

[36] M.K. Devaraju, I. Honma, *Advanced Energy Materials* **2** (2012) (3) 284.

[37] W.-J. Zhang, *Journal of The Electrochemical Society* **157** (2010) (10) A1040.

[38] O. Xiuqin, P. Lin, G. Haichen, W. Yichen, L. Jianwei, *Journal of Materials Chemistry* **22** (2012) (18) 9064.

[39] M. Talebi-Esfandarani, O. Savadogo, *Submitted to Journal of Applied electrochemistry* (2013).

[40] M. Talebi-Esfandarani, O. Savadogo, *Submitted to Electrochimica Acta* (2013).

[41] Bard a.J., L.R. Faulkner, Electrochemical Methods. Fundamentals and Applications., Wiley (2001).

CHAPTER 7 GENERAL DISCUSSION

As is well known, low electrical conductivity and poor ionic diffusion are the determining factors of $LiFePO_4$ which limit its application in LIB. Therefore, improvement in the electrical conductivity and its ionic diffusion can enhance the electrochemical behaviour of this material. In this regard, the first part of this study was devoted to carbon coating to improve the electrical conductivity of $LiFePO_4$ material. In the first step, it was attempted to synthesis a pure phase of $LiFePO_4$ material via hydrothermal method in the shortest duration time (6 h). Shorter time prevents the particle growth during synthesis and saves energy. Afterwards, carbon coating was performed with different amount of carbon to achieve the optimized, thin and uniform layer of carbon. Citric acid was used as the carbon source. XRD results showed that carbon did not affect the structure of $LiFePO_4$ since carbon coating was done after synthesis of the $LiFePO_4$. The result showed that optimized carbon content (about 30%) can lead to a more uniform and proper carbon distribution with high electrical conductivity. The samples with low amount of carbon delivered poor discharge capacity due to an insufficient carbon layer formation and low electrical conductivity. However, excessive carbon content formed a thick layer of carbon with agglomeration. This thick layer of carbon could impede the diffusion of Li^+ ions through the cathode material; thus, leading to the decrease of discharge capacity. In this way, the optimized amount of carbon was determined to obtain high performance $LiFePO_4$/C cathode material.

In addition, a pure phase of $LiFePO_4$ material was synthesized via sol-gel method and carbon coating was carried out with the optimized amount of carbon (30% of citric acid) to obtain $LiFePO_4$/C. However, the film of electrode (a mixture of $LiFePO_4$/C, carbon black and PVDF) peeled off from the aluminum current collector after drying during the fabrication of electrode.

After many efforts, it was found out that the peeling problem happened when citric acid was used as carbon source for coating of $LiFePO_4$ material prepared via sol-gel method. The carbon source was changed from citric acid to sucrose and the problem was solved. Therefore, sucrose was used as carbon source for coating of $LiFePO_4$ for the rest of the study although the sucrose requires high temperature processing for carbonization.

In the second part of this study an attempt was made to improve the ion diffusion rate of $LiFePO_4$/C material via a metal doping approach. In particular, palladium & platinum were doped in the $LiFePO_4$ material prepared via sol-gel method and then carbon coating was done by sucrose in the pristine $LiFePO_4$ and doped-$LiFePO_4$ material. The influence of doping on the physical-chemical properties and the electrochemical performance of the $LiFePO_4$/C material were investigated in details. At the beginning of this study, by doping $LiFePO_4$/C with the palladium and platinum elements, high discharge capacities and good cycling performances were expected. This is due to the high stability feature of palladium and platinum which can stabilize the crystal structure of $LiFePO_4$/C during charge/discharge process, resulting in high electrochemical performance.

The XRD results illustrated that Pd doping facilitated the formation of Li_3PO_4 impurity phase and the lattice parameters of $LiFePO_4$ structure decreased and shrunk in size by increasing the palladium content. In addition, it was observed from SEM images that the size of particles increased and agglomerated after doping. Also, palladium doping decreased the specific surface areas of the samples. Electrochemical results showed that discharge capacity and rate cycling capability of samples decreased by palladium doping. The correlation of impurity and morphological features on the electrochemical properties of doped material were examined. The reduction in the electrochemical properties can be attributed to the formation of Li_3PO_4 impurity

phase, shrinking in lattice parameter, agglomeration, large particle size and low surface area which were caused by palladium doping. In fact, the Li_3PO_4 impurity can act as an inert and inactive mass during the redox process and a shrinkage in lattice parameters makes the diffusion of Li^+ ions into the $LiFePO_4$ structure difficult due to the smaller space for the diffusion. Also, the large particle sizes increase the diffusion path for the movement of Li^+ ion during intercalation/de-intercalation process, reduces the rate of reaction and eventually decreases the electrochemical performance. These results suggest that palladium doping via sol-gel method is not a beneficial method to improve the electrochemical performance of $LiFePO_4$/C cathode material.

In contrast, Pt-doped material prepared via the sol-gel method revealed a significant enhancement in the electrochemical properties of $LiFePO_4$/C material, because Pt doping expanded the lattice parameters structure and increased the crystallinity of the material without forming any impurity. Enlargement and expansion in lattice parameters provided more space for the diffusion of Li^+ ions and facilitated the movement of Li^+ ions through the structure of $LiFePO_4$ material during process, enhancing the Li ion diffusion. In addition, Pt doping reduced the size of particle from 100-500 to 100-200 nm and particles with a better uniformity in size distribution and more homogeneity were observed. It is believed that the uniform particles with smaller sizes are favourable to reduce the diffusion path of Li^+ ion through the structure, resulting in the fast diffusion kinetics and enhancing the electrochemical performance. Pt-doped $LiFePO_4$/C sample delivered the discharge capacities of 166, 156, 142 and 140 mAh/g at 0.2C, 1C, 5C and 10C rates, respectively, as compared to 164, 150, 120 and 105 mAh/g for the undoped $LiFePO_4$/C.

In another set of experiments, a hydrothermal method was used for preparing $LiFePO_4$ and doped-$LiFePO_4$ materials followed by carbon coating with sucrose. The materials were synthesized at low temperature which is the most important advantage of the hydrothermal method because of energy saving. The influence of palladium and platinum doping on structure and morphology of $LiFePO_4$ material were particularly investigated and their correlations to the electrochemical properties of materials were studied in detail. The XRD results indicated that sample with a high amount of Pd (4%) contains unwanted Li_3PO_4 impurity phase. Therefore, the amount of palladium was optimized in (2%) to avoid formation of any impurity. As observed from SEM images and BET results, optimized palladium doping reduced the size of particles and increased the specific surface area unlike the 4% doping sample. As is well known in the literature, particles with smaller size reduce the distance for diffusion of Li^+ ions and improve the electrochemical performances of material which are compatible with our results. Electrochemical results illustrated that the $LiFe_{0.98}Pd_{0.02}PO_4/C$ sample delivered the discharge capacity of 168, 159, 130, 93, 70 mAh/g at 0.1C, 0.2C, 1C, 5C and 10C rates, respectively, in comparison with 117, 104, 83, 63 and 47 mAh/g for the $LiFePO_4/C$ sample. The electrochemical results indicated that $LiFe_{0.98}Pd_{0.02}PO_4/C$ sample enhanced the reversibility of reaction, and decreased the charge transfer resistance and potential polarization which confirmed better kinetic behavior from electrochemical consideration. The improvement can be attributed to two reasons. Firstly, the optimized Pd-doped might act as a pillar to prevent the shrinking and collapse of lattice structure, stabilizing the crystal structure during the intercalation/de-intercalation process of Li^+ ions. Another reason can be related to small particle with large surface area for more reaction. However, by increasing the Pd content, the discharge capacity decreased to 150, 122, 104, 84 and 63 mAh/g for the $LiFe_{0.96}Pd_{0.04}PO_4/C$ sample. This is probably due to the existence of the

Li_3PO_4 impurity phase, small surface area, and difficulty of Li^+ ion diffusion. Generally, the optimized palladium doping is helpful to improve the electrochemical performance of $LiFePO_4$/C material prepared via hydrothermal method.

In the final set of experiments, the effects of Pt doping on the chemical-physical properties and electrochemical performances of $LiFePO_4$/C sample prepared via hydrothermal method were examined. The XRD results revealed that the platinum could be successfully doped into the $LiFePO_4$ bulk structure. No observable peaks for Li_3PO_4 impurity phase were detected for the $LiFe_{0.96}Pt_{0.04}PO_4$ sample. The intensity of main diffraction peaks for Pt-doped sample was higher and sharper than $LiFePO_4$ sample, indicating better crystallinity for the Pt-doped sample which might imply crystal growth by platinum contribution. The same XRD result was observed for Pt-doped sample prepared via sol-gel method. The XPS results indicated that the oxidation state of the iron was +2. It should be noted that the Pt doping does not considerably change the chemical valence of Fe^{2+}. The SEM and BET results showed that platinum doping reduces the size of particles and increases specific surface area of particles, respectively. Particles with smaller sizes provide shorter path for diffusion and increase the rate of reaction due to increased reaction surface. This was confirmed by EIS technique which showed higher ion diffusion coefficient of (5.91×10^{-14}) for the Pt-doped sample in comparison to (2.47×10^{-14}) for undoped sample. Therefore, better electrochemical performance was observed for the Pt-doped sample. $LiFe_{0.96}Pt_{0.04}PO_4$/C delivered the specific capacity of 168, 162, 135, 120 and 102 mAh/g at 0.1C, 0.2C, 1C, 5C and 10C, respectively. The improvement in electrochemical performances for the Pt-doped sample can be attributed to the combination of homogeneous small particles and pillar effect of platinum on stabilizing the crystal structure.

The positive effect of doping on the electrochemical properties of $LiFePO_4$ was first reported by Chung et al. [71]. Since then, many studies reported that doping with V, Na, Mo, Ti, Mg, Nd, Ni, Al, Co, Zn, Sn, Cu, Cr, Cl, La and F improved the specific capacities of $LiFePO_4$ [7, 15, 84, 85, 107-140]. Figure 7-1 compares the specific discharge capacities of some doped-$LiFePO_4$ materials reported in the literature with the performance of the best sample in this work ($LiFe_{0.96}Pt_{0.04}PO_4$/C prepared by sol-gel method). $LiFe_{0.96}Pt_{0.04}PO_4$/C sample delivers the specific discharge capacities of 166, 156, 142, and 140 mAh/g at current rates of 0.2C, 1C, 5C, and 10C respectively, which are in the higher range of the reported data for $LiFePO_4$ in the literature, especially at high current rates, as shown in Figure 7-1. From the author's knowledge, $LiFe_{0.96}Pt_{0.04}PO_4$/C sample exhibits one of the best performances reported until now for $LiFePO_4$ materials tested in a regular cell. It is worthy to note that the contribution of Pt doping to achieve excellent performance at high current rates is more significant, because a huge amount of Li^+ ion tends to enter the structure of material in high current rates. Hence, Pt doping provides more space for the movement of Li^+ ions, facilitating the Li^+ ions diffusion as well as stabilizing the crystal structure during the charge/discharge process. However, a higher amount of pt doping (6%) prepared by sol-gel method reduced the performance. $LiFe_{0.94}Pt_{0.06}PO_4$/C sample delivers the specific discharge capacities of 135, 127, 102, and 77 mAh/g at current rates of 0.2C, 1C, 5C, and 10C, respectively.

In chapter 4, one interesting result is that the two samples (LF/40C and LF/50C) with higher BET surface area showed lower discharge capacities in comparison with LF/30C sample with lower BET surface area as shown in Figure 7-2. The variation of the discharge capacity with the BET surface area exhibited an optimum value at LF/30C which BET surface area is lower than those of LF/40C and LF/50C, but higher than of LF/20C. Accordingly, the sample with a BET

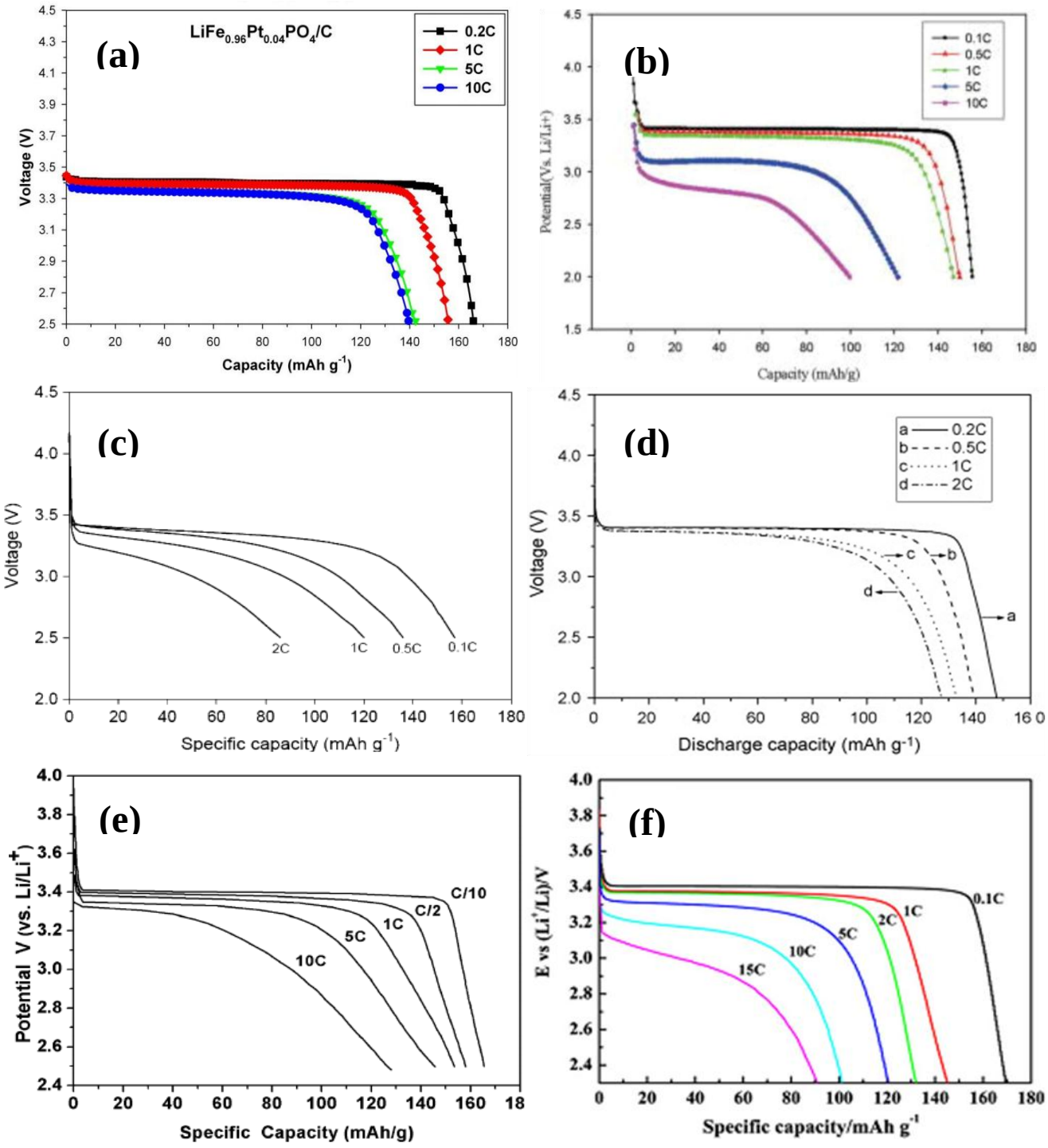

Figure 7-1: Specific discharge capacities of different doped LiFePO4/C materials at various current rates. (a) $LiFe_{0.96}Pt_{0.04}PO_4/C$ prepared by sol-gel in this work, (b) $LiFeP_{0.95}V_{0.05}O_4/C$ [108], (c) $LiFe_{0.9}Mg_{0.1}PO_4/C$ [120], (d) $LiFe_{0.98}Cu_{0.02}PO_4/C$ [131], (e) $LiFe_{0.97}Sn_{0.03}PO_4/C$ [133], (f) F-doped $LiFePO_4/C$ [138]

surface area of 34 m^2/g (LF/30C) exhibit better rate capacity than the samples with a BET of 45 m^2/g and 48 m^2/g (LF40/C and LF50/C). This result further suggested that a BET surface area is not the relevant parameter to probe the discharge capacity, because high BET surface area is not correlated to high electrochemically active surface area for Li-ion reaction processes.

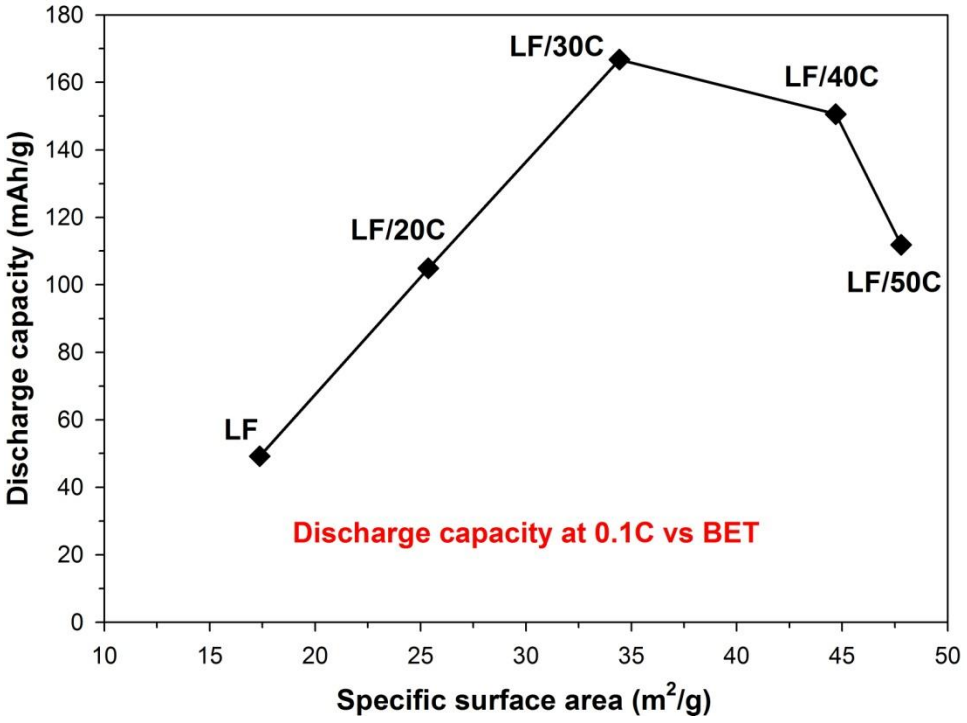

Figure 7-2: Specific discharge capacities at 0.1C rate of $LiFePO_4$ coated with different amount of carbon vs their specific surface area

Instead, there seems to be direct relationship between Li^+ ion diffusion coefficient and specific capacity. A high Li^+ ion diffusion coefficient may have a determining effect on the performance of $LiFePO_4$ cathode materials as shown in Figure 7-3. The specific capacity of $LiFePO_4$ has clear dependence on the Li^+ ion diffusion coefficient. LF/30C sample which exhibited the highest ion diffusion coefficient had the best discharge capacity.

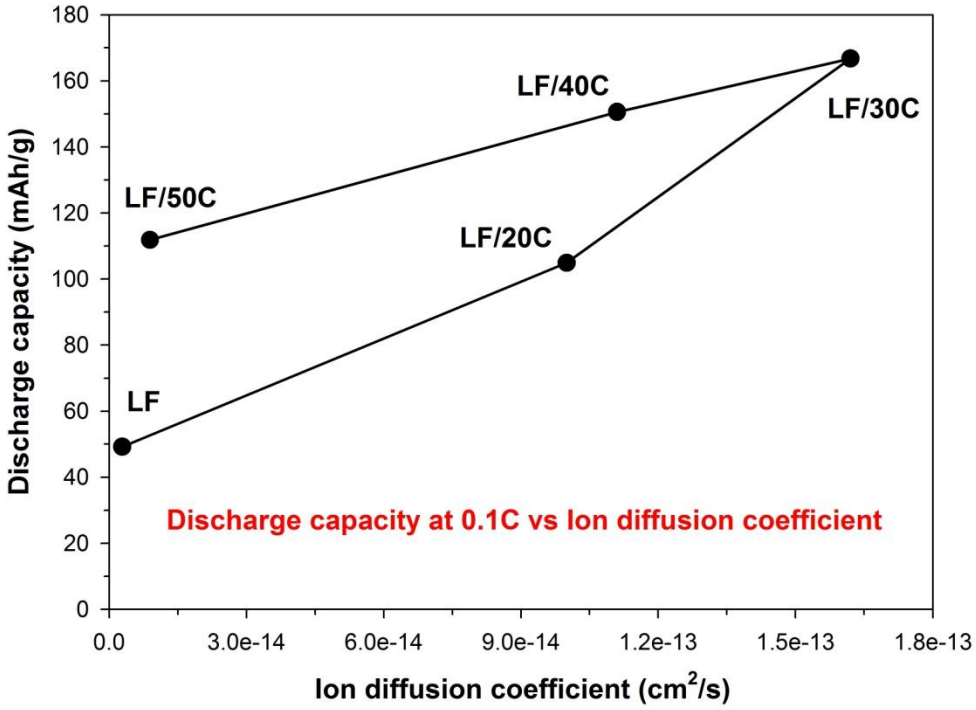

Figure 7-3: Specific discharge capacities at 0.1C rate of $LiFePO_4$ coated with different amounts of carbon vs the Li-ion diffusion coefficient in the electrode

It is well established that the particle size reduction appears to have significant positive effect on the improvement of the rate capacity. Figure 7-4 shows the variation of the specific capacity as a function of particle size for samples prepared by sol-gel method presented in chapter 5. The rate discharge capacity decreases almost linearly when the particle sizes increased. The benefit effect of adding Pt or Pd is the change of the particle size of the cathode. The Pt-doped sample with particle sizes of around 100-200 nm shows the best capacity of 140 mAh/g at 10C. Analysis of the experimental data also suggests that particle size reduction has the more significant effect in the improvement the performance rather than the surface area**.** The analysis points to the conclusion that doping appears to be a critical factor in controlling the capacity, especially at high discharge current rates by improving Li^+ ion diffusion rate.

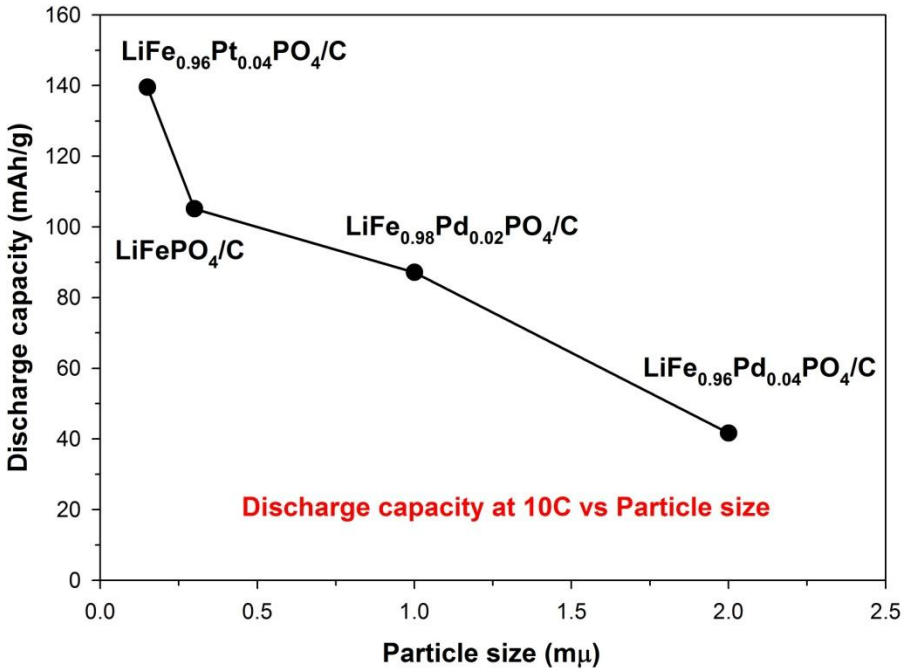

Figure 7-4: Specific discharge capacities at 10C rate of doped-$LiFePO_4$/C materials prepared by sol-gel vs their particle size

Generally, the results revealed a significant enhancement in the electrochemical performance caused via Pt doping prepared either by the sol-gel or hydrothermal method. In case of palladium doping attention must be paid carefully since it facilitates the formation of impurity phase in both methods. Optimized palladium content was defined to be around 2% to avoid impurity formation during the hydrothermal method. Furthermore, the impurity was formed via sol-gel method with any palladium content. Further study is still needed to address these issues. There is a correlation between impurity phase formation and particle sizes on the electrochemical performance of material. Samples with larger particle sizes and more impurity have lower electrochemical performance. The improvement achieved via doping approach can, however, increase the motivation of future works for further development of $LiFePO_4$ material.

CHAPTER 8 CONCLUSIONS AND RECOMMENDATIONS

8.1 Conclusions

In this dissertation, carbon coating and metal doping approaches of $LiFePO_4$ material were investigated to explore its applications as the positive cathode material for rechargeable LIBs. Hydrothermal and sol-gel methods were used for synthesis of $LiFePO_4$ and doped-$LiFePO_4$ materials. In the first part, the carbon coating of the $LiFePO_4$ was done with different amounts of citric acid as the carbon source to obtain $LiFePO_4$/C with high electrical conductivity. The optimized amount of carbon which exhibited high electrochemical performance was determined to be around 30%.

In the second part, $LiFe_{0.98}Pd_{0.02}PO_4$, $LiFe_{0.96}Pd_{0.04}PO_4$ and $LiFe_{0.96}Pt_{0.04}PO_4$ materials were successfully synthesized using the sol-gel method. The optimized amount of carbon was used to coat the doped materials to obtain $LiFe_{0.98}Pd_{0.02}PO_4$/C, $LiFe_{0.96}Pd_{0.04}PO_4$/C and $LiFe_{0.96}Pt_{0.04}PO_4$/C for electrochemical measurement testing. In the last part, $LiFe_{0.98}Pd_{0.02}PO_4$, $LiFe_{0.96}Pd_{0.04}PO_4$ and $LiFe_{0.96}Pt_{0.04}PO_4$ materials were successfully synthesized using a hydrothermal method and carbon coating was done with the optimized amount of carbon. The main focus of this thesis was to investigate the effects of palladium and platinum doping on the structure, purity, particle size and electrochemical properties of $LiFePO_4$/C material.

For the Pd-doped material prepared using sol-gel method, Pd facilitated the formation of Li_3PO_4 impurity phase and the lattice parameters decreased linearly with increasing Pd content. The particles became larger and agglomerated by incorporation of the palladium. The electrochemical results showed that the specific capacities of the $LiFePO_4$/C sample prepared using sol-gel method decreased by increasing the amount of Pd doping. The capacity loss of the Pd-doped samples synthesized via sol-gel method was found to have a liner relationship with the impurity

and particle sizes. On the other hand, among the Pd-doped samples prepared with hydrothermal method, $LiFe_{0.98}Pd_{0.02}PO_4/C$ sample showed a significant improvement with discharge capacities of 168, 159, 130, 93 and 70 mAh/g at 0.1C, 0.2C, 1C, 5C and 10C, respectively. The high electrochemical performance was due to the smaller uniform particles and the pillar effect of Pd which prevented the shrinking and collapse of structure, stabilizing the crystal structure during cycling. However, the electrochemical activity and cycle life degraded by increasing Pd content due to the large particle sizes and formation of Li_3PO_4 impurity phase in the $LiFe_{0.96}Pd_{0.04}PO_4/C$ sample.

In case of Pt doping, $LiFe_{0.96}Pt_{0.04}PO_4/C$ sample prepared via both hydrothermal and sol-gel methods exhibited superior electrochemical performances compared with $LiFePO_4/C$ sample. The improvement in electrochemical performance can be attributed to three reasons. Firstly, Pt doping expands the lattice parameters of crystal structure and provides more space for the movement of Li ions, facilitating the Li ion diffusion rate. Secondly, platinum doping helps to form homogeneous small particles for shorter diffusion path. Thirdly, platinum can act as pillar for stabilizing the crystal structure during charge/discharge process.

Overall, the electrochemical performances in the doped $LiFePO_4$ material depend on the existence of the impurity phase, particle size, specific surface area, changing lattice parameters and pillar effect of doped element. This study contributes to the advancement of the knowledge of fundamental properties of doped-$LiFePO_4$ materials and their correlations to electrochemical activities. Understanding the involved electrochemical processes from a fundamental point of view can provide valuable insight in recognizing the structure-properties relationship of the material and help design or search for new functional systems with desired performance features. The studies described in this dissertation have provided further insight into the features of

$LiFePO_4$ material and valuable information regarding the carbon coating and the metal doping strategies as well as the sol-gel and hydrothermal methods for preparation.

8.2 Recommendations

Although this thesis provides a new insight in understanding the preparation and characterization of $LiFePO_4$ cathode material for LIB application, using doping techniques, there are many issues which remain to be explored in this field. Therefore, the following opportunities have arisen and some suggestions are presented for future work, along the lines of this research, to understand the fundamental details, synthesis and characterization of $LiFePO_4$ material.

1. It is suspected that the low discharge capacity of most of the prepared Pd-doped materials is mainly due to the existence of Li_3PO_4 impurity. This impurity phase is thought to affect the poor performance and the ability to cycle of the cathodes in this work. Formation of this impurity on the cathodes is believed to limit the diffusion of Li^+ ions into the bulk of material, resulting in the low electrochemical performance of the cell. Further research is required to identify the reason of the Li_3PO_4 phase formation and find the possible remedies to remove it.

2. Substitution of other elements in the $LiFePO_4$ structure needs to be investigated for further improvement of its electrochemical properties. This might enable us to achieve a deeper insight of the doping strategy.

3. The doping content of Pt needs to be further optimized. This may enable us to further enhance the discharge capacity of Pt-doped $LiFePO_4$ materials.

4. An alternate approach is to investigate the properties and fundamental aspects of the doped material by a theoretical study. New scientific and technological knowledge related to these studies will provide us with valuable information regarding the Li^+ ion diffusion and electrical conductivity of $LiFePO_4$. The present research has shown that Pt doping and optimized Pd doping are affective approaches to improve the electrochemical performance of $LiFePO_4$ material. Therefore, the combination of experiment and simulation can offer deep insight into the $LiFePO_4$ properties.

REFERENCES

[1] J.M. Tarascon, M. Armand, Nature, 414 (2001) 359-367.

[2] M.S. Whittingham, Chemical Reviews, 104 (2004) 4271-4302.

[3] Z. Chen, J.R. Dahn, Electrochimica Acta, 49 (2004) 1079-1090.

[4] A.K. Padhi, K.S. Nanjundaswamy, J.B. Goodenough, Journal of The Electrochemical Society, 144 (1997) 1188-1194.

[5] A. Yamada, S.C. Chung, K. Hinokuma Journal of The Electrochemical Society, 148 (2001) A224-A229.

[6] N. Ravet, Y. Chouinard, J.F. Magnan, S. Besner, M. Gauthier, M. Armand, Journal of Power Sources, 97-98 (2001) 503-507.

[7] P.S. Herle, B. Ellis, N. Coombs, L.F. Nazar, Nat Mater, 3 (2004) 147-152.

[8] S. Ferrari, R.L. Lavall, D. Capsoni, E. Quartarone, A. Magistris, P. Mustarelli, P. Canton, The Journal of Physical Chemistry C, 114 (2010) 12598-12603.

[9] D. Jugovic, D. Uskokovic, Journal of Power Sources, 190 (2009) 538-544.

[10] Z. Gong, Y. Yang, Energy & Environmental Science, 4 (2011) 3223-3242.

[11] H.-K. Song, K.T. Lee, M.G. Kim, L.F. Nazar, J. Cho, Advanced Functional Materials, 20 (2010) 3818-3834.

[12] B. Ellis, W.H. Kan, W.R.M. Makahnouk, L.F. Nazar, Journal of Materials Chemistry, 17 (2007) 3248-3254.

[13] X. Qin, X. Wang, H. Xiang, J. Xie, J. Li, Y. Zhou, The Journal of Physical Chemistry C, 114 (2010) 16806-16812.

[14] J. Chen, M.S. Whittingham, Electrochemistry Communications, 8 (2006) 855-858.

[15] X. Ou, G. Liang, L. Wang, S. Xu, X. Zhao, Journal of Power Sources, 184 (2008) 543-547.

[16] J.-K. Kim, J.-W. Choi, G.S. Chauhan, J.-H. Ahn, G.-C. Hwang, J.-B. Choi, H.-J. Ahn, Electrochimica Acta, 53 (2008) 8258-8264.

[17] H. Huang, S.C. Yin, L.F. Nazar, Electrochemical and Solid-State Letters, 4 (2001) A170-A172.

[18] Y. Cui, X. Zhao, R. Guo, Materials Research Bulletin, 45 (2010) 844-849.

[19] M.S. Whittingham, Science, 192 (1976) 1126-1127.

[20] M. Armand, J.-M. Tarascon, Nature, 451 (2008) 652-657.

[21] P.G. Balakrishnan, R. Ramesh, T. Prem Kumar, Journal of Power Sources, 155 (2006) 401-414.

[22] B.M.L. Rao, R.W. Francis, H.A. Christopher, Journal of The Electrochemical Society, 124 (1977) 1490-1492.

[23] R. Yazami, P. Touzain, Journal of Power Sources, 9 (1983) 365-371.

[24] Nagaura .T, Tozawa.K, Lithium ion rechargeable battery, in: Batteries Solar Cells,, 1990, pp. 209.

[25] M. Winter, J.O. Besenhard, Electrochimica Acta, 45 (1999) 31-50.

[26] J. Cabana, Z. Stoeva, J.J. Titman, D.H. Gregory, M.R. Palacín, Chemistry of Materials, 20 (2008) 1676-1678.

[27] E. Ferg, R.J. Gummow, A. de Kock, M.M. Thackeray, Journal of The Electrochemical Society, 141 (1994) L147-L150.

[28] S. Yang, X. Feng, L. Zhi, Q. Cao, J. Maier, K. Müllen, Advanced Materials, 22 (2010) 838-842.

[29] P. Guo, H. Song, X. Chen, Journal of Materials Chemistry, 20 (2010) 4867-4874.

[30] M.-H. Park, M.G. Kim, J. Joo, K. Kim, J. Kim, S. Ahn, Y. Cui, J. Cho, Nano Letters, 9 (2009) 3844-3847.

[31] X.W. Lou, Y. Wang, C. Yuan, J.Y. Lee, L.A. Archer, Advanced Materials, 18 (2006) 2325-2329.

[32] L.-F. Cui, Y. Yang, C.-M. Hsu, Y. Cui, Nano Letters, 9 (2009) 3370-3374.

[33] B. Zhang, Q.B. Zheng, Z.D. Huang, S.W. Oh, J.K. Kim, Carbon, 49 (2011) 4524-4534.

[34] J.Y. Huang, L. Zhong, C.M. Wang, J.P. Sullivan, W. Xu, L.Q. Zhang, S.X. Mao, N.S. Hudak, X.H. Liu, A. Subramanian, H. Fan, L. Qi, A. Kushima, J. Li, Science, 330 (2010) 1515-1520.

[35] D. Wang, D. Choi, J. Li, Z. Yang, Z. Nie, R. Kou, D. Hu, C. Wang, L.V. Saraf, J. Zhang, I.A. Aksay, J. Liu, ACS Nano, 3 (2009) 907-914.

[36] M. Thackeray, Nat Mater, 1 (2002) 81-82.

[37] K. Mizushima, P.C. Jones, P.J. Wiseman, J.B. Goodenough, Materials Research Bulletin, 15 (1980) 783-789.

[38] G.G. Amatucci, J.M. Tarascon, L.C. Klein, Journal of The Electrochemical Society, 143 (1996) 1114-1123.

[39] Z. Chen, Z. Lu, J.R. Dahn, Journal of The Electrochemical Society, 149 (2002) A1604-A1609.

[40] J.K. Ngala, N.A. Chernova, M. Ma, M. Mamak, P.Y. Zavalij, M.S. Whittingham, Journal of Materials Chemistry, 14 (2004) 214-220.

[41] J.R. Dahn, U.v. Sacken, M.W. Juzkow, H. Al-Janaby, Journal of The Electrochemical Society, 138 (1991) 2207-2211.

[42] R. Kanno, H. Kubo, Y. Kawamoto, T. Kamiyama, F. Izumi, Y. Takeda, M. Takano, Journal of Solid State Chemistry, 110 (1994) 216-225.

[43] M. Song, S. Kwon, I. Kwon, H. Park, Journal of Applied Electrochemistry, 37 (2007) 421-427.

[44] Ohzuku. T., Makimura. Y., Chem Lett, 7 (2001) 642-643.

[45] E. Rossen, C.D.W. Jones, J.R. Dahn, Solid State Ionics, 57 (1992) 311-318.

[46] Y. Makimura, T. Ohzuku, Journal of Power Sources, 119–121 (2003) 156-160.

[47] M. Wu, Q. Zhang, H. Lu, A. Chen, Solid State Ionics, 169 (2004) 47-50.

[48] S.-h. Wu, M.-t. Yu, Journal of Power Sources, 165 (2007) 660-665.

[49] J. Cho, T.-J. Kim, B. Park, Journal of The Electrochemical Society, 149 (2002) A288-A292.

[50] M.M. Thackeray, W.I.F. David, P.G. Bruce, J.B. Goodenough, Materials Research Bulletin, 18 (1983) 461-472.

[51] R.J. Gummow, A. de Kock, M.M. Thackeray, Solid State Ionics, 69 (1994) 59-67.

[52] M.M. Thackeray, L.A. de Picciotto, W.I.F. David, P.G. Bruce, J.B. Goodenough, Journal of Solid State Chemistry, 67 (1987) 285-290.

[53] H.J. Dong, J.S. Young, M.O. Seung, Journal of The Electrochemical Society, 143 (1996) 2204-2211.

[54] X. Yongyao, Z. Yunhong, Y. Masaki, Journal of The Electrochemical Society, 144 (1997) 2593-2600.

[55] K. Amine, J. Liu, S. Kang, I. Belharouak, Y. Hyung, D. Vissers, G. Henriksen, Journal of Power Sources, 129 (2004) 14-19.

[56] R. Santhanam, B. Rambabu, Journal of Power Sources, 195 (2010) 5442-5451.

[57] N. Amdouni, F. Gendron, A. Mauger, H. Zarrouk, C.M. Julien, Materials Science and Engineering: B, 129 (2006) 64-75.

[58] X. Yong-Nian, C. Sung-Yoon, T.B. Jason, C. Yet-Ming, W.Y. Ching, Electrochemical and Solid-State Letters, 7 (2004) A131-A134.

[59] N. Terada, T. Yanagi, S. Arai, M. Yoshikawa, K. Ohta, N. Nakajima, A. Yanai, N. Arai, Journal of Power Sources, 100 (2001) 80-92.

[60] A. Yamada, S.C. Chung, K. Hinokuma, Journal of The Electrochemical Society, 148 (2001) A224-A229.

[61] Z.-R. Chang, H.-J. Lv, H.-W. Tang, H.-J. Li, X.-Z. Yuan, H. Wang, Electrochimica Acta, 54 (2009) 4595-4599.

[62] S. Okada, S. Sawa, M. Egashira, J.-i. Yamaki, M. Tabuchi, H. Kageyama, T. Konishi, A. Yoshino, Journal of Power Sources, 97–98 (2001) 430-432.

[63] N.N. Bramnik, K. Nikolowski, C. Baehtz, K.G. Bramnik, H. Ehrenberg, Chemistry of Materials, 19 (2007) 908-915.

[64] J. Liu, T.E. Conry, X. Song, L. Yang, M.M. Doeff, T.J. Richardson, Journal of Materials Chemistry, 21 (2011) 9984-9987.

[65] J. Wolfenstine, J. Allen, Journal of Power Sources, 136 (2004) 150-153.

[66] G. Chen, T.J. Richardson, Journal of Power Sources, 195 (2010) 1221-1224.

[67] T. Muraliganth, A. Manthiram, The Journal of Physical Chemistry C, 114 (2010) 15530-15540.

[68] A.S. Andersson, B. Kalska, L. Häggström, J.O. Thomas, Solid State Ionics, 130 (2000) 41-52.

[69] Z. Li, D. Zhang, F. Yang, Journal of Materials Science, 44 (2009) 2435-2443.

[70] M.S. Islam, D.J. Driscoll, C.A.J. Fisher, P.R. Slater, Chemistry of Materials, 17 (2005) 5085-5092.

[71] S.-Y. Chung, J.T. Bloking, Y.-M. Chiang, Nat Mater, 1 (2002) 123-128.

[72] M.D. Marca, H. Yaoqin, M. Frank, K. Robert, Electrochemical and Solid-State Letters, 6 (2003) A207-A209.

[73] E. Ali, Journal of The Electrochemical Society, 151 (2004) A1816-A1819.

[74] N.A. Chernova, M. Roppolo, A.C. Dillon, M.S. Whittingham, Journal of Materials Chemistry, 19 (2009) 2526-2552.

[75] C. Zhaohui, J.R. Dahn, Journal of The Electrochemical Society, 149 (2002) A1184-A1189.

[76] J.-M. Chen, C.-H. Hsu, Y.-R. Lin, M.-H. Hsiao, G.T.-K. Fey, Journal of Power Sources, 184 (2008) 498-502.

[77] C.H. Mi, X.G. Zhang, X.B. Zhao, H.L. Li, Journal of Alloys and Compounds, 424 (2006) 327-333.

[78] C. Lai, Q. Xu, H. Ge, G. Zhou, J. Xie, Solid State Ionics, 179 (2008) 1736-1739.

[79] S. Yang, P.Y. Zavalij, M. Stanley Whittingham, Electrochemistry Communications, 3 (2001) 505-508.

[80] A. Kuwahara, S. Suzuki, M. Miyayama, Ceramics International, 34 (2008) 863-866.

[81] K. Dokko, S. Koizumi, K. Sharaishi, K. Kanamura, Journal of Power Sources, 165 (2007) 656-659.

[82] G. Liang, L. Wang, X. Ou, X. Zhao, S. Xu, Journal of Power Sources, 184 (2008) 538-542.

[83] K. Kanamura, S. Koizumi, K. Dokko, Journal of Materials Science, 43 (2008) 2138-2142.

[84] F. Croce, A.D. Epifanio, J. Hassoun, A. Deptula, T. Olczac, B. Scrosati, Electrochemical and Solid-State Letters, 5 (2002) A47-A50.

[85] H. Yaoqin, M.D. Marca, K. Robert, F. Rita, Journal of The Electrochemical Society, 151 (2004) A1279-A1285.

[86] R. Dominko, M. Bele, M. Gaberscek, M. Remskar, D. Hanzel, S. Pejovnik, J. Jamnik, Journal of The Electrochemical Society, 152 (2005) A607-A610.

[87] H. Liu, J. Xie, K. Wang, Journal of Alloys and Compounds, 459 (2008) 521-525.

[88] R. Dominko, M. Bele, M. Gaberscek, M. Remskar, D. Hanzel, J.M. Goupil, S. Pejovnik, J. Jamnik, Journal of Power Sources, 153 (2006) 274-280.

[89] D. Choi, P.N. Kumta, Journal of Power Sources, 163 (2007) 1064-1069.

[90] S. Beninati, L. Damen, M. Mastragostino, Journal of Power Sources, 194 (2009) 1094-1098.

[91] J. Yao, K. Konstantinov, G. Wang, H. Liu, Journal of Solid State Electrochemistry, 11 (2007) 177-185.

[92] K.S. Park, J.T. Son, H.T. Chung, S.J. Kim, C.H. Lee, H.G. Kim, Electrochemistry Communications, 5 (2003) 839-842.

[93] B.Q. Zhu, X.H. Li, Z.X. Wang, H.J. Guo, Materials Chemistry and Physics, 98 (2006) 373-376.

[94] A.V. Murugan, T. Muraliganth, A. Manthiram, The Journal of Physical Chemistry C, 112 (2008) 14665-14671.

[95] S. Beninati, L. Damen, M. Mastragostino, Journal of Power Sources, 180 (2008) 875-879.

[96] K. Dong-Han, K. Jaekook, Electrochemical and Solid-State Letters, 9 (2006) A439-A442.

[97] D.-H. Kim, J. Kim, Journal of Physics and Chemistry of Solids, 68 (2007) 734-737.

[98] J.-F. Ni, H.-H. Zhou, J.-T. Chen, X.-X. Zhang, Materials Letters, 61 (2007) 1260-1264.

[99] B. Zhao, Y. Jiang, H. Zhang, H. Tao, M. Zhong, Z. Jiao, Journal of Power Sources, 189 (2009) 462-466.

[100] S. Ping Ong, L. Wang, B. Kang, G. Ceder, Chemistry of Materials, 20 (2008) 1798-1807.

[101] A.K. Padhi, K.S. Nanjundaswamy, C. Masquelier, S. Okada, J.B. Goodenough, Journal of The Electrochemical Society, 144 (1997) 1609-1613.

[102] B.-J. Hwang, K.-F. Hsu, S.-K. Hu, M.-Y. Cheng, T.-C. Chou, S.-Y. Tsay, R. Santhanam, Journal of Power Sources, 194 (2009) 515-519.

[103] C.M. Doherty, R.A. Caruso, B.M. Smarsly, C.J. Drummond, Chemistry of Materials, 21 (2009) 2895-2903.

[104] C. Liu, D. Ma, X. Ji, S. Zhao, S. Li, Applied Surface Science, 257 (2011) 4529-4531.

[105] M.S. Whittingham, Solid State Ionics, 134 (2000) 169-178.

[106] A. Kuwahara, S. Suzuki, M. Miyayama, Journal of Electroceramics, 24 (2010) 69-75.

[107] C.S. Sun, Z. Zhou, Z.G. Xu, D.G. Wang, J.P. Wei, X.K. Bian, J. Yan, Journal of Power Sources, 193 (2009) 841-845.

[108] H. Jian, C.S. Wang, X. Chen, S. Upreti, M.S. Whittingham, Electrochemical and Solid-State Letters, 12 (2009) A33-A38.

[109] X. Yin, K. Huang, S. Liu, H. Wang, H. Wang, Journal of Power Sources, 195 (2010) 4308-4312.

[110] N. Hua, C. Wang, X. Kang, T. Wumair, Y. Han, Journal of Alloys and Compounds, 503 (2010) 204-208.

[111] H. Gao, L. Jiao, W. Peng, G. Liu, J. Yang, Q. Zhao, Z. Qi, Y. Si, Y. Wang, H. Yuan, Electrochimica Acta, 56 (2011) 9961-9967.

[112] M. Zhang, L.-F. Jiao, H.-T. Yuan, Y.-M. Wang, J. Guo, M. Zhao, W. Wang, X.-D. Zhou, Solid State Ionics, 177 (2006) 3309-3314.

[113] G.-r. Hu, X.-g. Gao, Z.-d. Peng, K. Du, X.-y. Tan, Y.-j. Liu, Transactions of Nonferrous Metals Society of China, 17 (2007) 296-300.

[114] S. Venkat, N. John, Electrochemical and Solid-State Letters, 9 (2006) A110-A114.

[115] Z.-H. Wang, Q.-Q. Pang, K.-J. Deng, L.-X. Yuan, F. Huang, Y.-L. Peng, Y.-H. Huang, Electrochimica Acta, 78 (2012) 576-584.

[116] W. Huang, Q. Cheng, X. Qin, Russian Journal of Electrochemistry, 46 (2010) 359-362.

[117] Y. Mu-Rong, K. Wei-Hsin, Journal of The Electrochemical Society, 155 (2008) A729-A732.

[118] S.-h. Wu, M.-S. Chen, C.-J. Chien, Y.-P. Fu, Journal of Power Sources, 189 (2009) 440-444.

[119] D. Arumugam, G. Paruthimal Kalaignan, P. Manisankar, Journal of Solid State Electrochemistry, 13 (2009) 301-307.

[120] Z. Liu, X. Zhang, L. Hong, Journal of Applied Electrochemistry, 39 (2009) 2433-2438.

[121] D. Wang, H. Li, S. Shi, X. Huang, L. Chen, Electrochimica Acta, 50 (2005) 2955-2958.

[122] R.-r. Zhao, I.M. Hung, Y.-T. Li, H.-y. Chen, C.-P. Lin, Journal of Alloys and Compounds, 513 (2012) 282-288.

[123] D. Shanmukaraj, G.X. Wang, R. Murugan, H.K. Liu, Materials Science and Engineering: B, 149 (2008) 93-98.

[124] K.-F. Hsu, S.-Y. Tsay, B.-J. Hwang, Journal of Power Sources, 146 (2005) 529-533.

[125] A.Y. Shenouda, H.K. Liu, Journal of Alloys and Compounds, 477 (2009) 498-503.

[126] H. Liu, Q. Cao, L.J. Fu, C. Li, Y.P. Wu, H.Q. Wu, Electrochemistry Communications, 8 (2006) 1553-1557.

[127] Y. Hu, J. Yao, Z. Zhao, M. Zhu, L. Ying, H. Jin, H. Zhao, J. Wang, Materials Chemistry and Physics, 141 (2013) 835-841.

[128] X. Zhao, X. Tang, L. Zhang, M. Zhao, J. Zhai, Electrochimica Acta, 55 (2010) 5899-5904.

[129] R. Yang, X. Song, M. Zhao, F. Wang, Journal of Alloys and Compounds, 468 (2009) 365-369.

[130] J.B. Heo, S.B. Lee, S.H. Cho, J. Kim, S.H. Park, Y.S. Lee, Materials Letters, 63 (2009) 581-583.

[131] Z.-R. Chang, H.-J. Lv, H. Tang, X.-Z. Yuan, H. Wang, Journal of Alloys and Compounds, 501 (2010) 14-17.

[132] H.C. Shin, S.B. Park, H. Jang, K.Y. Chung, W.I. Cho, C.S. Kim, B.W. Cho, Electrochimica Acta, 53 (2008) 7946-7951.

[133] J. Ma, B. Li, H. Du, C. Xu, F. Kang, Journal of Solid State Electrochemistry, 16 (2012) 1-8.

[134] H. Liu, C. Li, Q. Cao, Y. Wu, R. Holze, Journal of Solid State Electrochemistry, 12 (2008) 1017-1020.

[135] Y. Wang, Y. Yang, X. Hu, Y. Yang, H. Shao, Journal of Alloys and Compounds, 481 (2009) 590-594.

[136] S. Luo, Y. Tian, H. Li, K. Shi, Z. Tang, Z. Zhang, Journal of Rare Earths, 28 (2010) 439-442.

[137] Y.-D. Cho, G. Fey, H.-M. Kao, Journal of Solid State Electrochemistry, 12 (2008) 815-823.

[138] F. Lu, Y. Zhou, J. Liu, Y. Pan, Electrochimica Acta, 56 (2011) 8833-8838.

[139] X.-Z. Liao, Y.-S. He, Z.-F. Ma, X.-M. Zhang, L. Wang, Journal of Power Sources, 174 (2007) 720-725.

[140] C.S. Sun, Y. Zhang, X.J. Zhang, Z. Zhou, Journal of Power Sources, 195 (2010) 3680-3683.

[141] H. Liu, C. Li, H.P. Zhang, L.J. Fu, Y.P. Wu, H.Q. Wu, Journal of Power Sources, 159 (2006) 717-720.

[142] H. Liu, L.J. Fu, H.P. Zhang, J. Gao, C. Li, Y.P. Wu, H.Q. Wu, Electrochemical and Solid-State Letters, 9 (2006) A529-A533.

[143] B.L. Ellis, K.T. Lee, L.F. Nazar, Chemistry of Materials, 22 (2010) 691-714.

[144] J.W. Fergus, Journal of Power Sources, 195 (2010) 939-954.

[145] M. Park, X. Zhang, M. Chung, G.B. Less, A.M. Sastry, Journal of Power Sources, 195 (2010) 7904-7929.

[146] Z. Wei-Jun, Journal of The Electrochemical Society, 157 (2010) A1040-A1046.

[147] W.-J. Zhang, Journal of Power Sources, 196 (2011) 2962-2970.

[148] L.-X. Yuan, Z.-H. Wang, W.-X. Zhang, X.-L. Hu, J.-T. Chen, Y.-H. Huang, J.B. Goodenough, Energy & Environmental Science, 4 (2010) 269-284.

[149] V.S. Saji, Y.-S. Kim, T.-H. Kim, J. Cho, H.-K. Song, Physical Chemistry Chemical Physics, 13 (2011) 19226-19237.